Tuning the size and surface of InP nanocrystals by microwave-assisted ionic liquid etching

by

Raghavender Siramdas

B.S., Osmania University, 2007
M.S., Indian Institute of Technology Madras, 2010

AN ABSTRACT OF A DISSERTATION

submitted in partial fulfillment of the requirements for the degree

DOCTOR OF PHILOSOPHY

Department of Chemistry
College of Arts and Sciences

KANSAS STATE UNIVERSITY
Manhattan, Kansas

2018

Abstract

Semiconductors are materials whose conductivity is between metals and insulators. Semiconductor nanocrystals (NCs) have sizes in the range 2 to 10 nm. Because of their unique optical properties like tunable emission wavelength, narrow emission peak, and stability over dyes, they have potential applications in displays. Indium phosphide (InP) is considered a less toxic alternative to commercially used cadmium-based semiconductor NCs. Microwave-assisted (MA) methods using ionic liquids (ILs) afford fast reaction heating rates because of the good MW absorbing capacity of ILs. For tuning size and surface, which are some of the important problems associated with the InP NCs, new synthetic methods are reported herein. In MAIL etching HF generated in the microwave reaction etches the InP NCs surface.

Pyridinium and imidazolium based ILs containing tetrafluoroborate (BF_4^-) and hexafluorophosphate (PF_6^-) ions yield luminescent NCs. In a silicon carbide (SiC) reaction vessel, which blocks most of the microwaves penetrating into the reaction, bigger NCs form than those from a Pyrex reaction vessel because of the higher reaction temperatures in the SiC vessel.

By changing microwave set-power (SP), different reaction times can be achieved. Though a small degree of change in average NC diameter of the NCs is observed at different SPs and reaction temperatures, addition of dodecylamine (DDA) yields NCs with average sizes between 3.2 to 4.2 nm with a broad size distribution. At lower SPs smaller NCs form and at higher SPs bigger NCs form. NC luminescence can be tuned from green (545 nm) to red (630 nm) in the visible region with quantum yields as high as 30%. Rapid heating and InP precursor activation might be

responsible for the larger change in NC size. The effect of DDA on NC size is also verified by microwave reactions in SiC vessels.

ILs containing PF_6^- ions at 280 °C will modify the surface of the NCs so the NC dispersibility changes from non-polar (toluene) to polar (DMSO) as the amount of IL increases. This is due to ligand stripping, which is the removal of large palmitic ligands from the NC surface. These NCs have broad absorption features and emission peaks with QYs of up to 30%. Fourier transform infrared spectroscopy indicates the absence of palmitic acid ligands on the NC surface and zeta potential measurements indicate the presence of anions on the NC surface. From X-ray photoelectron spectroscopy and nuclear magnetic resonance spectroscopy, the inorganic ion $PO_2F_2^-$ is identified on the NCs surface.

Tuning the size and surface of InP nanocrystals by microwave-assisted ionic liquid etching

by

Raghavender Siramdas

B.S., Osmania University, 2007
M.S., Indian Institute of Technology Madras, 2010

A DISSERTATION

submitted in partial fulfillment of the requirements for the degree

DOCTOR OF PHILOSOPHY

Department of Chemistry
College of Arts and Sciences

KANSAS STATE UNIVERSITY
Manhattan, Kansas

2018

Approved by:

Major Professor
Emily McLaurin

Copyright

Abstract

Semiconductors are materials whose conductivity is between metals and insulators. Semiconductor nanocrystals (NCs) have sizes in the range 2 to 10 nm. Because of their unique optical properties like tunable emission wavelength, narrow emission peak, and stability over dyes, they have potential applications in displays. Indium phosphide (InP) is considered a less toxic alternative to commercially used cadmium-based semiconductor NCs. Microwave-assisted (MA) methods using ionic liquids (ILs) afford fast reaction heating rates because of the good MW absorbing capacity of ILs. For tuning size and surface, which are some of the important problems associated with the InP NCs, new synthetic methods are reported herein. In MAIL etching HF generated in the microwave reaction etches the InP NCs surface.

Pyridinium and imidazolium based ILs containing tetrafluoroborate (BF_4^-) and hexafluorophosphate (PF_6^-) ions yield luminescent NCs. In a silicon carbide (SiC) reaction vessel, which blocks most of the microwaves penetrating into the reaction, bigger NCs form than those from a Pyrex reaction vessel because of the higher reaction temperatures in the SiC vessel.

By changing microwave set-power (SP), different reaction times can be achieved. Though a small degree of change in average NC diameter of the NCs is observed at different SPs and reaction temperatures, addition of dodecylamine (DDA) yields NCs with average sizes between 3.2 to 4.2 nm with a broad size distribution. At lower SPs smaller NCs form and at higher SPs bigger NCs form. NC luminescence can be tuned from green (545 nm) to red (630 nm) in the visible region with quantum yields as high as 30%. Rapid heating and InP precursor activation might be

responsible for the larger change in NC size. The effect of DDA on NC size is also verified by microwave reactions in SiC vessels.

ILs containing PF_6^- ions at 280 °C will modify the surface of the NCs so the NC dispersibility changes from non-polar (toluene) to polar (DMSO) as the amount of IL increases. This is due to ligand stripping, which is the removal of large palmitic ligands from the NC surface. These NCs have broad absorption features and emission peaks with QYs of up to 30%. Fourier transform infrared spectroscopy indicates the absence of palmitic acid ligands on the NC surface and zeta potential measurements indicate the presence of anions on the NC surface. From X-ray photoelectron spectroscopy and nuclear magnetic resonance spectroscopy, the inorganic ion $PO_2F_2^-$ is identified on the NCs surface.

Table of Contents

List of Figures

List of Abbreviations

BDMIm PF_6	1-butyl-2,3-dimethylimidazolium hexafluorophosphate
BMIm SbF_6	1-butyl-3-methylimidazolium hexafluoroantimonate
BMIm TFSI	1-butyl-3-methylimidazolium bis(trifluoromethylsulfonyl)-imide
BMPy BF_4	1-butyl-4-methylpyridinium tetrafluoroborate
BMPy PF_6	1-butyl-4-methylpyridinium hexafluorophosphate
$CDCl_3$	Deuterated chloroform
DDA	Dodecylamine
DLS	Dynamic light scattering
DMF	N,N-dimethyl formamide
DMSO	Dimethyl sulfoxide
DMSO-d_6	Deuterated dimethylsulfoxide
FA	Formic acid
FT-IR	Fourier transform infrared
FWHM	Full width at half maximum
HF	Hydrogen fluoride
HMIm BF_4	1-hexyl-3-methylimidazolium tetrafluoroborate
HT	Holding time
IL	Ionic liquid
$In(OAc)_3$	Indium acetate
InPA	Indium palmitate
MAIL	Microwave-assisted ionic liquid

MW	Microwave
NCs	Nanocrystals
NMR	Nuclear magnetic resonance
ODE	1-octadecene
PA	Palmitic acid
PC	Propylene carbonate
PL	Photoluminescence
SiC	Silicon carbide
SP	Set-power
TEM	Transmission electron microscopy
TGA	Thermogravimetric analysis
TMSP or $P(TMS)_3$	Tris(trimethylsilyl)phosphine
TOPO	Trioctylphosphine oxide
UV-Vis	UV-Visible
XPS	X-ray photoelectron spectroscopy
XRD	X-ray diffraction

Acknowledgements

I am very thankful to my PI, Dr. Emily McLaurin for her constant encouragement, guidance, and teachings to learn research and non-research skills required for a scientific researcher throughout my PhD journey. I would like to thank to Dr. Christopher M. Sorensen for giving an opportunity to work with him and to learn fundamental concepts in nanoscience. I would also like to thank my review committee members Dr. Christine Aikens, Dr. Tendai Gadzikwa, and Dr. Eric Maattaa for being in my review committee and for their support whenever I ask for any help. Finally, I would like to thank each and every one from my family, friends, colleagues, and staff at K-state for being helpful whenever I am in need of anything.

Chapter 1 - Introduction

1.1 Importance of III-V Semiconductors

III-V semiconductors have important applications in light emitting diodes (LEDs), infrared photodetectors, and solar cells.[1] Electron mobilities for some of the III-V semiconductors like GaAs or InGaAs are ten times higher than that of Si at a comparable sheet density.[2] Because of their exceptional electron transport properties, they are important components in transistors.[2] For photovoltaics, III-V semiconductors were first used in space until the late '90s.[1] Improvements in photovoltaic cell efficiencies led to the development of most efficient single- and multi-junction photovoltaics.[3] Besides their electrical applications, the optical properties of these materials make them stand apart from other semiconductors. Particularly, group-III nitrides such as AlN, GaN, and InN and their alloys emit light spanning from the visible[4] to the deep ultraviolet (UV)[5,6] useful for LEDs and laser diodes. Owing to advantages such as ideal spectral selectivity and thermal stability, group-III nitrides can also be used in high-performance UV photodetectors[7] and other III-V semiconductors, like GaInAs, in infrared photodetectors.[8]

1.2 Semiconductor Nanocrystals

Semiconductor nanocrystals (NCs) or quantum dots (QDs) are semiconductor materials whose size is often in the range of 2 to 10 nm.[9] Transformation from bulk material to nanomaterial is associated with changes in the distribution of energy levels at the edges of the valence band and conduction band as shown in Figure 1.1.[10] NC properties are strongly affected by size and ligands passivating the surface.[11,12] The optical properties of InP NCs in the wavelength region (450-750 nm) make these materials a potential alternative to Cd-based NCs.[13] Taking into account the covalent and ionic nature of bonds, the term "fractional ionic character (fi)" is used to quantify the bonding nature in semiconductors. Generally, III-V semiconductors possess higher covalent

character than that of II-VI and IV-VI semiconductors.[14] Specifically, the fi for InP is 0.42 and 0.70 for CdSe,.[14] Because they are more covalent, synthesis of III-V NCs often involves high reaction temperatures, long times and highly reactive precursors.[15]

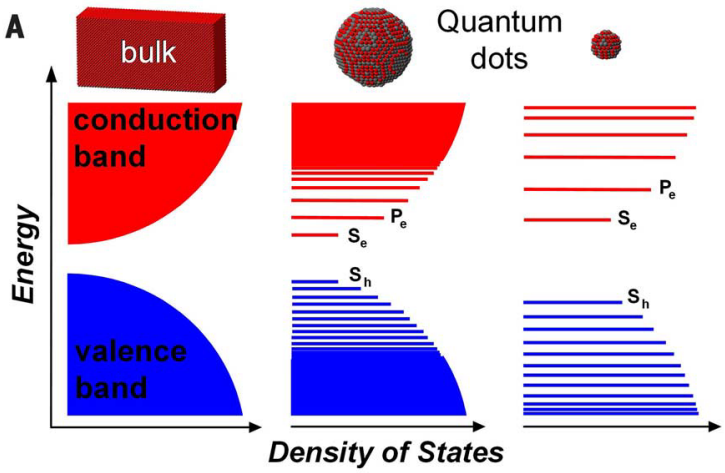

Figure 1.1 Distribution of energy levels and bands (valence and conduction) in semiconductor nanocrystals (quantum dots) and bulk semiconductors. As the physical dimensions of the semiconductor decrease, discrete energy levels form at the band edges. From reference 9. Reprinted with permission from AAAS.

Unique properties of semiconductor nanocrystals arise because of quantization of energy states. For instance, as shown in Figure 1.2, if the band gap is in the visible region when the NCs are excited by photons of equal or higher than the band gap energy, electrons from the valence band will be excited to the conduction band. After a certain time, electrons will relax to the valence band by combining with holes. During this recombination process, photons of energy lower than the energy of absorbed photons are emitted. Hence, there is emission of different colors based on size and as the size decreases, the color of the emission varies from red to blue.

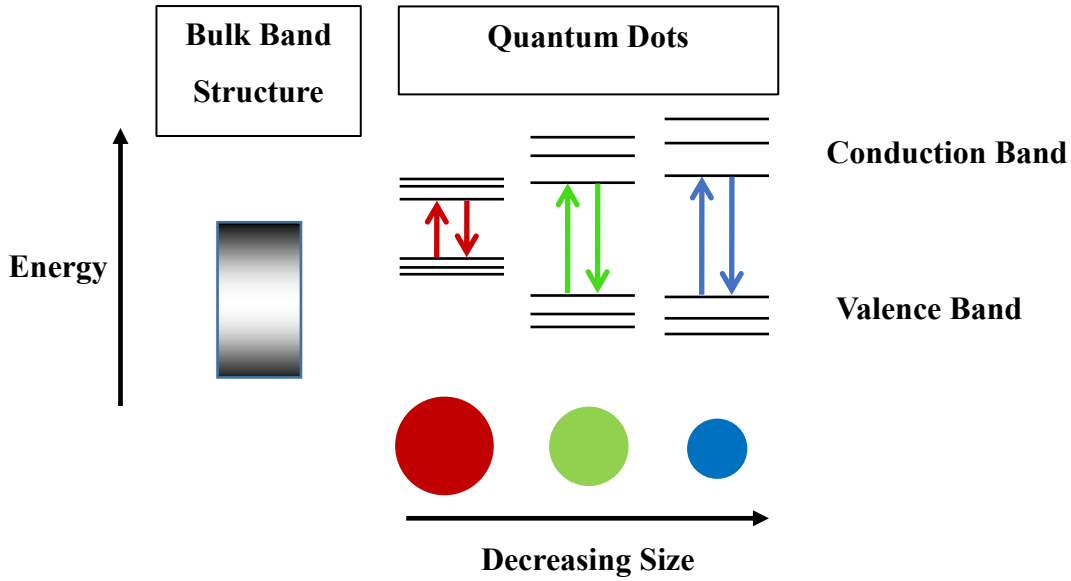

Figure 1.2 Schematic diagram showing quantum confinement and size-dependent absorption and photoluminescence in the visible region for semiconductor nanocrystals (quantum dots).

Size-dependent optical properties of semiconductor NCs have made these NCs attractive materials in various fields like solar cells, bio-imaging, and optoelectronics.[10,16–18] Figure 1.3 shows emission ranges obtainable in the visible and near-infrared (NIR) regions for different semiconductors.[19] For example, stable InAs NCs coated with ZnS and ZnCdS NCs with emission in the NIR region were used in biological imaging.[20,21] PL quantum yields can be obtained in the NIR region for InAs/InP/ZnSe NCs as high as 90% with narrow PL band and biocompatibility.[22] For solar cell applications, InAs NCs are a potential candidate for multiple exciton generation (MEG), generation of two or more excitons per one photon, because the bulk semiconductor band gap is 0.36 eV.[23]

As shown in Figure 1.3, emission of the InP NCs covers from around 480 to 740 nm in the visible region. InP NCs typically are associated with surface defects because of P dangling bonds, which act as electron traps.[11] A quantum yield of 40% is achieved by HF photoetching, which removes surface P atoms with dangling bonds.[11] To get very high quantum yields, these NCs often require

a shell of wider bandgap material (ZnS or ZnSe) for effective surface passivation.[24,25] The highest PL quantum yield of 87% and smallest full width at half maximum (FWHM) of 40 nm were achieved for In(Zn)P/ZnS and InP/ZnS, respectively.[24,26] The emission can also be tuned from blue to NIR (450-750 nm) for InP/ZnS NCs with quantum yields as high as 40%.[27]

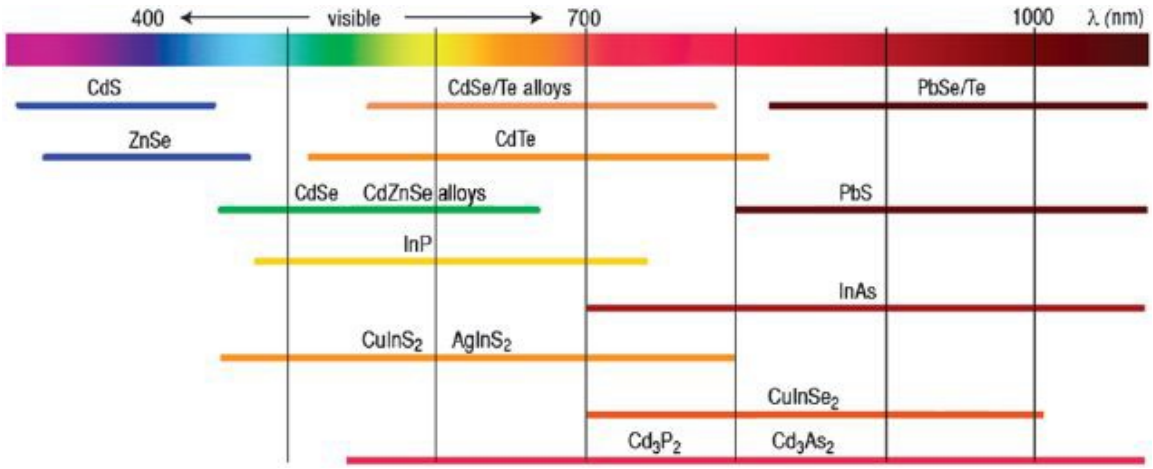

Figure 1.3 Reported spectral ranges of emission for different semiconductor quantum dots. Reprinted from ref 11. Copyright 2013 Cambridge University Press.

1.3 Importance of InP NCs Synthesis

The bulk band gap and exciton Bohr radius of InP are 1.35 eV and ~ 10 nm, so the emission wavelength for the NCs can be tuned in the visible and near-infrared regions by changing the NC size.[13] The use of cadmium-based materials in electronic equipment is prohibited by the European Union (EU) Restriction of Hazardous Substances (RoHS), whereas InP conforms to the RoHS directive of the EU.[13] So, development of InP based materials is required to make them as replacement for Cd-based NCs. High energy transfer efficiencies between InP/ZnS NCs and chromophoric dyes consisting of free anchoring groups were also reported, demonstrating their potential use in photovoltaic and biomedical applications.[28,29] InP/ZnS NCs are stable, retaining their luminescence for 24 hours under various physiological conditions, and are less cytotoxic than

CdSe/ZnS NCs. Leaching of Cd^{2+} ions causes damage to cell membranes and genetic materials whereas leaching of In^{3+} ions was found to have lower intrinsic toxicity.[30]

1.4 Synthetic Challenges of InP NCs

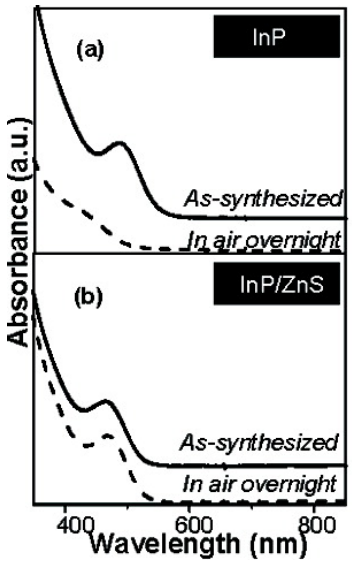

Figure 1.4 UV-Vis absorption spectra of InP NCs (A) and InP/ZnS NCs (B). InP NCs lose absorption features after 12 h in the air whereas InP/ZnS NCs are stable because of shell formation on the surface. Reprinted with permission from ref 24. Copyright 2007 American Chemical Society.

Because of the higher covalent nature of bonding between In and P (fractional ionic character, fi, 0.42), synthesis of InP NCs require high reaction temperatures[31] and very long reaction times[32] using aliphatic carboxylic acids[33], trioctylphosphine[34], or phosphonic acids[31]. Chemical instability of the InP NCs is a big issue due to oxidation in less than 12 h in air causing these NCs to lose their absorption features as shown in Figure 1.4.[27] Hence, they are often coated with inorganic shells (ZnS or ZnSe) to obtain chemical stability or luminescence.[27] Because of the high reactivity towards oxidation for P and In precursors, InP NCs synthesis is very sensitive to air.

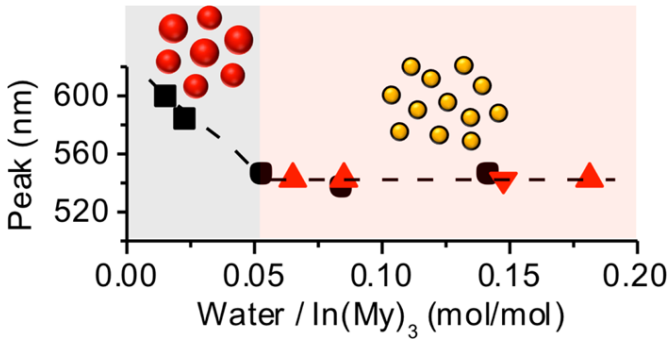

Figure 1.5 Effect of water on growth of the InP NCs. Higher concentrations of water in the reaction mixture prevent growth of the NCs, whereas at very low concentrations growth of the NCs can be tuned. Reprinted with permission from ref 31. Copyright 2015 American Chemical Society.

Another factor that serves as a disadvantage and boon is moisture/water in the synthesis.[35,36] The presence of water inhibits growth of the NCs with the first absorption peak remaining around 550 nm.[35] Without water in the reaction mixture, growth of the NCs can be effectively tuned with reaction temperature and time with the first absorption peak reaching 620 nm as shown in Figure 1.5. *In situ* generation of water during the synthesis leads to In_2O_3 shell formation over InP NCs enhancing luminescence by one order of magnitude.[37] Water present in the hot-injection method of synthesis can improve the optical properties of the InP/ZnS NCs.[36] XPS analysis revealed formation of an amorphous phosphate layer, which reduces the lattice mismatch between InP and ZnS. This, in turn, increases quantum yield to as high as 45%. It is possible to tune the emission from 525 to 625 nm by varying amount of the water in the system.

Other limitations associated with InP NC synthesis is the availability of a limited number of P precursors.[13] The most commonly used P precursor is tris(trimethylsilyl)phosphine and it is known for its depletion very quickly[13]. With this P precursor in the presence of coordinating solvents reaction times are reduced from days to 3 h.[38] Similar precursors such as Ge or Sn in place of Si are synthesized and used in the NC synthesis to improve size distribution moderately without

optimization.[39] Introducing electron-donating and electron-withdrawing groups in the organic moiety of this precursor did not lead to monodispersity of the synthesized InP NCs.[33] For economical synthesis, *in situ* generated PH_3 is used as the precursor for accessing larger sized InP NCs.[40] In recent times, tris(dimethylamino)phosphine, $P(NMe_2)_3$, emerged as potential candidate for InP NC synthesis.[41–43] Owing to some of these synthetic challenges, InP NCs synthesis is not as extensively studied as II-VI NCs such as CdSe.

1.5 Strategies and Problems Associated with Size, Emission, and Surface Tunability of the InP NCs

Size tunability is a challenging task in InP NCs synthesis. One method to tuning the size of the NCs is varying the concentration of aliphatic ligands, where optimum concentration gives monodisperse NCs.[38] In the same report, secondary injections of P and In precursors during the synthesis are also presented to achieve growth to tune the size. A similar strategy used sequential injections of precursors for growth of the NCs in a microfluidic reactor.[44] Separation of nucleation and growth by modifying the reactivity of the P precursor and choosing two suitable P precursors where one acts as a nucleating agent and the other precursor is responsible for growth was demonstrated.[33] However, separation of nucleation and growth is not sufficient to produce monodisperse particles for the covalent InP system.

Post-synthetic treatment by HF-photoetching showed that the emission can be tuned from 522 to 751 nm with quantum yields as high as around 40% and mean diameter changing from 1.7 to 6.5 nm.[12] Because of chemical instability shells over them are required.[27] Emission of InP/ZnS core/shell NCs is tuned in the visible region with quantum yields of around 50 and 70% and FWHM values of 60 and 40 nm, respectively.[24,41] There are no reports of tuning the emission without shells or HF-photoetching (post-treatment) for InP NCs.

Typical synthesis of the InP NCs involves long aliphatic ligands to obtain colloidal stability.[33,35] So, to modify the surface of the InP NCs from aliphatic ligands to very short ligands, the ligand exchange method is generally used.[45] Because of short ionic ligands on the surface, NC solubility changes from non-polar solvent (toluene) to polar solvent (DMSO) or more polar solvents.[45] Irrespective of the pristine ligand, upon ligand exchange the surface of the InP NCs can be replaced with S^{2-}, Se^{2-}, Te^{2-}, $SnSe_6^{4-}$, or $InCl_3$.[46,47] UV-etching of InP NCs in the presence of hydrofluoric and sulfuric acids yields NCs with sulfate (SO_4^{2-}) on the surface.[48] However, there is no report of *in situ* ligand exchange or ligand stripping of the InP NCs.

1.6 Microwave-Assisted Synthesis

Microwave-assisted synthesis is known for its advantages in organic and inorganic nanostructured materials synthesis because of fast reaction times and lower consumption of energy.[46–48] The mechanism of heating can be either dipolar polarization or ionic conduction.[52] In dipolar polarization, dipoles of molecules try to align with the changing alternating electric field and during this alignment molecules undergo friction, which generate heat.[50] In ionic conduction, ions will be in constant fluctuation under the oscillating electric field causing a rise in local temperatures due to collision and friction.[50] Heating is due to ionic conduction when ionic liquids (ILs) are used in the synthesis.[50] The power of the microwaves absorbed during the synthesis depends on the dielectric cross-section (real component, ε' and imaginary component, ε'') of the materials used.[53] To simplify, the ability to absorb microwaves is determined by loss tangent ($\tan \delta = \varepsilon''/\varepsilon'$).[50] Higher the loss tangent, better the microwave absorbing ability. Selective microwave absorption by the reactants enhances the reaction rates under increased pressure conditions.[50,52,54,55] The penetration depth of microwaves is deeper when there is a solution with a smaller loss tangent than a solution with a higher tangent.[56] Microwave leakage into the BS and

SiC vessels are found to be around 62 and 52 % of the impingent microwave field, respecectively.[57] Heating can be achieved as fast as 200-300 °C per minute in the microwave synthesis.[56] Generally, the frequency of the microwaves used for synthesis is 2.45 GHz.[51]

1.6.1 Microwave-Assisted Synthesis of Nanoparticles

Effect of microwave frequency on Ni nanoparticles (NPs) was studied by the Strouse group as the dielectric cross-section is frequency dependent.[53] Kinetics for nucleation and growth are enhanced with increasing MW field strength for Ni NPs.[53] For Au NPs, there is no effect of frequency (2.45 and 5.8 GHz) on size and shape for synthesis in polar media.[58] The microwave-assisted method is used to synthesize uniform and stable spherical Ag NPs in glycerol, which acts as solvent and reducing agent.[59] By changing the concentrations or reactants in the microwave synthesis, sizes of Ag NPs are controlled.[60] For Ag nanostructures, morphology can be changed to nanosheets, nanorods, and nanowires by the microwave-assisted method.[61] Bulk quantities of Ag nanocomposites are synthesized by using biodegradable polymer.[62] Synthesis of nanoalloys is also reported for Ag with Au and Pt by a microwave-assisted method.[63] Microwave synthesis is demonstrated for other metallic particles also like Au[64,65], Rh[66], Co[67], Ni[68], and Cu[69]. Ligand exchange reactions are carried out for Rh NPs in microwave synthesis to replace PVP ligands with ammonium carboxylates at 150 °C.[66] Morphology can be changed to get nanorods and nanowires for gold.[70] Core-shell NPs like Au@Pd[71], Au@Rh[72], and Au@Ag NPs[73] were reported. The Microwave-assisted method is also used for the synthesis of QDs of II-VI (CdSe[74–78], CdTe[79], CdS[80]) and IV-VI (PdSe[81]) semiconductors. For CdSe QDs, similar heating rates were occurred in both Pyrex and SiC vessels.[78] Core-shell QDs (CdSe/ZnS[82,83], CdTe/CdS/ZnS[84]), alloyed QDs (ZnSe(S)[85]), and doped QDs (Mn:ZnSe/ZnS[86]) can also be synthesized. For III-V materials, luminescent InP NCs were synthesized in 2008 using ionic liquids as microwave absorbers and a

fluoride ion source for etching the surface of the NCs.[50,51]

1.6.2 Ionic Liquids for Microwave-Assisted Synthesis of Nanomaterials

Ionic liquids (ILs) are organic salts, whose melting points are generally below 100 °C.[51] They are used as solvents in the microwave-assisted synthesis of inorganic nanostructures because of their low vapor pressure, high decomposition temperature, and good coupling with the applied microwaves.[51] Their ability to absorb microwaves increases with temperature due to the ionic conduction effect.[88] This facilitates fast heating rates of reaction mixtures.[75] These properties of ILs have advantages in the synthesis of nanomaterials. The microwave-assisted ionic liquid (MAIL) method was reported in 2004 for the preparation of Te nanorods and nanowires.[89] Some of the examples for the application of ILs in nanomaterials syntheses are Au[90,91], Co[92], ZnS[93], PbSe[94], Bi_2Se_3[95], Ni_2P[96], Fe_2O_3[97], Bi_2Te_3[98], ZnO[99], and CuO[100]. ILs not only act as microwave absorbers but their decomposed species will be responsible for luminescence of InP NCs in the microwave synthesis.[87,101,102] The effect of different ionic liquids containing BF_4^-, PF_6^-, F^-, and Cl^- and the effect of their concentrations in the reaction mixture were studied ultimately achieving a quantum yield of around 50% for InP NCs.[87]

1.7 Structure of the Thesis

Our work of the InP NCs synthesis by the microwave-assisted method is an extension of the reported work[87] to investigate the effect of temperature, microwave power and vessel, an aliphatic amine, and ionic liquids containing BF_4^- and PF_6^- for tuning the size and surface of the InP NCs. In chapter 3, an alternative method is developed to tune the size of InP NCs instead of using different concentrations of ligands, different P precursors, or multiple injections of precursors by using microwave powers and reaction temperatures. But, addition of ionic liquids in the reaction mixture prevents from using post-synthetic etching step or inorganic shell (ZnS or ZnSe) formation

to get luminescent NCs. However, NCs still does not possess good size distribution. Chapter 4 discusses a synthesis of luminescent InP NCs dispersible in a polar solvent (DMSO). Characterization by XPS, NMR, TGA, and Zeta potential measurements identified the presence of an inorganic ion ($PO_2F_2^-$). The presented method offers a new way to modify InP NC surface in such a way to get dispersibility in polar solvents.

1.8 References

(1) Mokkapati, S.; Jagadish, C. III-V Compound SC for Optoelectronic Devices. *Mater. Today* **2009**, *12* (4), 22–32.

(2) Alamo, J. A. del. Nanometer-Scale Electronics with III–V Compound Semiconductors. *Nature* **2011**, *479* (7373), 317–323.

(3) Greenaway, A. L.; Boucher, J. W.; Oener, S. Z.; Funch, C. J.; Boettcher, S. W. Low-Cost Approaches to III–V Semiconductor Growth for Photovoltaic Applications. *ACS Energy Lett.* **2017**, *2* (10), 2270–2282.

(4) Nakamura, S. The Roles of Structural Imperfections in InGaN-Based Blue Light-Emitting Diodes and Laser Diodes. *Science* **1998**, *281* (5379), 956–961.

(5) Taniyasu, Y.; Kasu, M.; Makimoto, T. An Aluminium Nitride Light-Emitting Diode with a Wavelength of 210 Nanometres. *Nature* **2006**, *441* (7091), 325–328.

(6) Rinke, P.; Winkelnkemper, M.; Qteish, A.; Bimberg, D.; Neugebauer, J.; Scheffler, M. Consistent Set of Band Parameters for the Group-III Nitrides AlN, GaN, and InN. *Phys. Rev. B* **2008**, *77* (7), 075202.

(7) Sang, L.; Liao, M.; Sumiya, M. A Comprehensive Review of Semiconductor Ultraviolet Photodetectors: From Thin Film to One-Dimensional Nanostructures. *Sensors* **2013**, *13* (8), 10482–10518.

(8) Pearsall, T. $Ga_{0.47}In_{0.53}As$: A Ternary Semiconductor for Photodetector Applications. *IEEE J. Quantum Electron.* **1980**, *16* (7), 709–720.

(9) Xu, G.; Zeng, S.; Zhang, B.; Swihart, M. T.; Yong, K.-T.; Prasad, P. N. New Generation Cadmium-Free Quantum Dots for Biophotonics and Nanomedicine. *Chem. Rev.* **2016**, *116* (19), 12234–12327.

(10) Kagan, C. R.; Lifshitz, E.; Sargent, E. H.; Talapin, D. V. Building Devices from Colloidal Quantum Dots. *Science* **2016**, *353* (6302), aac5523.

(11) Adam, S.; Talapin, D. V.; Borchert, H.; Lobo, A.; McGinley, C.; de Castro, A. R. B.; Haase, M.; Weller, H.; Möller, T. The Effect of Nanocrystal Surface Structure on the Luminescence Properties: Photoemission Study of HF-Etched InP Nanocrystals. *J. Chem. Phys.* **2005**, *123* (8), 084706.

(12) Talapin, D. V.; Gaponik, N.; Borchert, H.; Rogach, A. L.; Haase, M.; Weller, H. Etching of Colloidal InP Nanocrystals with Fluorides: Photochemical Nature of the Process Resulting in High Photoluminescence Efficiency. *J. Phys. Chem. B* **2002**, *106* (49), 12659–12663.

(13) Tamang, S.; Lincheneau, C.; Hermans, Y.; Jeong, S.; Reiss, P. Chemistry of InP Nanocrystal Syntheses. *Chem. Mater.* **2016**, *28* (8), 2491–2506.

(14) Reiss, P.; Carrière, M.; Lincheneau, C.; Vaure, L.; Tamang, S. Synthesis of Semiconductor Nanocrystals, Focusing on Nontoxic and Earth-Abundant Materials. *Chem. Rev.* **2016**, *116* (18), 10731–10819.

(15) Heath, J. R. Covalency in Semiconductor Quantum Dots. *Chem. Soc. Rev.* **1998**, *27* (1), 65–71.

(16) Carey, G. H.; Abdelhady, A. L.; Ning, Z.; Thon, S. M.; Bakr, O. M.; Sargent, E. H. Colloidal Quantum Dot Solar Cells. *Chem. Rev.* **2015**, *115* (23), 12732–12763.

(17) Bruchez, M.; Moronne, M.; Gin, P.; Weiss, S.; Alivisatos, A. P. Semiconductor Nanocrystals as Fluorescent Biological Labels. *Science* **1998**, *281* (5385), 2013–2016.

(18) Pichaandi, J.; van Veggel, F. C. J. M. Near-Infrared Emitting Quantum Dots: Recent Progress on Their Synthesis and Characterization. *Coord. Chem. Rev.* **2014**, *263-264*, 138–150.

(19) Chen, O.; Wei, H.; Maurice, A.; Bawendi, M.; Reiss, P. Pure Colors from Core–shell Quantum Dots. *MRS Bull.* **2013**, *38* (9), 696–702.

(20) Choi, H. S.; Ipe, B. I.; Misra, P.; Lee, J. H.; Bawendi, M. G.; Frangioni, J. V. Tissue- and Organ-Selective Biodistribution of NIR Fluorescent Quantum Dots. *Nano Lett.* **2009**, *9* (6), 2354–2359.

(21) Allen, P. M.; Liu, W.; Chauhan, V. P.; Lee, J.; Ting, A. Y.; Fukumura, D.; Jain, R. K.; Bawendi, M. G. InAs(ZnCdS) Quantum Dots Optimized for Biological Imaging in the Near-Infrared. *J. Am. Chem. Soc.* **2010**, *132* (2), 470–471.

(22) Xie, R.; Chen, K.; Chen, X.; Peng, X. InAs/InP/ZnSe Core/Shell/Shell Quantum Dots as Near-Infrared Emitters: Bright, Narrow-Band, Non-Cadmium Containing, and Biocompatible. *Nano Res.* **2008**, *1* (6), 457–464.

(23) Yu, P.; Zhu, K.; Norman, A. G.; Ferrere, S.; Frank, A. J.; Nozik, A. J. Nanocrystalline TiO_2 Solar Cells Sensitized with InAs Quantum Dots. *J. Phys. Chem. B* **2006**, *110* (50), 25451–25454.

(24) Li, L.; Reiss, P. One-Pot Synthesis of Highly Luminescent InP/ZnS Nanocrystals without Precursor Injection. *J. Am. Chem. Soc.* **2008**, *130* (35), 11588–11589.

(25) Lim, J.; Bae, W. K.; Lee, D.; Nam, M. K.; Jung, J.; Lee, C.; Char, K.; Lee, S. InP@ZnSeS, Core@Composition Gradient Shell Quantum Dots with Enhanced Stability. *Chem. Mater.* **2011**, *23* (20), 4459–4463.

(26) Altıntas, Y.; Talpur, M. Y.; Mutlugün, E. Efficient Förster Resonance Energy Transfer Donors of In(Zn)P/ZnS Quantum Dots. *J. Phys. Chem. C* **2017**, *121* (5), 3034–3043.

(27) Xie, R.; Battaglia, D.; Peng, X. Colloidal InP Nanocrystals as Efficient Emitters Covering Blue to Near-Infrared. *J. Am. Chem. Soc.* **2007**, *129* (50), 15432–15433.

(28) Thomas, A.; Nair, P. V.; George Thomas, K. InP Quantum Dots: An Environmentally Friendly Material with Resonance Energy Transfer Requisites. *J. Phys. Chem. C* **2014**, *118* (7), 3838–3845.

(29) Devatha, G.; Roy, S.; Rao, A.; Mallick, A.; Basu, S.; Pillai, P. P. Electrostatically Driven Resonance Energy Transfer in “cationic” Biocompatible Indium Phosphide Quantum Dots. *Chem. Sci.* **2017**, *8* (5), 3879–3884.

(30) Brunetti, V.; Chibli, H.; Fiammengo, R.; Galeone, A.; Malvindi, M. A.; Vecchio, G.; Cingolani, R.; Nadeau, J. L.; Pompa, P. P. InP/ZnS as a Safer Alternative to CdSe/ZnS Core/shell Quantum Dots: In Vitro and in Vivo Toxicity Assessment. *Nanoscale* **2012**, *5* (1), 307–317.

(31) Gary, D. C.; Terban, M. W.; Billinge, S. J. L.; Cossairt, B. M. Two-Step Nucleation and Growth of InP Quantum Dots via Magic-Sized Cluster Intermediates. *Chem. Mater.* **2015**, *27* (4), 1432–1441.

(32) Mićić, O. I.; Cheong, H. M.; Fu, H.; Zunger, A.; Sprague, J. R.; Mascarenhas, A.; Nozik, A. J. Size-Dependent Spectroscopy of InP Quantum Dots. *J. Phys. Chem. B* **1997**, *101* (25), 4904–4912.

(33) Gary, D. C.; Glassy, B. A.; Cossairt, B. M. Investigation of Indium Phosphide Quantum Dot Nucleation and Growth Utilizing Triarylsilylphosphine Precursors. *Chem. Mater.* **2014**, *26* (4), 1734–1744.

(34) Moreels, I.; Martins, J. C.; Hens, Z. Ligand Adsorption/Desorption on Sterically Stabilized InP Colloidal Nanocrystals: Observation and Thermodynamic Analysis. *ChemPhysChem* **2006**, *7* (5), 1028–1031.

(35) Xie, L.; Harris, D. K.; Bawendi, M. G.; Jensen, K. F. Effect of Trace Water on the Growth of Indium Phosphide Quantum Dots. *Chem. Mater.* **2015**, *27* (14), 5058–5063.

(36) Ramasamy, P.; Kim, B.; Lee, M.-S.; Lee, J.-S. Beneficial Effects of Water in the Colloidal Synthesis of InP/ZnS Core–shell Quantum Dots for Optoelectronic Applications. *Nanoscale* **2016**, *8* (39), 17159–17168.

(37) Protière, M.; Reiss, P. Amine-Induced Growth of an In_2O_3 Shell on Colloidal InP Nanocrystals. *Chem. Commun.* **2007**, *0* (23), 2417–2419.

(38) Battaglia, D.; Peng, X. Formation of High Quality InP and InAs Nanocrystals in a Noncoordinating Solvent. *Nano Lett.* **2002**, *2* (9), 1027–1030.

(39) Harris, D. K.; Bawendi, M. G. Improved Precursor Chemistry for the Synthesis of III–V Quantum Dots. *J. Am. Chem. Soc.* **2012**, *134* (50), 20211–20213.

(40) Li, L.; Protière, M.; Reiss, P. Economic Synthesis of High Quality InP Nanocrystals Using Calcium Phosphide as the Phosphorus Precursor. *Chem. Mater.* **2008**, *20* (8), 2621–2623.

(41) Song, W.-S.; Lee, H.-S.; Lee, J. C.; Jang, D. S.; Choi, Y.; Choi, M.; Yang, H. Amine-Derived Synthetic Approach to Color-Tunable InP/ZnS Quantum Dots with High Fluorescent Qualities. *J. Nanoparticle Res.* **2013**, *15* (6), 1750.

(42) Tessier, M. D.; De Nolf, K.; Dupont, D.; Sinnaeve, D.; De Roo, J.; Hens, Z. Aminophosphines: A Double Role in the Synthesis of Colloidal Indium Phosphide Quantum Dots. *J. Am. Chem. Soc.* **2016**, *138* (18), 5923–5929.

(43) Buffard, A.; Dreyfuss, S.; Nadal, B.; Heuclin, H.; Xu, X.; Patriarche, G.; Mézailles, N.; Dubertret, B. Mechanistic Insight and Optimization of InP Nanocrystals Synthesized with Aminophosphines. *Chem. Mater.* **2016**, *28* (16), 5925–5934.

(44) Baek, J.; Allen, P. M.; Bawendi, M. G.; Jensen, K. F. Investigation of Indium Phosphide Nanocrystal Synthesis Using a High-Temperature and High-Pressure Continuous Flow Microreactor. *Angew. Chem. Int. Ed.* **2011**, *50* (3), 627–630.

(45) Boles, M. A.; Ling, D.; Hyeon, T.; Talapin, D. V. The Surface Science of Nanocrystals. *Nat. Mater.* **2016**, *15* (2), 141–153.

(46) Liu, W.; Lee, J.-S.; Talapin, D. V. III–V Nanocrystals Capped with Molecular Metal Chalcogenide Ligands: High Electron Mobility and Ambipolar Photoresponse. *J. Am. Chem. Soc.* **2013**, *135* (4), 1349–1357.

(47) Dirin, D. N.; Dreyfuss, S.; Bodnarchuk, M. I.; Nedelcu, G.; Papagiorgis, P.; Itskos, G.; Kovalenko, M. V. Lead Halide Perovskites and Other Metal Halide Complexes As Inorganic Capping Ligands for Colloidal Nanocrystals. *J. Am. Chem. Soc.* **2014**, *136* (18), 6550–6553.

(48) Mnoyan, A. N.; Kirakosyan, A. G.; Kim, H.; Jang, H. S.; Jeon, D. Y. Electrostatic Stabilized InP Colloidal Quantum Dots with High Photoluminescence Efficiency. *Langmuir* **2015**, *31* (25), 7117–7121.

(49) Spargo, P. Microwaves in Organic Synthesis Edited by Andre Loupy. Wiley-VCH: Weinheim. 2002. 159 Euro. 499 Pp. ISBN 3-527-30514-9. *Org. Process Res. Dev.* **2004**, *8* (2), 298–298.

(50) Baghbanzadeh, M.; Carbone, L.; Cozzoli, P. D.; Kappe, C. O. Microwave-Assisted Synthesis of Colloidal Inorganic Nanocrystals. *Angew. Chem. Int. Ed.* **2011**, *50* (48), 11312–11359.

(51) Zhu, Y.-J.; Chen, F. Microwave-Assisted Preparation of Inorganic Nanostructures in Liquid Phase. *Chem. Rev.* **2014**, *114* (12), 6462–6555.

(52) Gabriel, C.; Gabriel, S.; Grant, E. H.; Grant, E. H.; Halstead, B. S. J.; Mingos, D. M. P. Dielectric Parameters Relevant to Microwave Dielectric Heating. *Chem. Soc. Rev.* **1998**, *27* (3), 213–224.

(53) Ashley, B.; Dyer, C. M.; Owens, J.; Strouse, G. F. Influence of Microwave Frequency and Power on Nanometal Growth. *J. Phys. Chem. C* **2018**, *122* (6), 3617–3627.

(54) Washington, Aaron L.; Strouse, G. F. Selective Microwave Absorption by Trioctyl Phosphine Selenide: Does It Play a Role in Producing Multiple Sized Quantum Dots in a Single Reaction? *Chem. Mater.* **2009**, *21* (13), 2770–2776.

(55) Bilecka, I.; Niederberger, M. Microwave Chemistry for Inorganic Nanomaterials Synthesis. *Nanoscale* **2010**, *2* (8), 1358–1374.

(56) Chikan, V.; McLaurin, E. J. Rapid Nanoparticle Synthesis by Magnetic and Microwave Heating. *Nanomaterials* **2016**, *6* (5).

(57) Ashley, B.; Lovingood, D. D.; Chiu, Y.-C.; Gao, H.; Owens, J.; Strouse, G. F. Specific Effects in Microwave Chemistry Explored through Reactor Vessel Design, Theory, and Spectroscopy. *Phys. Chem. Chem. Phys.* **2015**, *17* (41), 27317–27327.

(58) Horikoshi, S.; Abe, H.; Sumi, T.; Torigoe, K.; Sakai, H.; Serpone, N.; Abe, M. Microwave Frequency Effect in the Formation of Au Nanocolloids in Polar and Non-Polar Solvents. *Nanoscale* **2011**, *3* (4), 1697–1702.

(59) Nirmala Grace, A.; Pandian, K. One Pot Synthesis of Polymer Protected Pt, Pd, Ag and Ru Nanoparticles and Nanoprisms under Reflux and Microwave Mode of Heating in glycerol—A Comparative Study. *Mater. Chem. Phys.* **2007**, *104* (1), 191–198.

(60) He, B.; Tan, J. J.; Liew, K. Y.; Liu, H. Synthesis of Size Controlled Ag Nanoparticles. *J. Mol. Catal. Chem.* **2004**, *221* (1), 121–126.

(61) Tsuji, M.; Nishizawa, Y.; Matsumoto, K.; Kubokawa, M.; Miyamae, N.; Tsuji, T. Effects of Chain Length of Polyvinylpyrrolidone for the Synthesis of Silver Nanostructures by a Microwave-Polyol Method. *Mater. Lett.* **2006**, *60* (6), 834–838.

(62) Nadagouda, M. N.; Varma, R. S. Synthesis of Thermally Stable Carboxymethyl Cellulose/Metal Biodegradable Nanocomposites for Potential Biological Applications. *Biomacromolecules* **2007**, *8* (9), 2762–2767.

(63) Abdelsayed, V.; Aljarash, A.; El-Shall, M. S.; Al Othman, Z. A.; Alghamdi, A. H. Microwave Synthesis of Bimetallic Nanoalloys and CO Oxidation on Ceria-Supported Nanoalloys. *Chem. Mater.* **2009**, *21* (13), 2825–2834.

(64) Ngo, V. K. T.; Nguyen, H. P. U.; Huynh, T. P.; Tran, N. N. P.; Lam, Q. V.; Huynh, T. D. Preparation of Gold Nanoparticles by Microwave Heating and Application of Spectroscopy to Study Conjugate of Gold Nanoparticles with Antibody E. Coli O157:H7. *Adv. Nat. Sci. Nanosci. Nanotechnol.* **2015**, *6* (3), 035015.

(65) Bayazit, M. K.; Yue, J.; Cao, E.; Gavriilidis, A.; Tang, J. Controllable Synthesis of Gold Nanoparticles in Aqueous Solution by Microwave Assisted Flow Chemistry. *ACS Sustain. Chem. Eng.* **2016**, *4* (12), 6435–6442.

(66) Dahal, N.; García, S.; Zhou, J.; Humphrey, S. M. Beneficial Effects of Microwave-Assisted Heating versus Conventional Heating in Noble Metal Nanoparticle Synthesis. *ACS Nano* **2012**, *6* (11), 9433–9446.

(67) Cheng, W.-T.; Cheng, H. W. Synthesis and Characterization of Cobalt Nano-Particles through Microwave Polyol Process. *AIChE J.* **2009**, *55* (6), 1383–1389.

(68) Li, D.; Komarneni, S. Microwave-Assisted Polyol Process for Synthesis of Ni Nanoparticles. *J. Am. Ceram. Soc.* **2006**, *89* (5), 1510–1517.

(69) Sreeju., N.; Rufus, A.; Philip, D. Microwave-Assisted Rapid Synthesis of Copper Nanoparticles with Exceptional Stability and Their Multifaceted Applications. *J. Mol. Liq.* **2016**, *221*, 1008–1021.

(70) Tsuji, M.; Hashimoto, M.; Nishizawa, Y.; Tsuji, T. Synthesis of Gold Nanorods and Nanowires by a Microwave–polyol Method. *Mater. Lett.* **2004**, *58* (17), 2326–2330.

(71) Harpeness, R.; Gedanken, A. Microwave Synthesis of Core−Shell Gold/Palladium Bimetallic Nanoparticles. *Langmuir* **2004**, *20* (8), 3431–3434.

(72) García, S.; Anderson, R. M.; Celio, H.; Dahal, N.; Dolocan, A.; Zhou, J.; Humphrey, S. M. Microwave Synthesis of Au–Rh Core–shell Nanoparticles and Implications of the Shell Thickness in Hydrogenation Catalysis. *Chem. Commun.* **2013**, *49* (39), 4241–4243.

(73) Tsuji, M.; Miyamae, N.; Lim, S.; Kimura, K.; Zhang, X.; Hikino, S.; Nishio, M. Crystal Structures and Growth Mechanisms of Au@Ag Core−Shell Nanoparticles Prepared by the Microwave−Polyol Method. *Cryst. Growth Des.* **2006**, *6* (8), 1801–1807.

(74) Chu, M.; Shen, X.; Liu, G. Microwave Irradiation Method for the Synthesis of Water-Soluble CdSe Nanoparticles with Narrow Photoluminescent Emission in Aqueous Solution. *Nanotechnology* **2006**, *17* (2), 444.

(75) Gerbec, J. A.; Magana, D.; Washington, A.; Strouse, G. F. Microwave-Enhanced Reaction Rates for Nanoparticle Synthesis. *J. Am. Chem. Soc.* **2005**, *127* (45), 15791–15800.

(76) Moghaddam, M. M.; Baghbanzadeh, M.; Keilbach, A.; Kappe, C. O. Microwave-Assisted Synthesis of CdSe Quantum Dots: Can the Electromagnetic Field Influence the Formation and Quality of the Resulting Nanocrystals? *Nanoscale* **2012**, *4* (23), 7435–7442.

(77) Panda, A. B.; Glaspell, G.; El-Shall, M. S. Microwave Synthesis of Highly Aligned Ultra Narrow Semiconductor Rods and Wires. *J. Am. Chem. Soc.* **2006**, *128* (9), 2790–2791.

(78) Luo, H.; Kebede, B. A.; McLaurin, E. J.; Chikan, V. Rapid Induction and Microwave Heat-Up Syntheses of CdSe Quantum Dots. *ACS Omega* **2018**, *3* (5), 5399–5405.

(79) Washington II, A. L.; Strouse, G. F. Microwave Synthesis of CdSe and CdTe Nanocrystals in Nonabsorbing Alkanes. *J. Am. Chem. Soc.* **2008**, *130* (28), 8916–8922.

(80) Washington, Aaron L.; Strouse, G. F. Microwave Synthetic Route for Highly Emissive TOP/TOP-S Passivated CdS Quantum Dots. *Chem. Mater.* **2009**, *21* (15), 3586–3592.

(81) Zhu, J.; Palchik, O.; Chen, S.; Gedanken, A. Microwave Assisted Preparation of CdSe, PbSe, and Cu2-xSe Nanoparticles. *J. Phys. Chem. B* **2000**, *104* (31), 7344–7347.

(82) Schumacher, W.; Nagy, A.; Waldman, W. J.; Dutta, P. K. Direct Synthesis of Aqueous CdSe/ZnS-Based Quantum Dots Using Microwave Irradiation. *J. Phys. Chem. C* **2009**, *113* (28), 12132–12139.

(83) Ziegler, J.; Merkulov, A.; Grabolle, M.; Resch-Genger, U.; Nann, T. High-Quality ZnS Shells for CdSe Nanoparticles: Rapid Microwave Synthesis. *Langmuir* **2007**, *23* (14), 7751–7759.

(84) He, Y.; Lu, H.-T.; Sai, L.-M.; Su, Y.-Y.; Hu, M.; Fan, C.-H.; Huang, W.; Wang, L.-H. Microwave Synthesis of Water-Dispersed CdTe/CdS/ZnS Core-Shell-Shell Quantum Dots with Excellent Photostability and Biocompatibility. *Adv. Mater.* **2008**, *20* (18), 3416–3421.

(85) Qian, H.; Qiu, X.; Li, L.; Ren, J. Microwave-Assisted Aqueous Synthesis: A Rapid Approach to Prepare Highly Luminescent ZnSe(S) Alloyed Quantum Dots. *J. Phys. Chem. B* **2006**, *110* (18), 9034–9040.

(86) Xue, X.; Chen, L.; Zhao, C.; Chang, L. One-Pot Synthesis of Highly Luminescent and Color-Tunable Water-Soluble Mn:ZnSe/ZnS Core/shell Quantum Dots by Microwave-Assisted Method. *J. Mater. Sci. Mater. Electron.* **2018**, *29* (11), 9184–9192.

(87) Lovingood, D. D.; Strouse, G. F. Microwave Induced In-Situ Active Ion Etching of Growing InP Nanocrystals. *Nano Lett.* **2008**, *8* (10), 3394–3397.

(88) Robinson, J.; Kingman, S.; Irvine, D.; Licence, P.; Smith, A.; Dimitrakis, G.; Obermayer, D.; Kappe, C. O. Understanding Microwave Heating Effects in Single Mode Type Cavities—theory and Experiment. *Phys. Chem. Chem. Phys.* **2010**, *12* (18), 4750–4758.

(89) Zhu, Y.-J.; Wang, W.-W.; Qi, R.-J.; Hu, X.-L. Microwave-Assisted Synthesis of Single-Crystalline Tellurium Nanorods and Nanowires in Ionic Liquids. *Angew. Chem. Int. Ed.* **2004**, *43* (11), 1410–1414.

(90) Redel, E.; Walter, M.; Thomann, R.; Vollmer, C.; Hussein, L.; Scherer, H.; Krüger, M.; Janiak, C. Synthesis, Stabilization, Functionalization And, DFT Calculations of Gold Nanoparticles in Fluorous Phases (PTFE and Ionic Liquids). *Chem. – Eur. J.* **2009**, *15* (39), 10047–10059.

(91) Ren, L.; Meng, L.; Lu, Q.; Fei, Z.; Dyson, P. J. Fabrication of Gold Nano- and Microstructures in Ionic Liquids--a Remarkable Anion Effect. *J. Colloid Interface Sci.* **2008**, *323* (2), 260–266.

(92) Marquardt, D.; Xie, Z.; Taubert, A.; Thomann, R.; Janiak, C. Microwave Synthesis and Inherent Stabilization of Metal Nanoparticles in 1-Methyl-3-(3-Carboxyethyl)-Imidazolium Tetrafluoroborate. *Dalton Trans.* **2011**, *40* (33), 8290–8293.

(93) Shahid, R.; Gorlov, M.; El-Sayed, R.; Toprak, M. S.; Sugunan, A.; Kloo, L.; Muhammed, M. Microwave Assisted Synthesis of ZnS Quantum Dots Using Ionic Liquids. *Mater. Lett.* **2012**, *89*, 316–319.

(94) Ding, K.; Lu, H.; Zhang, Y.; Snedaker, M. L.; Liu, D.; Maciá-Agulló, J. A.; Stucky, G. D. Microwave Synthesis of Microstructured and Nanostructured Metal Chalcogenides from Elemental Precursors in Phosphonium Ionic Liquids. *J. Am. Chem. Soc.* **2014**, *136* (44), 15465–15468.

(95) Jiang, Y.; Zhu, Y.-J.; Cheng, G.-F. Synthesis of Bi_2Se_3 Nanosheets by Microwave Heating Using an Ionic Liquid. *Cryst. Growth Des.* **2006**, *6* (9), 2174–2176.

(96) Zhang, C.; Xin, B.; Xi, Z.; Zhang, B.; Li, Z.; Zhang, H.; Li, Z.; Hao, J. Phosphonium-Based Ionic Liquid: A New Phosphorus Source toward Microwave-Driven Synthesis of Nickel Phosphide for Efficient Hydrogen Evolution Reaction. *ACS Sustain. Chem. Eng.* **2018**, *6* (1), 1468–1477.

(97) Hu, H.; Yang, H.; Huang, P.; Cui, D.; Peng, Y.; Zhang, J.; Lu, F.; Lian, J.; Shi, D. Unique Role of Ionic Liquid in Microwave-Assisted Synthesis of Monodisperse Magnetite Nanoparticles. *Chem. Commun.* **2010**, *46* (22), 3866–3868.

(98) Ji, G.; Shi, Y.; Pan, L.; Zheng, Y. Effect of Ionic Liquid Amount ($C_8H_{15}BrN_2$) on the Morphology of Bi_2Te_3 Nanoplates Synthesized via a Microwave-Assisted Heating Approach. *J. Alloys Compd.* **2011**, *509* (20), 6015–6020.

(99) Rabieh, S.; Bagheri, M.; Heydari, M.; Badiei, E. Microwave Assisted Synthesis of ZnO Nanoparticles in Ionic Liquid [Bmim]cl and Their Photocatalytic Investigation. *Mater. Sci. Semicond. Process.* **2014**, *26*, 244–250.

(100) Wang, W.-W.; Zhu, Y.-J.; Cheng, G.-F.; Huang, Y.-H. Microwave-Assisted Synthesis of Cupric Oxide Nanosheets and Nanowhiskers. *Mater. Lett.* **2006**, *60* (5), 609–612.

(101) Siramdas, R.; McLaurin, E. J. InP Nanocrystals with Color-Tunable Luminescence by Microwave-Assisted Ionic-Liquid Etching. *Chem. Mater.* **2017**, *29* (5), 2101–2109.

(102) Lee, S. K.; McLaurin, E. J. Recent Advances in Colloidal Indium Phosphide Quantum Dot Production. *Curr. Opin. Green Sustain. Chem.* **2018**, *12*, 76–82.

Chapter 2 - Effects of Microwave-Assisted Method on InP Nanocrystals Synthesis

2.1 Introduction

Colloidal synthesis of indium phosphide (InP) nanocrystals (NCs) has gained momentum in the recent times owing to a possible replacement for currently used Cd-based semiconductor NCs in commercial applications in displays or solid-state lighting.[1] Their relatively less-toxicity compels them utilize in display technologies in place of CdSe-based nanocrystals or compete with organic light emitting diodes (OLEDs).[2,3] However, their synthesis is not trivial because of the difficulties associated with them during the synthesis like very high sensitivity of reaction precursors to oxidation and moisture and very high reactivity of phosphorous precursors, and limited number of P precursors availability.[4–7] In addition, their higher covalent nature than II-VI counterparts requires high reaction temperatures for the synthesis. In InP NC synthesis, separation of nucleation and growth events is not easy to achieve.[3,6,8] The synthesis often uses alkylsilylphosphine precursor for the synthesis of high quality InP NCs.[9,10] In recent times less expensive P precursor has been used widely to get tetrahedral shaped InP NCs.[11,12] To improvise the synthesis or synthesizing high-quality InP NCs, a new cluster of InP was discovered a few years back.[9] Though there exist many synthetic methods of InP NCs by the hot-injection method and micro-fluidic method, we adopted a method developed by Strouse & coworkers, who developed a precursor to synthesize luminescent InP NCs by a microwave-assisted method as there are advantages associated with microwave-assisted synthesis over conventional synthesis of semiconductor nanocrystals.[9,10,13]

So, this chapter consists of several experiments of microwave-assisted method of InP NCs synthesis. We studied the effect of different MW vessels (SiC and Pyrex), holding times, reaction temperatures, and different ionic liquids (ILs) on the quality of the InP NCs synthesized in terms of size and surface defects with the InP precursor we developed.

2.2 Experimental Section

Materials.

The following chemicals were used as received: indium acetate ($In(OAc)_3$, 99.99% trace metals basis), palmitic acid (PA, ≥99%), 1-butyl-4-methylpyridinium tetrafluoroborate (BMPy BF_4, ≥97%), 1-butyl-3-methylimidazolium tetrafluoroborate (BMIm BF_4, ≥97%), 1-butyl-4-methylimidazolium hexafluoroantimonate (BMIm SbF_6, ≥97%), 1-butyl-3-methylimidazolium hexafluoroantimonate (BMIm PF_6, ≥97%), 1-butyl-4-methylpyridinium hexafluorophosphate (BMPy PF_6, ≥97%), 1-butyl-2,3-dimethylimidazolium hexafluorophosphate (BDMIm PF_6, ≥97%), decane (≥99%), and dodecylamine (DDA, 98%) from Sigma-Aldrich; tris(trimethylsilyl)phosphine ($P(TMS)_3$), min. 98% (10% in hexane), and indium acetate ($In(OAc)_3$, 99.99%) from Strem.

Indium Palmitate (InPA)

InPA was synthesized using a method adopted from Strouse and co-workers.[13] A 100 mL two-neck round-bottom (RB) flask was attached to a Schlenk line using a condenser; a rubber septum was attached, and the flask was put under vacuum. After filling the flask with N_2, 0.5462 g (2.13 mmol) of PA was added. The solid was heated under vacuum while stirring in an oil bath at 105 °C for 5−10 min. After cooling the PA to room temperature under vacuum, the flask was put under N_2, and 0.207 g (0.710 mmol) of $In(OAc)_3$ was added. After putting the flask under vacuum, the solids were heated to 150 °C. Any solid that formed on the walls of the flask was melted using a

heat gun. This process was repeated until the pressure reached baseline, about an hour. The flask was cooled to room temperature under vacuum, yielding a white solid. Here, moles ratio of In:PA = 1:3

InP Precursor

In an inert atmosphere glovebox, decane (47 mL) was added to the flask containing the InPA and left stirring until the solid was well-suspended (12 h). In the glovebox, $P(TMS)_3$ (1.15 mL, 0.393 mmol) was diluted in decane (3 mL) and slowly added to the InPA suspension. After obtaining an orange solution (1−2 h), the InP precursor solution was transferred to a Schlenk line and heated in an oil bath set to 65 °C under N_2. After the solution turned optically clear (~10 min), the flask was returned to the glovebox. The orange solution was immediately used as the precursor for the InP NC syntheses. This is essential for formation of high-quality NCs reproducibly. In the following photograph orange InP precursor is shown. The precursor is orange in color prior to exposing to air. After exposing to air for few seconds and storing it for a week with vial closed, color of the precursor turns to yellow gradually over a week period of time indicating sensitivity of the precursor to air.

Microwave-Assisted Synthesis of InP NCs

The following methods were used for the synthesis of NCs. The ratio of InP precursor:IL was 1:10. All samples were prepared in a glovebox under inert atmosphere in tightly capped 10 mL microwave vessels with a stir bar. The microwave method used the “heat as fast as possible” mode and a reaction time (holding time) of 15 min and 800 W set-power (SP), unless otherwise indicated, followed by cooling to 55 °C using compressed air. After the microwave synthesis, the red/brown solution was separated from the dark-brown IL side product, which settled at the bottom, by a pipette. The sample was precipitated using acetone. The solid was isolated after centrifugation at

5100 rpm for 5 min and suspended in toluene. The precipitation and suspension (washing) procedures were repeated two more times, and the NCs were suspended in toluene for characterization.

Method I. For all UV-Vis measurments, 2 μL of IL taken from 3 samples each is added to 5 mL of water. The three samples are pure BMPy BF_4 IL, BMPy BF_4 IL from a MW reaction done at 270 °C, and BMPy BF_4 IL from a MW control reaction done at 270 °C without InP precursor. These two MW reactions contained dodecylamine (DDA, 0.0462 g) in the reaction mixture. Then 0.1 mL from the above 5 mL solution is taken into a cuvette containing 2.9 mL of water. For collecting IL after MW reactions, decane layer has been separated and then 2 μL of IL is taken from IL layer. Here, In to PA ratio used for InP precursor preparation is 1:3.3 and SP is 150 W.

Calculations

For pure IL, 2 μL of it contains 10.12×10^{-6} moles. 0.1 mL of 5 mL solution of 10.12×10^{-6} moles of IL contains 20.24×10^{-8} moles. After transferring 0.1 mL into 2.9 mL of water, absorbance value is measured as 0.3264 at 255 nm. Similarly, same solutions have been prepared by using 2 μL of ILs after MW reactions. Their absorbances are 0.2192 and 0.1650 at 255 nm for ILs from MW reactions of without InP precursor and with InP precursor, respectively. Then number of moles of undissociated ILs are found to be 13.58×10^{-8} and 10.23×10^{-8}. % IL decomposed is 16.7 ± 11 and 25.8 ± 17% for 3 batches of samples.

Method II. InP precursor (3 mL) is combined with BMIm BF_4 ionic liquid (0.426 mmol, 78 μL) in a Pyrex microwave vessel. The vessel is capped, brought out of the glovebox, and put in the microwave reactor immediately. The mixture is heated to temperatures ranging 250, 265, and 280 °C. In second case, instead of BMIm BF_4, BMPy BF_4 IL (82.5 μL) is used for MW reactions of temperatures 250 and 280 °C.

Method III. InP precursor (3 mL) was combined with BMIm SbF_6 ionic liquid (0.426 mmol, 0.15 g) in a Pyrex microwave vessel. The vessel was capped, brought out of the glovebox, and put in the microwave reactor immediately. The mixture was heated to 280 °C at low (200 W) set-power (SP). After the reaction, black solution is formed.

Method IV. InP precursor (3 mL) is combined with BMPy BF_4 ionic liquid (0.426 mmol, 82.5 µL) in a microwave Pyrex vessel. The vessel is capped, brought out of the glovebox, and put in the microwave reactor immediately. The mixture is heated to different temperatures 250, 270, and 290 °C in Pyrex and SiC vessels separately. In addition, a MW reaction at 250 °C is carried out without BMIm BF_4 IL in SiC vessel.

Method V. InP precursor (3 mL) is combined with BMPy BF_4 ionic liquid (0.426 mmol, 82.5 µL) in a microwave vessel. The vessel is capped, brought out of the glovebox, and put in the microwave reactor immediately. The mixture is heated to different temperatures 250 and 270 °C in Pyrex and SiC vessels, which are equipped with Ruby thermometer to measure internal reaction temperature.

Method VI. InP precursor (3 mL) is combined with BMPy BF_4 ionic liquid (0.426 mmol, 82.5 µL) in a microwave vessel. The vessel is capped, brought out of the glovebox, and put in the microwave reactor immediately. The reaction mixture is heated to 250 °C with 15 and 60 min holding times (HT) in Pyrex and SiC vessels separately.

Method VII. InP precursor (3 mL) is combined with BMIm BF_4 ionic liquid (0.426 mmol, 78 µL) in a Pyrex microwave vessel. The vessel is capped, brought out of the glovebox, and put in the microwave reactor immediately. The mixture is heated to temperatures ranging 250, 260, and 270 °C. The NCs obtained at 250, 260, and 270 °C are subjected to microwave reactions of 250 °C without any IL and 260 and 270 °C with 78 µL of BMIm BF_4 IL each, respectively.

2.3 Results and Discussions

Prior to designing MW reactions of InP NCs synthesis, stability of tetrafluoroborate (BF_4^-), hexafluorophosphate (PF_6^-), and hexafluoroantimonate (SbF_6^-) ion containing ionic liquids is compared by thermogravimetric analysis (TGA). Figure 2.1 shows TGA curves and derivative of weight % curves of BMIm SbF_6, BMIm BF_4, and BMPy BF_4, BMIm PF_6, and BDMIm PF_6 heated under inert atmosphere.

2.3.1 Thermal Properties of Ionic liquids

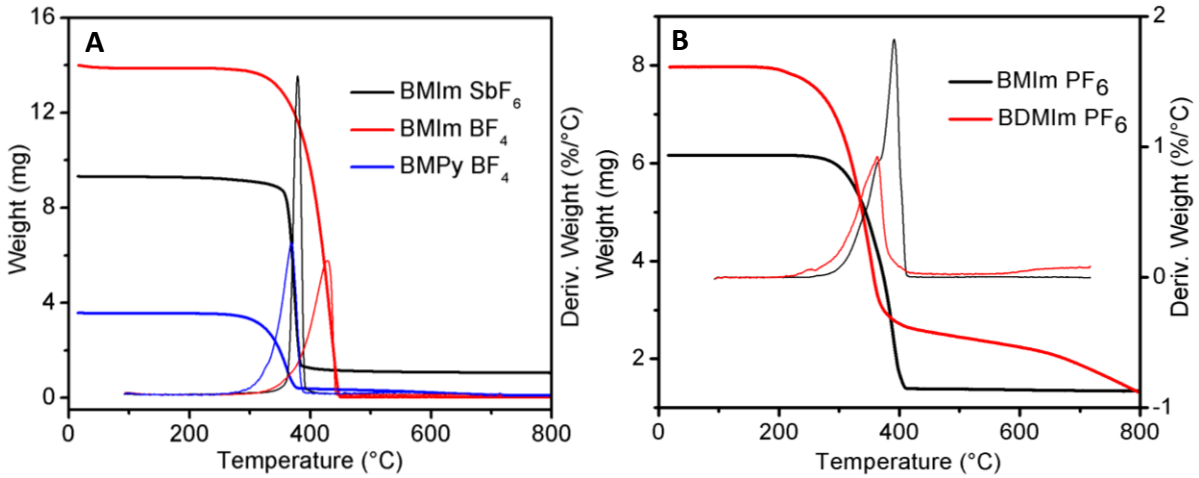

Figure 2.1 Thermogravimetric Analysis (TGA) curves of tetrafluoroborate (BF_4^-), hexafluorophosphate (PF_6^-), and hexafluoroantimonate (SbF_6^-) based ionic liquids (BMIm SbF_6, BMIm BF_4, BMPy BF_4, BMIm PF_6, and BDMIm PF_6) in thick colors along with their derivative curves in thin colors. Decomposition temperatures is higher for BMIm BF_4 than that of BMPy BF_4.

High decomposition temperatures of ionic liquids (ILs) are responsible for *in situ* etching of InP NCs because of fluoride release upon decomposition of the IL. The decomposition temperatures from derivative TGA curves can be identified as 370, 379, and 430 °C for BMPy BF_4, BMIm SbF_6, and BMIm BF_4, respectively as shown in Figure 2.1. Decomposition temperature of pyridinium

ionic liquid of tetrafluoroborate ion is lower by 60 °C than that of imidazolium ionic liquid for tetrafluoroborate ion. For BMIm PF_6 and BDMIm PF_6 ILs, the decomposition temperatures are 363 and 390 °C, respectively. The distinctive feature for BDMIm PF_6 IL is that it resumes decomposing after reaching 600 °C temperatures. It should be noted that the decomposition of all ILs starts well before their main decomposition temperature. However, they do not need to have necessarily the same decomposition temperatures in typical InP microwave reactions. Because their decomposition temperatures can also be affected by mass and surrounding chemical species in microwave reactions might lower their decomposition temperature as surface etching by the released fluoride ion might drive the decomposition of IL forward. Inaccuracies in reading the temperatures by IR sensor cannot also be ruled out for different decomposition temperatures.

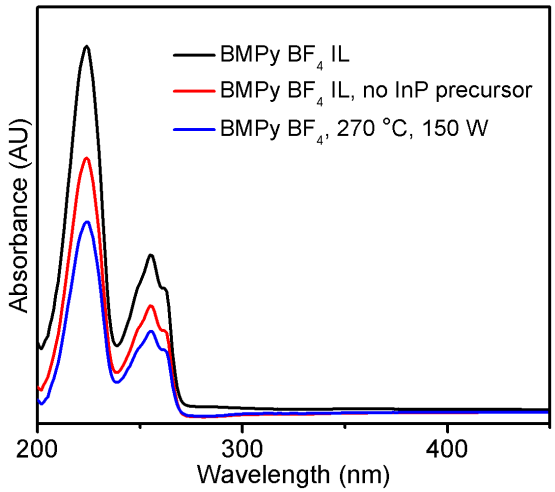

Figure 2.2 UV-Vis absorption spectra of BMPy BF_4 IL from pure IL, a MW control experiment, without InP precursor, and a MW reaction. Both MW reactions are done at 270 °C with dodecylamine in the reaction mixtures. Decreasing of absorbance from pure IL to MW reaction with InP precursor confirms decomposition of IL. All samples are recorded in water.

To confirm IL decomposition, absorption of ILs are recorded. Figure 2.2 shows absorption spectra of same concentration of pure BMPy BF_4 IL, BMPy BF_4 IL from a MW control experiment

without InP precursor, and BMPy BF_4 IL from a MW experiment as described in Method I. Absorbance values of the peaks at 224, 255, and 264 nm decrease from pure IL to IL from MW experiment with InP precursor. It must be due to decomposition of IL at 270 °C causing reduction of unreacted IL amount after MW reaction. Addition of InP precursor might be causing even more decomposition probably etching of surface of the NCs by fluoride ion driving the decomposition of IL forward. It is found that decomposition of BMPy BF_4 IL is 16.7 ± 11 and 25.8 ± 17% in the control MW experiment without InP precursor and MW experiment with InP precursor, respectively for 3 batches of samples.

2.3.2 Effect of Different ILs

Having compared decomposition temperatures of tetrafluoroborate-based ILs, their effect on InP NCs synthesis is examined as shown in Figure 2.3. In absorption spectra, irrespective of temperature in the region 250-280 °C, excitonic peaks are located around 540 nm without any significant change in their positions for InP NCs synthesized with BMIm BF_4. Similarly, emission peak for these NCs is located around 570 nm without any considerable changes with tails at higher wavelengths indicating surface defects or traps.[14] However, as described in method II same type of reactions with BMPy BF_4 are carried out at 250 °C and 280 °C. Here, NCs of slightly larger size at 280 °C are formed as excitonic peak has little red shift. At the moment we could not give any plausible reason for this effect. Emission peak as well has a little red shift indicating increase in average size of the NCs with decrease in tail intensity because of surface passivation probably caused by more decomposition of BMPy BF_4 IL.

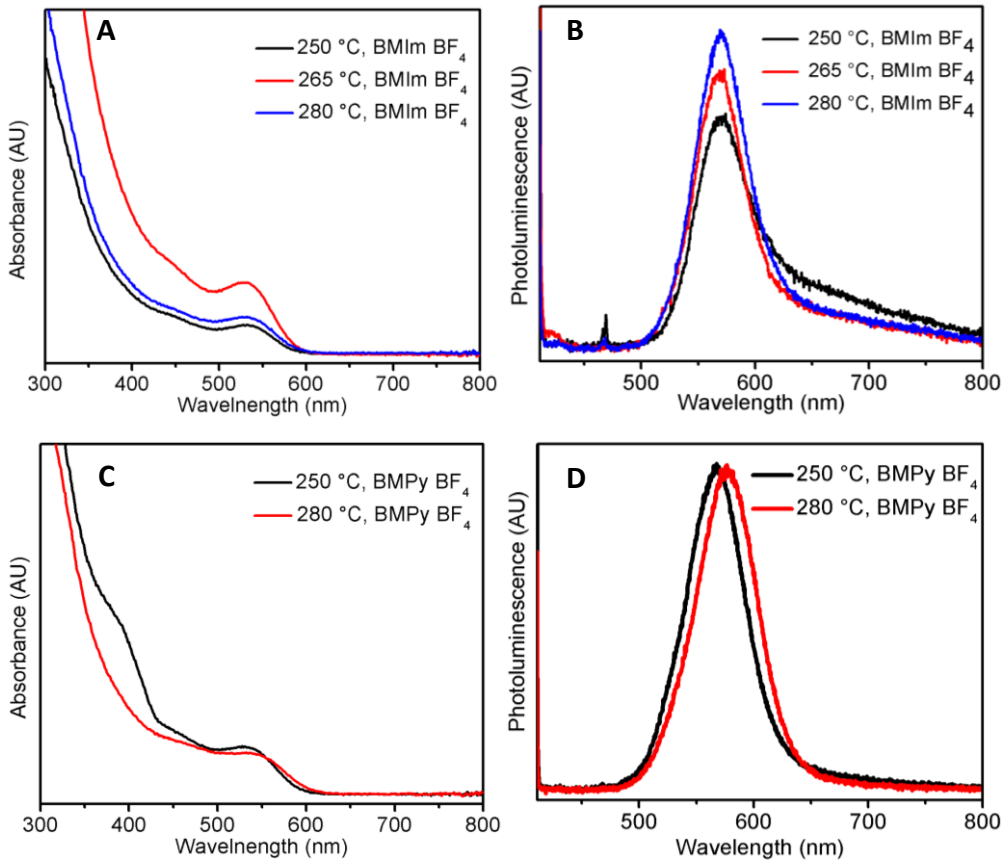

Figure 2.3 UV-Vis absorption (A & C) and photoluminescence (B & D) spectra of InP NCs at different temperatures with imidazolium-containing tetrafluoroborate ionic liquids on the top (A & B) and with pyridinium containing tetrafluoroborate ionic liquids on the bottom (C & D). Excitonic peaks positions of InP NCs are not varied significantly with BMIm BF_4 ionic liquid though temperature is increased from 250 to 280 °C whereas red shift in excitonic peak can be seen with BMPy BF_4 IL with same changes in the reaction temperatures. Red shift for emission peak is also observed in the photoluminescence spectra.

As described in Method III instead of tetrafluoroborate containing ILs, fluorine containing antimony-based IL, 1-butyl-3-methylimidazolium hexafluoroantimonate, BMIm SbF_6, is used for etching of the InP NCs. MW reaction is carried out at 280 °C and 200 W set-power since higher power generated sparks in MW reaction vessel and caused abrupt shutting MW reaction off, which

could be due to higher MW field density causing sparks in the reaction mixture. Figure 2.4 shows absorption spectra and X-ray diffraction spectrum (B) and inset in A shows black solution of crude reaction mixture in MW vessel after the MW reaction. Solid obtained after size selective precipitation of a portion of crude mixture is dispersed in toluene and its absorption spectrum shows broad absorption feature centered around 510 nm. The solid from crude solution is used for XRD characterization to figure out structure and composition of the black solid. XRD pattern reflects formation of bulk antimony.[15] It might be due to aggressive etching caused by fluoride ion produced from SbF_6^- ion yielding Sb (0) reduced from Sb (V). So, bulk antimony is being formed predominantly in MW reaction with BMIm SbF_6 IL.

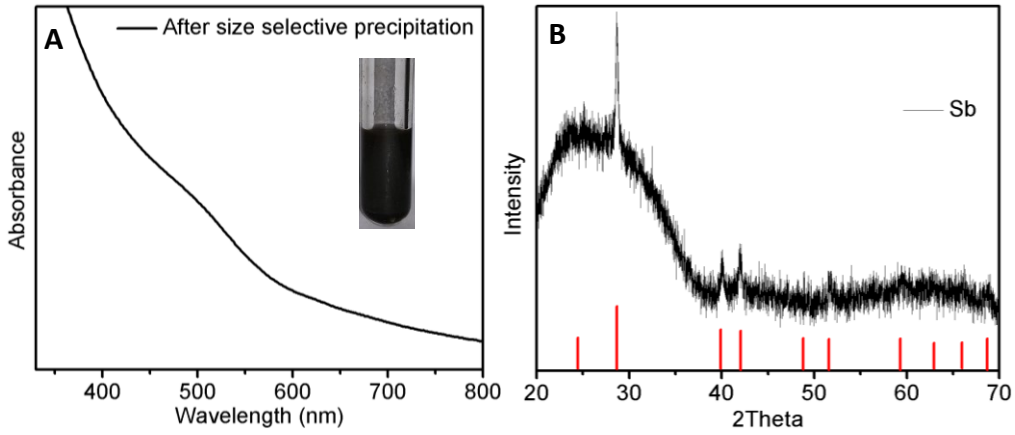

Figure 2.4 UV-Visible absorption spectra (A) and X-ray diffraction pattern (B) of final reaction product of a microwave reaction by BMIm SbF_6. Inset (A) shows crude black solution and upon size-selective precipitation obtained solid can be suspended in toluene. XRD pattern shows sharp peaks indicating possible bulk antimony formation in the crude mixture after the MW reaction. The reflections (red) correspond to rhombohedral Sb (JCPDS 01-0802).

2.3.3 Effect of Microwave Vessels

Having compared effect of MAIL etching with different anions of ILs containing BF_4 and SbF_6, next we investigated the effect of reaction vessel. Since penetration depth of microwave radiation is higher in Pyrex vessel than that of SiC vessel,[16] we hypothesized poor emission features for the NCs from the SiC vessel. As described in Method IV, MW reactions are carried out in SiC vessel at 250, 270, 290 °C and their absorption spectra are shown in Figure 2.5. As temperature increases from 250 to 290 °C, excitonic peak shifts from 513 nm to 527 nm indicating increase in size of the NCs. If no IL is used in the MW reaction for instance at 250 °C there is shift in excitonic peak from 513 to 500 nm denoting smaller size NCs formation signifying a good size distribution of NCs because of narrow absorption peak. Pyrex vessel is used in place of SiC vessel and similar reactions are done at the same temperatures. As the temperature increases from 250 to 290 °C, excitonic peak shifts from 496 to 516 nm resulting in smaller NCs than those from the SiC vessel.

These trends are also seen in the photoluminescence spectra. As temperature increases, the emission peak shifts from 552 to 564 nm indicating increase in size of the NCs though no considerable shift is observed for 260 °C. However, these peaks possess tails at higher wavelengths denoting surface defects. Whereas NCs from 250 °C reaction without any IL addition have less intense emission at lower wavelength 538 nm with a long tail signifying smaller size NCs formation with surface defects. In Pyrex vessels, as temperature increases from 250 to 290 °C, emission peak shifts from 539 to 559 nm indicating increase in size of the NCs. Since tails at higher wavelengths are flattening it could be inferred that surface defects might be minimized because of higher decomposition of IL in Pyrex vessel. Higher decomposition of IL in Pyrex vessel is due to higher penetration of microwaves in Pyrex vessel. Overall, it can be concluded that at a particular temperature NCs from SiC vial will have bigger size than that of Pyrex vessel and they possess

surface defects, which might be due to absence of MW heating in SiC vessel lowering decomposition of IL in the SiC vessel. Since IL couple well with microwaves, they heat very fast and might decompose more in microwave heating.

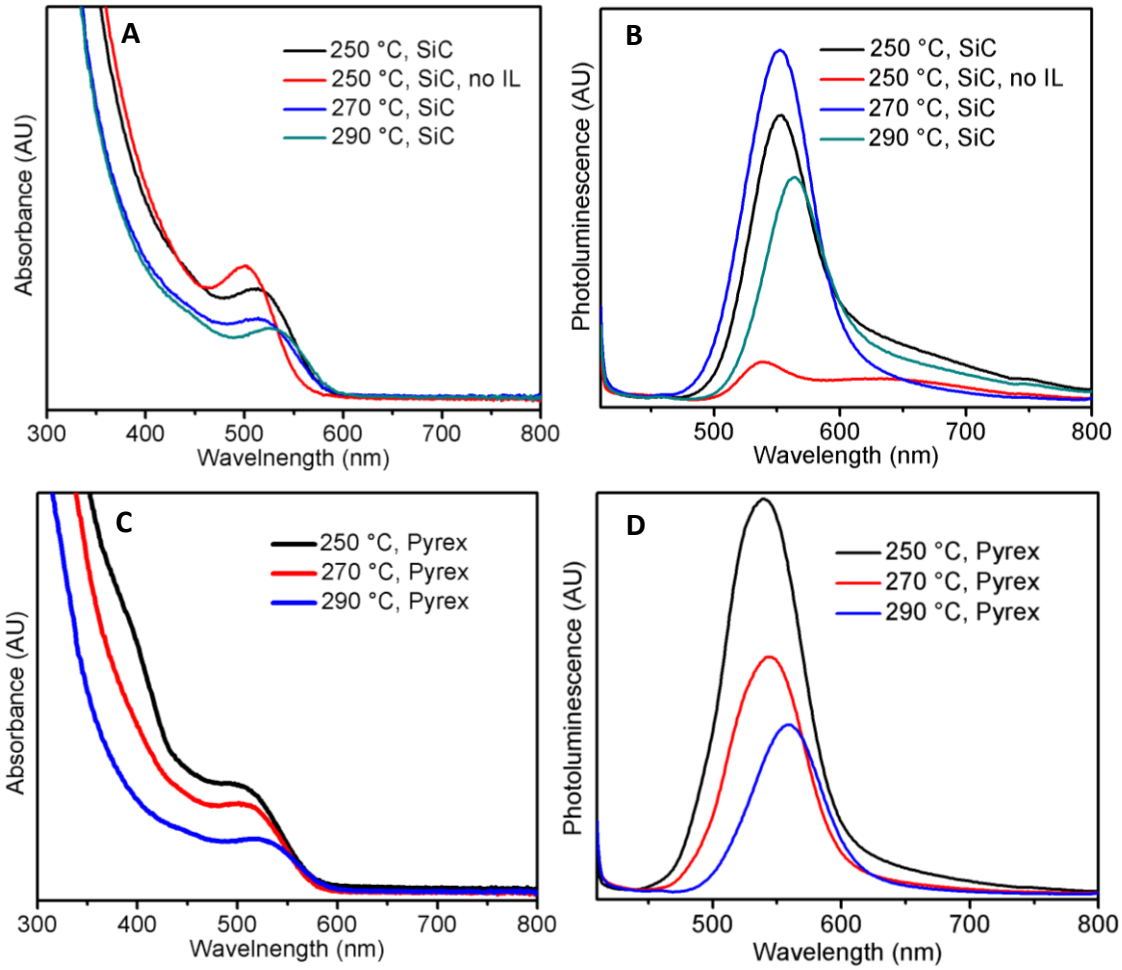

Figure 2.5 UV-Vis absorption and photoluminescence spectra of InP NCs synthesized at different temperatures in SiC vessels (A & B) and Pyrex vessels (C & D). In the absorption spectra, as temperature increases for SiC vessels excitonic peak has a very little red shift to 513 nm whereas if ionic liquid is not used in the MW reaction, excitonic peak has blue shift with narrow excitonic feature. In photoluminescence spectra as well, red shift is observed with increase in temperature

to 290 °C. A red-shift in the absorption and photoluminescence spectra is seen for MW reactions using Pyrex vessel (C & D).

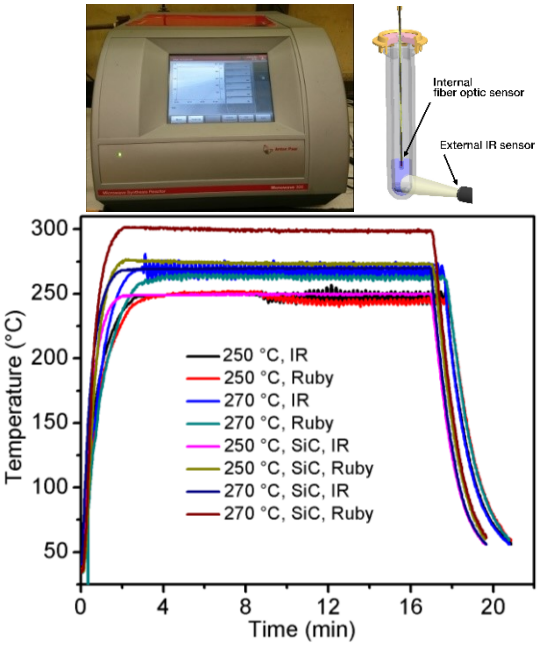

Figure 2.6 Microwave reactor (Anton Paar Monowave 300) along with a picture of MW vessel showing temperature IR sensor located on the bottom and outside (top). Plot of temperature versus time showing IR (vessel outside) and Ruby (vessel inside) temperatures for reactions carried out at 250 and 270 °C in SiC and Pyrex vessels, separately. Here, IR temperature is temperature control for all the MW reactions.

In Anton Paar Monowave 300 Microwave Reactor, IR sensor is located at the bottom of the vial as shown in Figure. 2.6 and it measures the temperature outside of the MW vessel. It does not take into account the inside temperature of reaction mixture so to see the differences inside and outside temperatures of MW vessel and to figure out the variations of getting different sizes of NCs from SiC and Pyrex vessels, their IR temperature (outside of reaction vessel) and Ruby temperatures (inside of reaction vessel) are measured simultaneously by inserting Ruby thermometer into MW vessel.

Figure 2.6 shows Ruby temperature and IR temperature curves for two reactions at two different temperatures for Pyrex and SiC vessels. Synthetic conditions of these reactions are described in Method V. In Pyrex vessel at lower temperature 250 °C, IR and Ruby temperatures are very close until 9 minutes and thereafter IR temperatures are higher than that of Ruby temperatures with oscillations of temperatures to maintain the set reaction temperature because of auto-program set up in microwave reactor. Here, as IR sensor is located at bottom of the vessel the IR temperature is high probably because IL is denser and it is not uniformly distributed in entire reaction mixture during course of the MW reaction. Since IR sensor is located at the bottom of outside of MW vessel, IR temperatures could be higher. Similarly, IR temperatures are higher than that of Ruby temperatures at 270 °C. Oscillations have started right from 3 minutes because of higher temperature more IL decomposes. In contrast, in SiC vessel Ruby temperatures are higher than that of Pyrex vessels by around 26 and 31 °C at both 250 and 270 °C, respectively. Here, IR temperature is temperature control of the MW reactions. This higher internal temperature might be the reason for getting bigger size NCs in SiC vessel. It should be noted that both temperature curves are flat without any oscillations because of uniform heating in the reaction mixture caused by convective heating. In addition, it indicates that convective heating is faster than that of MW heating in microwave reactors. It could be due to the fact some of the microwaves penetrate SiC vessel so both convective and MW heating might be contributing to higher Ruby temperatures.

2.3.4 Effect of Holding Time

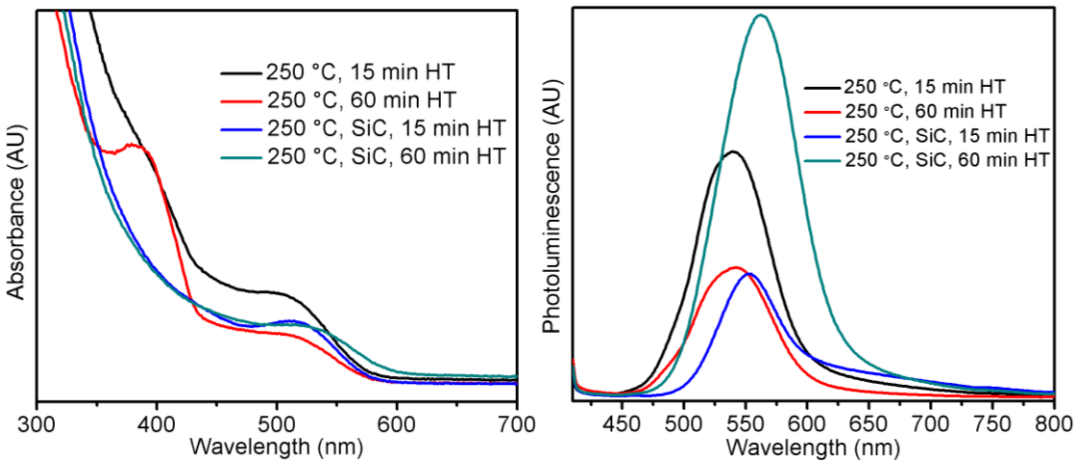

Figure 2.7 UV-Vis absorption and photoluminescence spectra of InP NCs synthesized at different holding times in Pyrex and SiC vessels. For Pyrex and SiC vessels, as holding time (HT) increases excitonic peaks get broadened because of increased etching and longer reaction times with a new absorption peak appearing around 400 nm. In photoluminescence spectra, as HT increases FWHM values increase from 70 to 73 nm and 57 to 75 nm for Pyrex and SiC vessels, respectively. Surface defects of NCs from SiC vessel are minimized as HT increases since tail at longer wavelengths flattens.

To remove surface defects, effect of holding time is examined as we hypothesized that longer holding time can cause more IL decomposition. As described in method VI, MW reactions are carried out at holding times 15 minutes and 60 minutes. NCs in Pyrex vessel at 250 °C with 15 min HT have excitonic peak around 500 nm with a little hump around 400 nm, which could be due to InP cluster formation, as shown in Figure 2.7.[9] As HT increases to 60 minutes, no considerable change is observed in the excitonic peak position with little broadening. However, emergence of peak around 383 nm confirming higher etching time (or HT) produces InP cluster formation[9] because of surface etching. In SiC vessel, NCs produced have a shift in their excitonic peak from 513 to 523 nm with broader excitonic feature indicating MAIL etching results in increased size

distribution. However, no peak around 400 nm is observed here probably due to gradual etching by IL in the SiC vessel. In photoluminescence spectra, NCs in Pyrex vessel at 250 °C with 15 min HT have emission peak around 540 nm and shoulder peaks in the region 450 to 550 nm can be implicated probably because of InP cluster formation. As HT increases to 60 min, emission peak has a very little shift to 542 nm with shoulder peaks at smaller wavelengths. In SiC vessel, NCs produced have a red shift in their excitonic peak from 552 to 562 nm with increase in FWHM from 57 to 75 nm indicating increase in size of the NCs with large size distribution because of increased MAIL etching. It can be noted that there is a tail with a hump around at 675 nm for 15 min HT reaction but as HT increases to 60 min, tail flattens showing it requires longer holding time to remove surface defects of the NCs in SiC vessel.

2.3.5 Post-etching by ILs

Apart from shells of higher band gap formation on InP NCs, which results in core/shell or alloy NCs, HF photoetching had been used as post-synthetic step to obtain luminescent InP NCs.[17–19] This HF photoetching produced varying sizes of 6.5 nm to 1.7 nm with quantum yields of 20-40%. Motivated by this post-etching of surface of the InP NCs, analogous reaction has been devised in our work. InP NCs synthesized by MAIL method have been used for etching by ionic liquid again in a microwave-assisted method to carry out a post-synthetic etching as we hypothesized that NCs size reduction and improvement in quantum yield of the NCs.

As described in method VII, InP NCs synthesized at 250 °C have excitonic feature around 540 nm and these NCs after washing with toluene (solvent) and acetone (anti-solvent) are again heated to same 250 °C in a MW reaction without addition of BMIm BF_4 IL. They still possess their excitonic feature as shown in Figure 2.8 However, NCs with BMIm BF_4 after subjecting to MW reactions of temperatures (260 and 270 °C), which were originally used to synthesize them at the same

temperatures, completely lose their inherent absorption features indicating complete digestion of the NCs. In photoluminescence spectra emission from the InP NCs are shown but emission for the post-etch MW reactions are not shown as they did not have any emission.

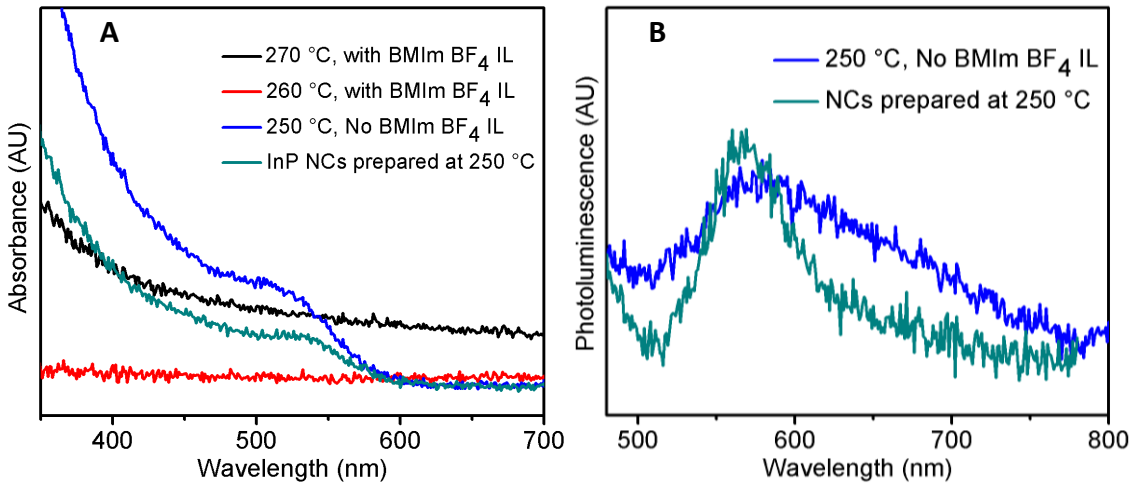

Figure 2.8 UV-Vis absorption and photoluminescence spectra of InP NCs synthesized by BMIm BF_4 IL. Excitonic peak is seen for InP NCs prepared at 250 °C (cyan) and after heating them to 250 °C without any IL (blue) as well. However, NCs with BMIm BF_4 IL after subjecting to MW reactions of temperatures 260 (red) and 270 °C (black), respectively, lose excitonic features indicating complete digestion or very aggressive etching of the NCs. Photoluminescence spectra of InP NCs prepared at 250 °C and after a post-etching MW reaction.

2.4 Summary

Factors that affect microwave-assisted method of InP NCs synthesis are investigated by optical characterization of synthesized InP NCs. Since quantification of MAIL etching is difficult, effect of MAIL etching has been inferred mainly by PL spectra herein. Lower decomposition temperature of ILs might be driving force for the etching of InP NCs; BMIm BF_4 IL decomposition temperature is higher than that of BMPy BF_4 by 60 °C in thermal heating. There is difference in final size of the InP NCs with BMPy BF_4 along with minimization of surface defects but not with BMIm BF_4.

Absence of MAIL etching by IL produces InP NCs with narrow absorption peak indicating MAIL etching imparts broadening of excitonic peak. Higher reaction temperatures result in bigger size NCs in both SiC and Pyrex vessels. However, surface defects are associated with NCs in SiC vessels probably due to minimal surface etching caused by convective heating. MAIL etching increases with increased holding time as well because of minimization of surface defects. MAIL etching in post-synthetic step yields complete digestion of the NCs probably because of higher concentration of ionic liquid.

2.5 References

(1) McKittrick Joanna; Shea-Rohwer Lauren E.; Green D. J. Review: Down Conversion Materials for Solid-State Lighting. *J. Am. Ceram. Soc.* **2014**, *97* (5), 1327–1352.

(2) Lin, G.; Ouyang, Q.; Hu, R.; Ding, Z.; Tian, J.; Yin, F.; Xu, G.; Chen, Q.; Wang, X.; Yong, K.-T. In Vivo Toxicity Assessment of Non-Cadmium Quantum Dots in BALB/c Mice. *Nanomedicine Nanotechnol. Biol. Med.* **2015**, *11* (2), 341–350.

(3) Tamang, S.; Lincheneau, C.; Hermans, Y.; Jeong, S.; Reiss, P. Chemistry of InP Nanocrystal Syntheses. *Chem. Mater.* **2016**, *28* (8), 2491–2506.

(4) Xie, R.; Battaglia, D.; Peng, X. Colloidal InP Nanocrystals as Efficient Emitters Covering Blue to Near-Infrared. *J. Am. Chem. Soc.* **2007**, *129* (50), 15432–15433.

(5) Xie, L.; Harris, D. K.; Bawendi, M. G.; Jensen, K. F. Effect of Trace Water on the Growth of Indium Phosphide Quantum Dots. *Chem. Mater.* **2015**, *27* (14), 5058–5063.

(6) Gary, D. C.; Glassy, B. A.; Cossairt, B. M. Investigation of Indium Phosphide Quantum Dot Nucleation and Growth Utilizing Triarylsilylphosphine Precursors. *Chem. Mater.* **2014**, *26* (4), 1734–1744.

(7) Allen, P. M.; Walker, B. J.; Bawendi, M. G. Mechanistic Insights into the Formation of InP Quantum Dots. *Angew. Chem. Int. Ed.* **2010**, *49* (4), 760–762.

(8) Reiss, P.; Carrière, M.; Lincheneau, C.; Vaure, L.; Tamang, S. Synthesis of Semiconductor Nanocrystals, Focusing on Nontoxic and Earth-Abundant Materials. *Chem. Rev.* **2016**, *116* (18), 10731–10819.

(9) Gary, D. C.; Terban, M. W.; Billinge, S. J. L.; Cossairt, B. M. Two-Step Nucleation and Growth of InP Quantum Dots via Magic-Sized Cluster Intermediates. *Chem. Mater.* **2015**, *27* (4), 1432–1441.

(10) Baek, J.; Allen, P. M.; Bawendi, M. G.; Jensen, K. F. Investigation of Indium Phosphide Nanocrystal Synthesis Using a High-Temperature and High-Pressure Continuous Flow Microreactor. *Angew. Chem. Int. Ed.* **2011**, *50* (3), 627–630.

(11) Tessier, M. D.; De Nolf, K.; Dupont, D.; Sinnaeve, D.; De Roo, J.; Hens, Z. Aminophosphines: A Double Role in the Synthesis of Colloidal Indium Phosphide Quantum Dots. *J. Am. Chem. Soc.* **2016**, *138* (18), 5923–5929.

(12) Buffard, A.; Dreyfuss, S.; Nadal, B.; Heuclin, H.; Xu, X.; Patriarche, G.; Mézailles, N.; Dubertret, B. Mechanistic Insight and Optimization of InP Nanocrystals Synthesized with Aminophosphines. *Chem. Mater.* **2016**, *28* (16), 5925–5934.

(13) Gerbec, J. A.; Magana, D.; Washington, A.; Strouse, G. F. Microwave-Enhanced Reaction Rates for Nanoparticle Synthesis. *J. Am. Chem. Soc.* **2005**, *127* (45), 15791–15800.

(14) Fu, H.; Zunger, A. InP Quantum Dots: Electronic Structure, Surface Effects, and the Redshifted Emission. *Phys. Rev. B* **1997**, *56* (3), 1496–1508.

(15) Zhou, X.; Zhong, Y.; Yang, M.; Hu, M.; Wei, J.; Zhou, Z. Sb Nanoparticles Decorated N-Rich Carbon Nanosheets as Anode Materials for Sodium Ion Batteries with Superior Rate Capability and Long Cycling Stability. *Chem. Commun.* **2014**, *50* (85), 12888–12891.

(16) Ashley, B.; Lovingood, D. D.; Chiu, Y.-C.; Gao, H.; Owens, J.; Strouse, G. F. Specific Effects in Microwave Chemistry Explored through Reactor Vessel Design, Theory, and Spectroscopy. *Phys. Chem. Chem. Phys.* **2015**, *17* (41), 27317–27327.

(17) Li, L.; Reiss, P. One-Pot Synthesis of Highly Luminescent InP/ZnS Nanocrystals without Precursor Injection. *J. Am. Chem. Soc.* **2008**, *130* (35), 11588–11589.

(18) Adam, S.; Talapin, D. V.; Borchert, H.; Lobo, A.; McGinley, C.; de Castro, A. R. B.; Haase, M.; Weller, H.; Möller, T. The Effect of Nanocrystal Surface Structure on the Luminescence Properties: Photoemission Study of HF-Etched InP Nanocrystals. *J. Chem. Phys.* **2005**, *123* (8), 084706.

(19) Talapin, D. V.; Gaponik, N.; Borchert, H.; Rogach, A. L.; Haase, M.; Weller, H. Etching of Colloidal InP Nanocrystals with Fluorides: Photochemical Nature of the Process Resulting in High Photoluminescence Efficiency. *J. Phys. Chem. B* **2002**, *106* (49), 12659–12663.

Chapter 3 - InP Nanocrystals with Color-Tunable Luminescence by Microwave-Assisted Ionic-Liquid Etching

3.1 Introduction

The popularity of colloidal semiconductor nanocrystals (NCs) can be attributed to their use in electronic[1–3] and biological[4–6] technologies as well as the fundamental interest in their physical and chemical properties.[7,8] Related to the latter, interest in their surfaces has grown due to the large effect small changes in surface composition and structure have on NC behavior and capabilities.[9] Understanding and controlling these surfaces is an enticing area for chemists. Unfortunately, the best materials for these applications are often heavy metal containing materials, such as CdSe and PbS, whose toxicity provides a barrier to growth of NC usage.[10–12]

One alternative is III−V semiconductors, which are ubiquitous in bulk technologies.[13,14] NCs of these materials have proven challenging to reproducibly synthesize with high quality (quantum yield, narrow size-distribution).[15,16] In particular, InP NCs exhibit luminescence in the visible range but have poor tunability with respect to NC size and, thus, optical properties. Unlike syntheses of II−VI nanocrystals, InP syntheses frequently require different precursors to obtain different sizes.[17,18] Alternatively, changing ratios of ligands or sequential additions of precursors can be used to obtain InP NCs with different diameters.[17,19] More recently, reaction temperature was used to tune InP NC size,[20,21] but despite these and other recent advances in InP NC synthesis,[22–29] postreaction processing is generally required to obtain luminescent InP NCs.

The two most popular techniques for obtaining luminescent InP NCs are 1) addition of shells to InP cores[30] and 2) etching using HF.[31–33] Shells are frequently ZnS, or related materials, and can be generated in single-step syntheses.[34–38] A recent report demonstrated addition of shells to InP cores results in QYs of up to 79%.[39] HF etching achieves quantum yields of more than 50%.[40] The

mechanism for etching is hypothesized to involve removal of surface P vacancies (electron traps)[41] and activation of surface P dangling bonds (hole traps) for attack by fluoride.[31] Despite these advances, additional synthetic steps or modifications to InP NC cores are often problematic. Addition of shells can prevent transfer of charge-carriers from the NCs, which hinders many electronic applications.[42,43] Etching is associated with removal of native NC surface ligands or ligand stripping,[44] a process that can improve NC charge transfer,[45] but it can also change the size of the NCs.[23,31,33] The use of HF is also dangerous as it is both highly corrosive and a contact poison.[46,47]

Although there are many examples of microwave-assisted synthesis of NCs in the literature, there is a strong bias toward metal and oxide nanoparticles prepared in polar solvent.[48–50] For other II−VI NCs and III−V NCs, colloidal preparations often involve high-boiling, hydrophobic solvents, and ligands.[51–53] These solvents allow for reaction at high temperature to obtain higher quality, more crystalline NCs. For microwave-assisted NC syntheses they highlight a key issue with the use of this synthetic method: a material with a good microwave dissipation factor (loss tangent) is required for heating.[54] In the absence of polar solvent, heating is achieved either through the reactants or the reaction vessel (usually glass). This can lead to very slow heating rates and, often, large size distributions.[53,55]

One way to increase heating rates in microwave-assisted syntheses is the addition of ionic liquids (ILs). ILs have low melting points but are not necessarily liquid at room temperature.[56] Their ionic nature makes them ideal for microwave-assisted syntheses as ionic conduction can markedly increase heating rates.[54] The microwave-assisted ionic-liquid (MAIL) method uses ILs in conjunction with organic solvents to promote rapid microwave heating.[57–59] The ILs couple well with microwaves and efficiently dissipate microwave energy as heat. As with any additive, the IL

can interfere with the synthesis itself, and a less intrusive heating method may be desired.[60] One well-established process is microwave-assisted decomposition of ILs with fluoride-containing anions.[61] Even though it is not always desirable,[62] IL fluoride release was used to successfully synthesize fluoridic nanomaterials,[63] and nearly a decade ago, luminescent InP NCs were obtained using MAIL decomposition.[64] In the procedure developed by Strouse and co-workers, ILs and related fluoride-containing salts were combined with an InP precursor and rapidly heated in a microwave reactor to obtain NCs. The NCs had diameters of 2.7 ± 0.3 nm and QYs approaching 50%, which changed with the amount and composition of IL. The method was also used to form luminescent InGaP NCs,[65] but despite its success and simplicity, it has not been popularized. To the best of our knowledge there are no subsequent literature reports of its use for luminescent InP NC formation.

Here, we report expansion of this work to obtain luminescent shell-free InP NCs of different sizes. By varying the reaction temperature and microwave set-power (SP) and adding amine, the NC diameter could be tuned from 3.2 to 4.2 nm calculated corresponding to PL ranging from green to red with quantum yields of up to 30% without optimization. By investigating microwave powers up to 800 W, much larger than the commonly used maximum of 300 W, we obtain insight into the interplay between MAIL heating and NC formation. The NC growth and possible processes that lead to luminescent InP NCs were investigated by performing syntheses in the presence or absence of amine and IL. A silicon carbide (SiC) vessel was used to help mimic convective heating methods, and comparison with a conventional reaction done using an analogous procedure provides insight into the real advantages of microwave reactors for NC synthesis.

3.2 Experimental Section

Materials

The following chemicals were used as received: indium acetate ($In(OAc)_3$, 99.99% trace metals basis), palmitic acid (PA, ≥99%), 1-butyl-4-methylpyridinium tetrafluoroborate (BMPy BF_4, ≥97%), 1-butyl-3-methylimidazolium bis(trifluoromethylsulfonyl)-imide (BMIm TFSI, ≥98%), 1-butyl-4-methylpyridinium hexafluorophosphate (BMPy PF_6, ≥97%), 1-butyl-2,3-dimethylimidazolium hexafluorophosphate (BDMIm PF_6, ≥97%), decane (≥99%), 1-octadecene (ODE, 90%), and dodecylamine (DDA, 98%) from Sigma-Aldrich; tris(trimethylsilyl)phosphine ($P(TMS)_3$), min. 98% (10% in hexane), and indium acetate ($In(OAc)_3$, 99.99%) from Strem; Fluorescein and Rhodamine B from Fisher Scientific; deuterated chloroform ($CDCl_3$) from Cambridge Isotope Laboratories.

Indium Palmitate (InPA)

InPA was synthesized using a method adopted from Strouse and co-workers.[66] A 100 mL two-neck round-bottom (RB) flask was attached to a Schlenk line using a condenser; a rubber septum was attached, and the flask was put under vacuum. After filling the flask with N_2, 0.605 g (2.36 mmol) of PA was added. The solid was heated under vacuum while stirring in an oil bath at 105 °C for 5−10 min. After cooling the PA to room temperature under vacuum, the flask was put under N_2, and 0.207 g (0.710 mmol) of $In(OAc)_3$ was added. After putting the flask under vacuum, the solids were heated to 150 °C. Any solid that formed on the walls of the flask was melted using a heat gun. This process was repeated until the pressure reached baseline, about an hour. The flask was cooled to room temperature under vacuum, yielding a white solid.

InP Precursor

In an inert atmosphere glovebox, decane (47 mL) was added to the flask containing the InPA and left stirring until the solid was well-suspended (12 h). In the glovebox, $P(TMS)_3$ (1.15 mL, 0.393 mmol) was diluted in decane (3 mL) and slowly added to the InPA suspension. After obtaining an orange solution (1−2 h), the InP precursor solution was transferred to a Schlenk line and heated in an oil bath set to 65 °C under N_2. After the solution turned optically clear (∼10 min), the flask was returned to the glovebox. The orange solution was immediately used as the precursor for the InP NC syntheses. This is essential for formation of high quality NCs reproducibly.

Microwave-Assisted InP NC Synthesis

The following methods were used for the synthesis of NCs. The ratio of InP precursor:IL was 1:10, and the ratio of InP precursor:DDA was 1:6. All samples were prepared in a glovebox under inert atmosphere in tightly capped 10 mL microwave vessels with a stir bar. The microwave method used the "heat as fast as possible" mode and a reaction time (holding time) of 15 min, unless otherwise indicated, followed by cooling to 55 °C using compressed air. After the microwave synthesis, the red/brown solution was separated from the dark-brown IL side product, which settled at the bottom, by a pipet. The sample was precipitated using acetone. The solid was isolated after centrifugation at 5100 rpm for 5 min and suspended in toluene. The precipitation and suspension (washing) procedures were repeated two more times, and the NCs were suspended in toluene for characterization.

Method I. InP precursor (3 mL) was combined with the ionic liquid (0.426 mmol) in a Pyrex microwave vessel. The vessel was capped, brought out of the glovebox, and put in the microwave reactor immediately. The mixture was heated to temperatures ranging from 250 to 300 °C at high (800 W) and low (150 W) set-powers (SPs).

Method II. InP precursor (3 mL) was added to BMPy BF_4 (82.5 μL) in a Pyrex microwave vessel followed by addition of DDA (0.046 g, 0.248 mmol). After the vessel was tightly capped, the mixture was stirred in the vessel for 3 min, brought out of the glovebox, and put in the microwave reactor immediately. The mixture was heated to temperatures ranging from 250 to 300 °C at 800 and 150 W SPs.

Method III. InP precursor (3 mL) was combined with DDA (0.046 g) in a silicon carbide (SiC) vessel. After tightly capping the vessel, the solution was stirred for 3 min, brought out of the glovebox, and immediately put in the microwave reactor. The mixture was heated to 280 °C at 800 or 150 W SP.

Conventional InP NC Synthesis

$In(OAc)_3$ (30.39 mg, 104.1 μmol) and PA (88.72 mg, 349.9 μmol) were combined in a 25 mL three-neck RB flask and heated to 150 °C. At this temperature, the RB flask was degassed for 20 min and then cooled to room temperature under vacuum. After taking the resulting white solid into a glovebox, 7.4 mL of a 7.73 mM solution of $P(TMS)_3$ in ODE was added to the RB flask. After 2 h of stirring, the mixture was transferred to a Schlenk flask and brought out of the glovebox to heat to 65 °C under N_2 gas supply in an oil bath. After obtaining an optically clear solution (InP precursor), the mixture was brought into a glovebox. To 3.7 mL of this InP precursor solution in a 20 mL three-neck RB flask was added 0.1 mL (0.51 mmol) of BMPy BF_4. The flask was brought out of the glovebox and attached to a Schlenk line through a condenser. After the RB flask was degassed for 20 min, it was heated to 300 °C using a thermocouple and temperature controller. It took 9.5 min to reach 300 °C. After heating at 300 °C for 15 min, the flask was cooled to room temperature. The resulting NC solution was washed with acetone and toluene 2 times, as described above.

Physical Measurements

Microwave syntheses were done using an Anton Paar Monowave 300 Microwave Reactor. In situ monitoring was accomplished using an IR sensor (for temperature) and a built-in camera (for changes in appearance). UV−vis absorption spectra were recorded with a Cary 500 or a Cary 5000 UV−vis-NIR spectrophotometer. Photoluminescence spectra were recorded using an Ocean Optics 2000+ spectrometer with 405 nm excitation or with a PTI Quanta Master 400 fluorometer. This fluorometer was also used for quantum yield measurements. Relative quantum yields of samples, Φ_{sam}, were calculated using Fluorescein and Rhodamine B in 0.1 N NaOH or water as the reference according to where A is the measured absorbance, η is the refractive index of the solvent, I is the integrated photoluminescence, and Φ_{ref} is the emission quantum yield of the reference. Φ_{ref} was taken to be 0.95 for Fluorescein in 0.1 N NaOH and 0.31 for Rhodamine B in water.[67,68] The first absorption features and PL peaks were fit to Gaussian distributions to determine their peak position and width. Photoluminescence spectra were fit to two Gaussian distributions to represent trap emission, if present. For TEM analysis, a drop of sample was dried on a copper grid. TEM images were recorded using an FEI Tecnai G2 Spirit BioTWIN microscope. Powder X-ray diffraction (XRD) patterns were recorded by a Bruker D8 X-ray diffractometer or a PANalytical Empyrean multipurpose X-ray diffractometer. NMR spectra were recorded on Varian 400 MHz NMR in $CDCl_3$ solvent.

3.3 Results and Discussion

The microwave-assisted method presented here is key to the luminescent InP NC synthesis. Two specific advantages over conventional heating are the use of a solvent at elevated pressures and selective heating of the IL. The first is one of the known advantages of microwave reactors (or other pressurized methods) and can provide enhanced reaction rates.[69] Here, decane was chosen as the solvent to enhance microwave interactions with the IL and increase the reaction speed. We

expect the reaction to go faster at the elevated pressures (20 bar) reached in the solvent, and decane is more readily separated from the NCs than oily alternatives such as octadecene.[70] Second, decane provides a "window" for the microwaves, as it has little coupling with the field, allowing the waves to interact with the IL and "selectively heat".

Here, we exploit the IL for heating and as a reactant. As reactants, the ILs with BF_4^- anions decompose to release fluoride. Although the mechanism of release was not studied, subsequent etching is similar to processes associated with etching of bulk semiconductor surfaces.[71,72] These methods can leave fluoride on the semiconductor surfaces and previous MAIL etching of InP NCs confirmed the presence of fluorine using ^{19}F MAS NMR.[64] In conjunction with release of fluoride, the corresponding neutral halide (BF_3) forms. This quintessential Lewis acid is used for removal of native ligands from NC surfaces, so-called ligand stripping. Recent work using PbSe and BF_3:Et_2O demonstrated an elegant mechanistic pathway for this ligand-stripping process, which forms "naked" NCs.[44] The native PbSe oleate ligands are "stripped", ultimately forming BF_4^- and $OA_x(B_yF_z)$ byproducts and cationic NCs, which can be well dispersed in polar solvent such as DMF. Thus, using these BF_4^--containing ILs as reactants can modify the NC surfaces in multiple ways.

Luminescent InP NCs by In Situ Etching

The general procedure used for InP NC synthesis was adapted from the work of Lovingood and Strouse.[64] A simplified procedure is shown in Scheme 1. Briefly, an "InP" precursor is synthesized using InPA and $P(TMS)_3$. After heating the mixture in decane to obtain a clear solution, InP NCs are synthesized by combining the IL and precursor in an inert atmosphere in a Pyrex vessel. The vessel is then heated in a microwave reactor, while stirring. The precursor must be used immediately after preparation to obtain high quality NCs reproducibly. Variations in products were

Scheme 3.2. Microwave-Assisted Synthesis of InP NCs

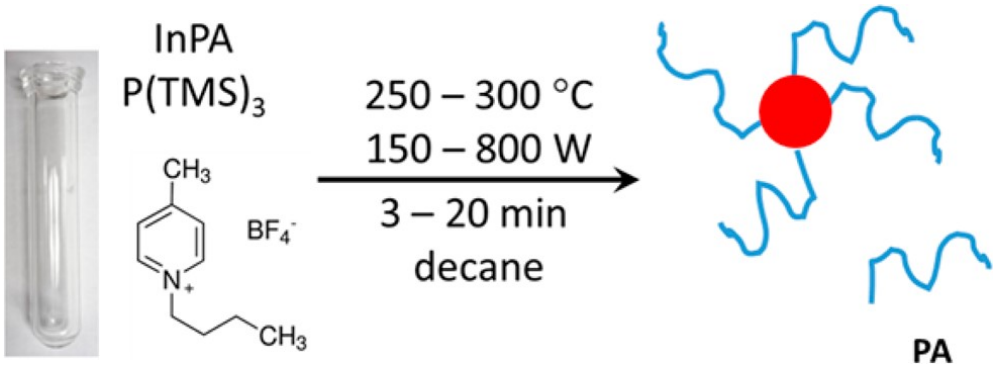

observed for reactions done at different temperatures, times, and SPs. Initially, the SP of the microwave was changed to assess the effect of microwaves on the synthesis, as previous experiments were limited to 300 W SP.[64] The effect of microwave SP is examined with respect to heating rate and reaction temperature. This effect is best demonstrated with a high (800 W) and low (150 W) SP. Plots of power and temperature vs time are shown in Figure 3.1. At the high SP (Figure 3.1A), the microwave applies the full 800 W to the solution for less than 5 s before decreasing the power to prevent overheating and modulating the power to maintain a temperature of 297 ± 3 °C. This results in power oscillations of about 200 W and a ramp time of ~100 s. The total reaction time is thus ~16.5 min (plus ~5 min cooling time). In contrast, low SP (Figure 1B) requires the reactor to apply the maximum power for more than 5 min before dropping. Oscillations of 150 W maintain the reaction temperature of 295 ± 4 °C. The ramp time jumps to 6 min, with a total reaction time of ~21 min (plus ~5 min cooling). Thus, the 150 W SP provides a limiting heating condition for comparison to a higher, 800 W SP.

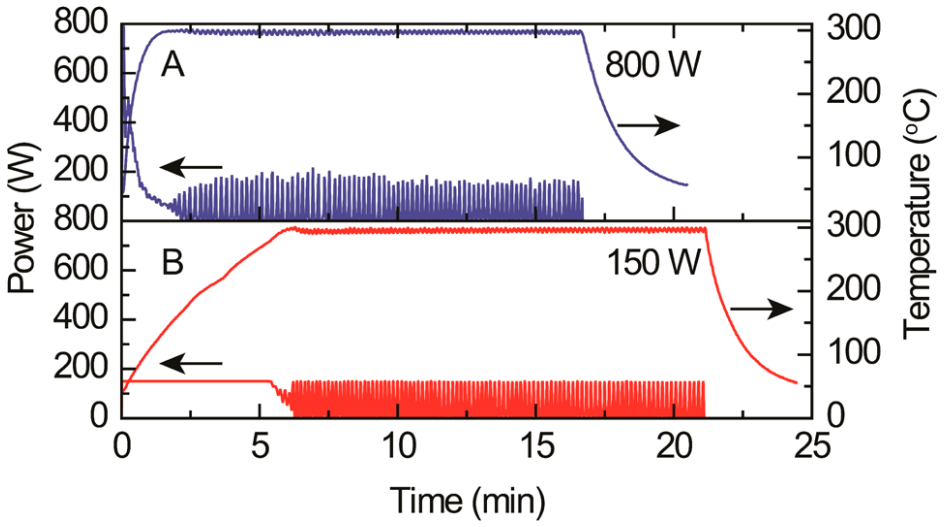

Figure 3.1 Power and temperature vs time plots at different powers. (A) At the high set-power (SP) extreme, 800 W power is applied for <5 s and oscillates nearly 200 W to maintain the set-temperature of 300 °C. This results in a ramp time of <2 min and a total reaction time of ~16.5 min plus ~5 min cooling. (B) At low SP, 150 W power is applied to the solution for >5 min before dropping. A ramp time of 6 min is required to reach 300 °C, and a total reaction time of 21 min plus 5 min cooling is required. The oscillations are limited to the SP of 150 W.

By comparing the photophysical properties of the NCs prepared at different temperatures and SPs, the effect of reaction conditions at high and low power can be parsed out. Figure 3.2 shows the absorption and photoluminescence spectra of InP NCs prepared at the 800 and 150 W SPs. The reaction temperature was varied to obtain different sizes, as was demonstrated recently by Xie et al.[25] Based on the absorption spectra, there is a small increase in size with increasing temperature. At 150 W SP and 250 °C, the smallest NCs form, as indicated by the first absorption feature near 500 nm and PL peak near 550 nm. The PL of this sample is low (QY < 3%), and the broad shoulder at lower energy is indicative of poorly defined surfaces (surface defects).[73] This shoulder decreases as the reaction temperature increases from 250 to 300 °C. This is true for the NCs prepared at a SP of 800 W as well, but the shoulder is not as prominent. The 800 W samples exhibit a noticeable

broadening in their absorption feature at reaction temperatures ≥270 °C. This is likely due to a broad size-distribution and was observed with post-synthetic HF etching of InP NCs as well.[40,65] The PL fullwidth at half-maximum (FWHM) values also suggest a broader size distribution for the samples prepared at 800 W and temperatures ≥270 °C with values of 0.25 ± 0.1 eV (69 ± 4 nm) vs 0.23 ± 0.1 eV (60 nm ±3 nm) for the samples prepared at 150 W and temperatures ≥270 °C. Low-resolution transmission electron microscopy (TEM) on samples indicates the NCs are spherical in shape as shown in Figure 3.3 and 3.4 and confirms a small overall increase in diameter for these samples. Sample aggregation made size-distribution determination a challenge, but, in general, larger distributions were obtained for larger NCs. These samples were prepared at higher temperatures requiring longer overall heating times, which can cause size broadening. Despite their broad absorption spectra, QYs were higher for the 800 W samples prepared at higher temperatures with values of 15 ± 5% vs <10% for the 150 W SP samples.

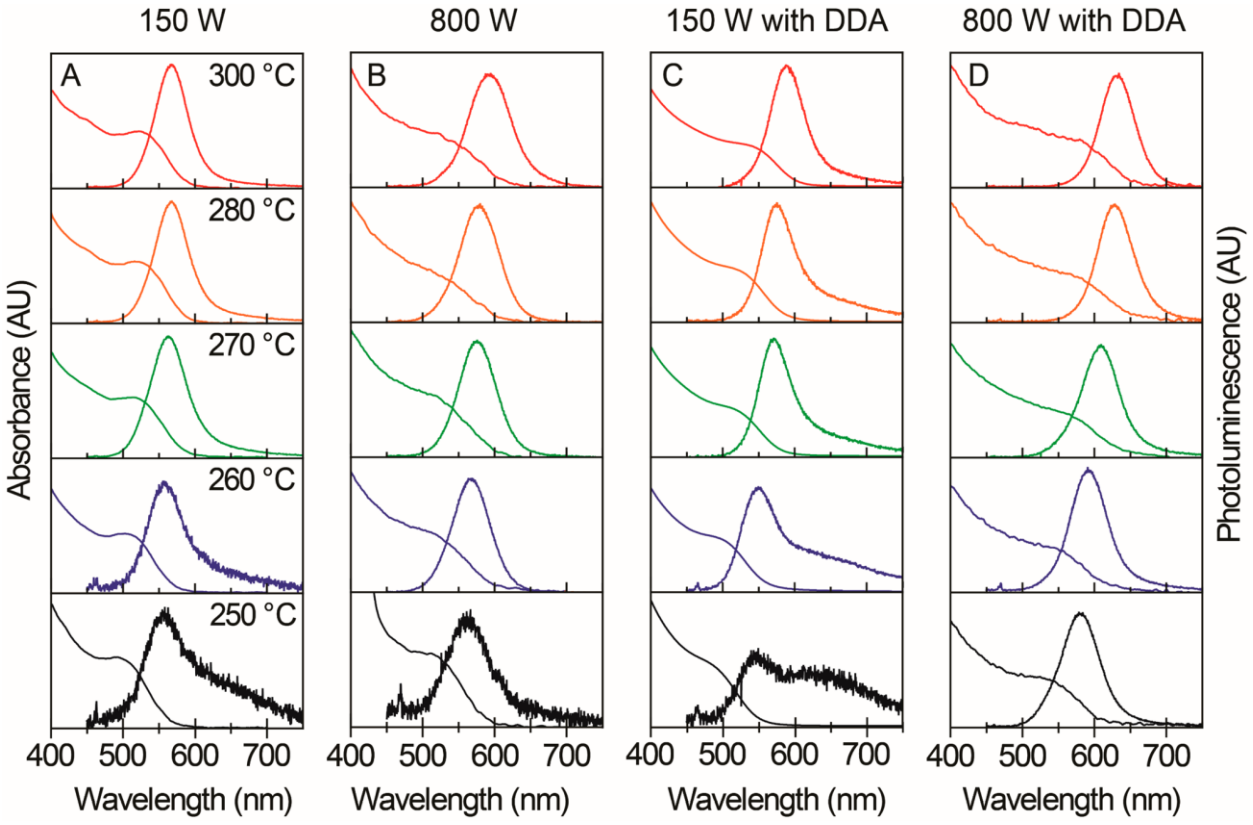

Figure 3.2 Absorption and photoluminescence (PL) spectra of InP NCs. (A) InP NCs prepared with 150 W set-power (SP) at 250 °C, 260 °C, 270 °C, 280 °C, and 300 °C. The InP PL is low at lower reaction temperatures and has a shoulder at lower energy, likely due to surface defects. The first absorption feature shifts from 497 to 522 nm, and the PL peak shifts from 553 nm to 574, indicating an overall increase in calculated diameter of 0.26 nm. (B) InP NCs prepared with 800 W SP at 250 °C, 260 °C, 270 °C, 280 °C, and 300 °C. The InP PL is low at 250 °C reaction temperature. The first absorption feature shifts from 508 to 528 nm, and the PL peak shifts from 562 to 596 nm indicating an overall increase in calculated diameter of 0.25 nm. (C) InP NCs prepared with 150 W SP with dodecylamine (DDA) at 250 °C, 260 °C, 270 °C, 280 °C, and 300 °C. The InP PL is low at lower temperatures, especially at 250 °C, with a broad shoulder. As temperature increases, the shoulder decreases, indicating an increase in surface passivation, and a red-shift in the PL and absorption peak are observed. The first absorption feature shifts from 484

to 529 nm, and the PL peak shifts from 544 nm to 588 indicating an overall increase in calculated diameter of 0.56 nm. (D) InP NCs prepared with 800 W SP with DDA at 250 °C, 260 °C, 270 °C, 280 °C, and 300 °C. As temperature increases, the first absorption feature shifts from 534 to 578 nm, and the PL peak shifts from 578 to 632 nm, indicating an overall increase in calculated diameter of 0.33 nm.

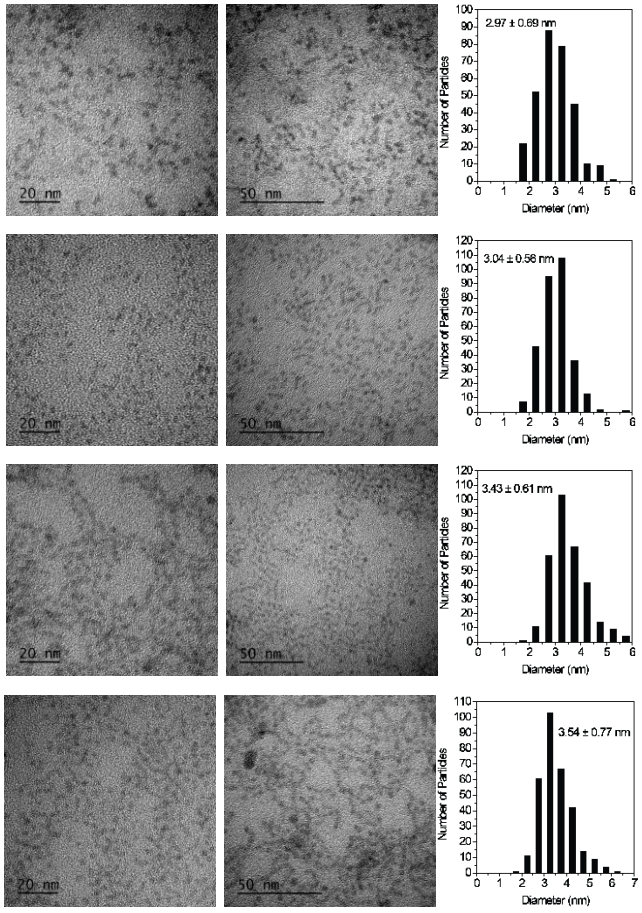

Figure 3.3 TEM images and corresponding histograms of InP NCs prepared using microwave-assisted synthesis at 800 W SP and temperatures ranging from 250-300 °C. The NCs exhibit spherical shapes, although they are somewhat aggregated.

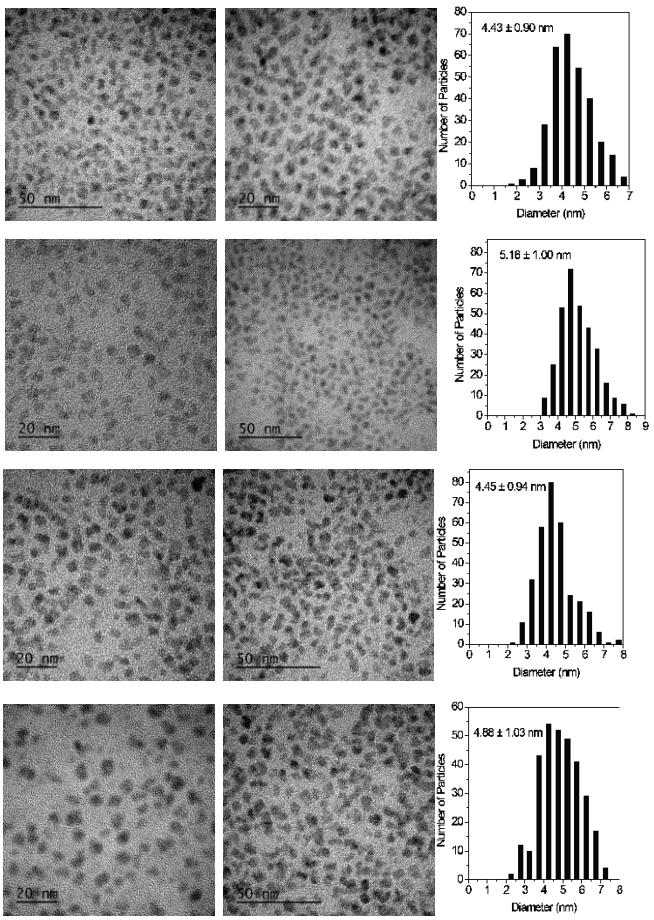

Figure 3.4 TEM images and corresponding histograms of InP NCs prepared using microwave-assisted synthesis at 150 W SP and temperatures ranging from 250-300 °C. The NCs exhibit aggregated shapes likely due to aging of the samples for 8 months before imaging.

To further examine the effects of limiting reaction power, the synthesis was done with different hold times. As opposed to a hold time of 15 min at the reaction temperature, times were varied from 0 to 15 min at 280 °C. Absorption and photoluminescence spectra are shown in Figure 3.5. Only a small shift in the first absorption feature is observed, as it increases from ~505 nm at 0 min to ~525 nm at 15 min. A more interesting effect is present in the luminescence spectra. At short reaction times, very little or no luminescence is observed from the NCs. After 5 min hold time a defined PL peak is observed, increasing in intensity at 10 and 15 min hold times. This, along with the luminescence from samples prepared without amine (Figure 3.2A and 3.2B), suggests higher

temperatures are required to obtain luminescent InP NCs because IL decomposition and related etching processes are known to occur at higher temperatures.[74]

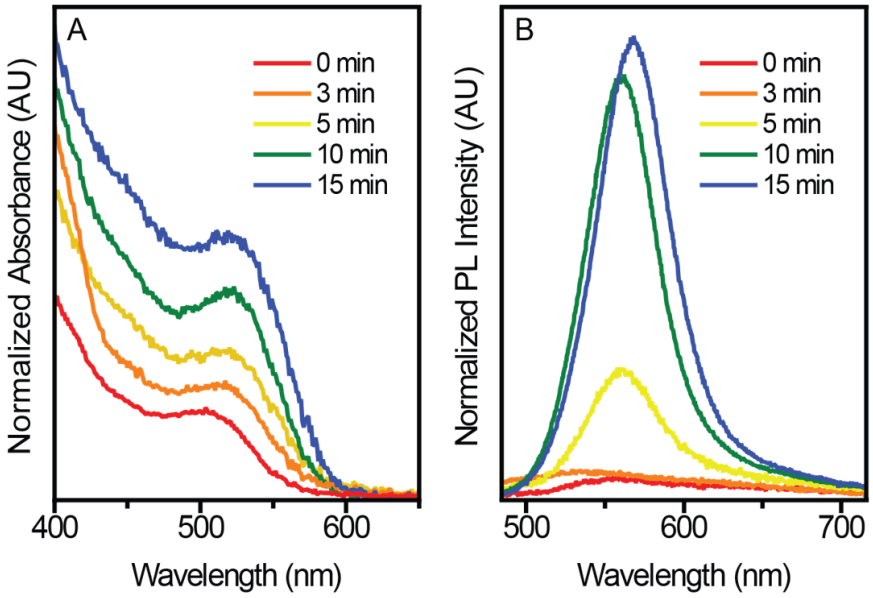

Figure 3.5 (A) UV-Vis absorption and (B) photoluminescence spectra of InP NCs prepared with 150 W SP at constant temperature 280 °C with holding times of 0, 3, 5, 10, and 15 min. The excitonic peak in the absorption spectra at 0 min indicates formation of InP NCs before entering into the holding stage of the reaction. After 15 min, the excitonic peak has a small red-shift indicating little growth of the NCs during the etching stage of the reaction. PL peaks at 0 min and 3 min indicate negligible emission from the InP NCs. As time progresses, a defined PL peak appears and a small red-shift in the PL peak is seen, but there is little growth of the InP NCs during the etching stage of the reaction.

The etching process affects the NC properties in multiple ways. To determine effects not realized by examination of their photophysical properties, further characterization was done using ^{1}H and ^{19}F NMR. Figure 3.6 shows the ^{1}H NMR spectrum of an InP NC sample prepared at high power and temperature. The presence of palmitate ligands associated with the NC surface is indicated by the broad peaks centered at 1.6 and 2.3 ppm, corresponding to the hydrogens nearest to the NC

surface. The multiplets around 7.17 and 7.25 ppm correspond to toluene, which is used while washing the NCs. One of the multiplets also contains the solvent ($CHCl_3$) peak as well. The singlet at 3.49 ppm might be due to methanol, which was also used for NC washing.

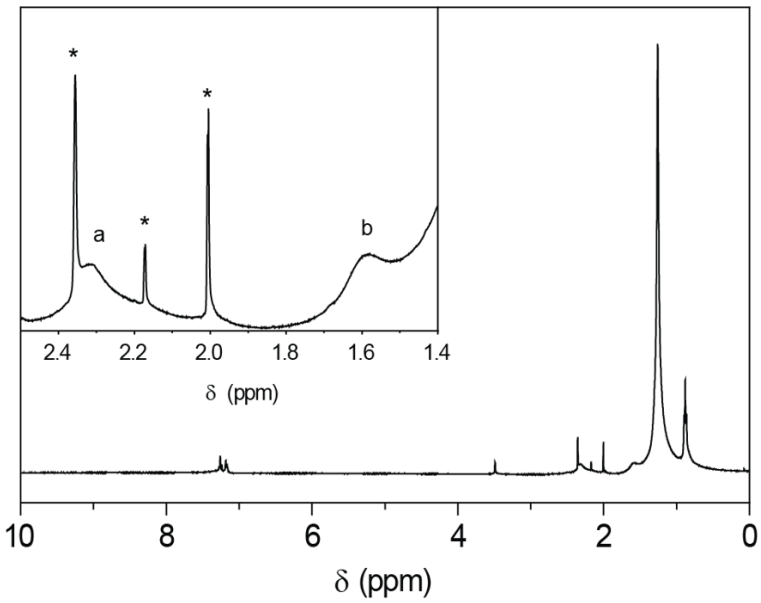

Figure 3.6 ^{1}H NMR spectrum of InP NCs synthesized at 300 °C, 800 W, 15 min. in $CDCl_3$. Inset: Peaks a and b exhibit broadening, associated with ligands bound to nanoparticles.1 The sharp peaks (*) correspond to residual solvent.

The ^{19}F NMR spectra on these reaction products did not show any new peaks, despite analysis of many reactions. An example spectrum is shown in Figure 3.7 along with spectra of the IL alone and heated with and without palmitic acid. All of these spectra show strong peaks centered at −152 ppm with a 1:4 integrated intensity ratio, corresponding to BF_4^-. No other fluorine-containing species from the reactions were observed. Previously, ^{19}F MAS NMR on similar NCs indicated the presence of fluorine-containing species.[64] However, fluorine concentrations may be too low to observe here using solution techniques as signals associated with the NC surface are often broadened.[75]

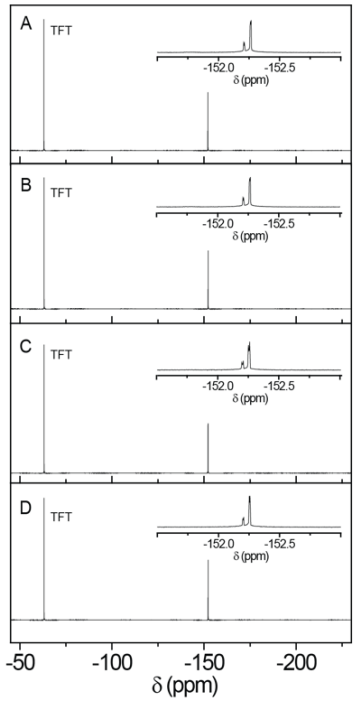

Figure 3.7 Representative ^{19}F NMR spectra of (A) BMPy BF_4 heated at 300 °C, 800 W, 15 min. (B) BMPy BF_4 heated with palmitic acid (same molar ratio as the NC synthesis) at 300 °C, 800 W, 15 min. (C) BMPy BF_4 heated with InP precursor at 300 °C, 800 W, 15 min. (D) BMPy BF_4 ionic liquid. All spectra show a peak from the trifluorotoluene (TFT) standard and a large peak corresponding to BF_4^-. No other fluorine-containing species are observed. Insets expand the BF_4^- region and show there is little change in the peak positions from sample-to-sample**.**

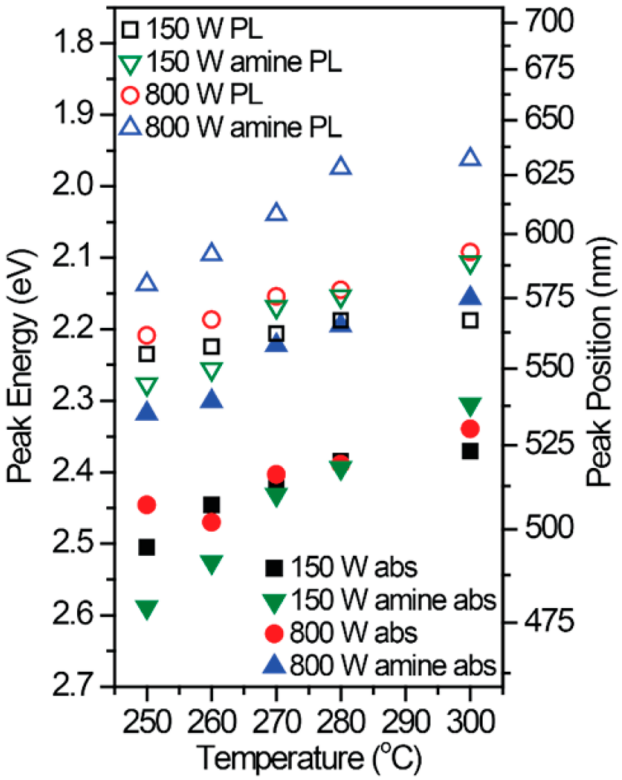

Figure 3.8 Scatter plot of absorption peak energy (eV) and PL peak position (nm) vs reaction temperature (°C). The degree of change in peak position is highest for the NCs prepared at 800 W set-power with amine, increasing from 578 to 632 nm (empty blue up-triangles). At 150 W with amine, the degree of increase in PL peak position is also high, ranging from 544 to 588 nm (empty green down-triangles). Without amine the magnitude of change in peak positions is lower at 800 and 150 W ranging from 562 to 596 nm and 553−574 nm, respectively.

In addition to the BMPy BF_4 IL, ILs with different cations and anions were utilized to assess the effects of the IL on the reaction and demonstrate the generality of the method. First, the analogous BMPy PF_6 IL was used. Although this IL did not yield luminescent InP NCs previously, employing lower temperatures and powers provided a pathway to luminescent InP NCs, as shown in Figure 3.9A. An IL with a more stable cation (BDMIm PF_6) could also successfully be exploited for luminescent InP NC synthesis (Figure 3.9B), although the NCs were not as bright (QYs < 10%), probably because of lower decomposition of BDMIm PF_6. Finally, BMIm TFSI provided a

fluoride-free IL control. Although NCs formed when using this IL, they did not luminesce (Figure 3.9C), suggesting a fluoride-containing anion is required for luminescent InP NCs since TFSI does not release fluoride upon decomposition. Assessing additional effects due to the IL is complicated by the different heating rates shown in the temperature vs time plots in Figure 3.10. The ILs heat the reaction solution more rapidly with BMIm TFSI > BMPy BF_4 > BDMIm PF_6 at 280 °C and 800 W. At 260 °C and 800 W, BMPy PF_6 resulted in faster heating than BMPy BF_4. Thus, the resulting InP NC products depend on the IL contribution to heating rate as well as the ability of the IL to influence the reaction chemically.

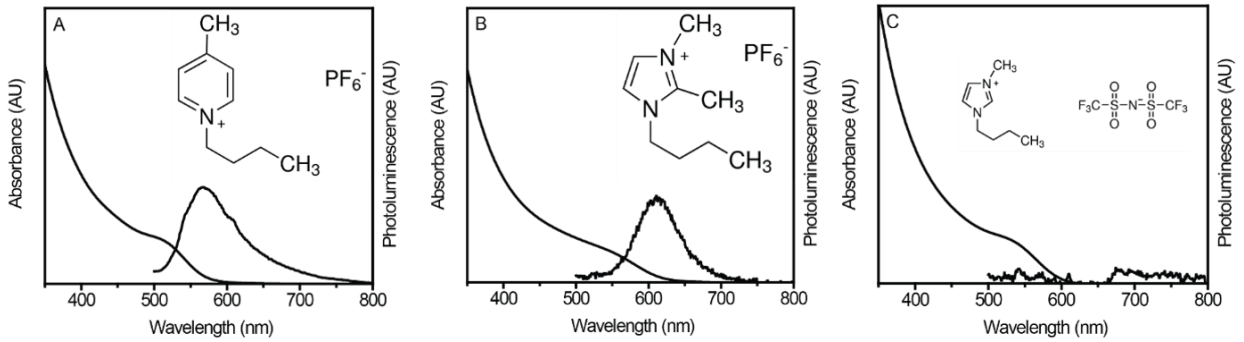

Figure 3.9 UV-Vis absorption and photoluminescence spectra (405 nm excitation) of InP NCs prepared with different ionic liquids. (A) 1-butyl-4-methylpyridinium hexafluorophosphate (BMPy PF_6), 260 °C, 150 W (B) 1-butyl-2,3-dimethylimidazolium hexafluorophosphate (BDMIm PF_6), 280 °C, 800 W (C) 1-butyl-3-methylimidazolium bis(trifluoromethylsulfonyl)imide (BMIm TFSI), 280 °C, 800 W. Synthetic conditions were adjusted to obtain luminescent NCs using BMPy PF_6, reducing power and temperature. The syntheses with the ionic liquids BDMIm PF_6 and BMIm TFSI represent new examples of the generality of this synthesis. Although all reactions form NCs, photoluminescence is not observed with the TFSI-containing ionic liquid, likely due to the absence of a fluorine-containing anion.

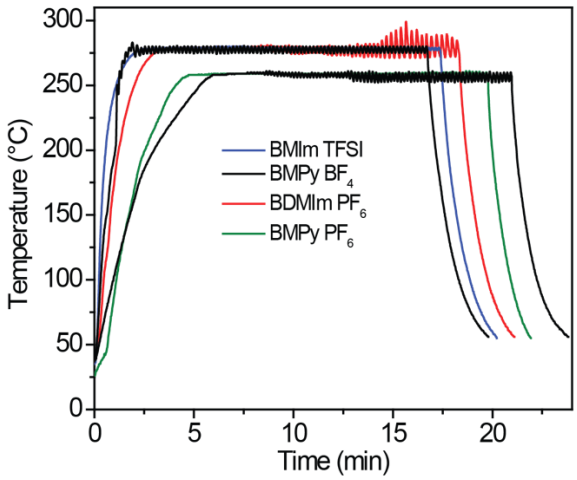

Figure 3.10 Temperature vs time plot for InP NC syntheses using different ionic liquids. Reactions done with a set-temperature of 280 °C and set-power of 800 W show slightly faster heating for the BMIm TFSI IL (blue) than the BMPy BF_4 IL (black) and the slowest heating with BDMIm PF_6 (red). Reactions done with a set-temperature of 260 °C and set-power of 150 W show slower heating for the BMPy BF_4 IL (black) than the analogous PF_6 salt (green).

Microwave-Assisted Synthesis of Luminescent InP NCs with Amine

It is well-established that amines have an effect on InP NC formation.[27,28,76,77] A detailed study by Gary et al. found primary amines destabilized InP clusters, facilitating NC formation.[27] In more recent work, primary amines were shown to activate phosphorus precursors,[28,78] and Abolhasani et al. found the presence of amine increased the rate of nucleation of InP NCs.[26] Here, we add dodecylamine (DDA) to the microwave-assisted syntheses to obtain higher quality, larger InP NCs, examining the effects of power and temperature on the resulting NCs.

In general, InP NCs prepared with DDA were brighter and larger. Figure 3.2C and 3.2D show the absorption and photoluminescence spectra of InP NCs formed at temperatures ranging from 250 to 300 °C and 150 or 800 W SP in the presence of DDA. The highest QYs were obtained for NCs prepared at 300 °C (800 W, DDA) with a QY of 30%. In fact, the luminescence of samples prepared at 800 W with DDA is well-defined even for the sample prepared at 250 °C (Figure 3.2D).

In Figure 3.2C a shoulder is observed in samples prepared at temperatures ≤260 °C with a very broad, lower energy emission present in the sample prepared at 250 °C. Samples prepared with DDA had absorption and PL peaks that could be tuned from ~490 to ~575 nm and ~545 to ~630 nm, respectively. This range is larger than that of samples prepared with no amine. These values are plotted along with the intermediate values obtained at different temperatures and in the absence of DDA in Figure 3.8. This plot shows the range of absorption peak and PL peak energies obtainable using this microwave-assisted method. It is readily apparent the samples prepared with DDA (triangles) show a larger range than those prepared without DDA (black squares and red circles). In fact, the DDA 150 W SP samples (green down-triangles) encompass the sizes obtainable with both 150 and 800 W in the absence of DDA. The higher QYs with amine addition might be due to more decomposition of IL caused by Lewis acid (BF_3) and Lewis base (DDA) reaction at higher temperatures.

The NC spectra varied slightly from synthesis-to-synthesis but consistently produced NCs with similar UV−vis absorptions and luminescence peak positions. Since amines provide the largest NC color-tunability, spectra for NCs synthesized using 150 and 800 W at 300 °C with amine were compared (Figure 3.11). Deviations in the first absorption feature were limited to ±5 nm (±0.02 eV) at 800 W and ±7 nm (±0.03 eV) at 150 W, likely due to the longer overall heating time required at lower powers. Corresponding photoluminescence spectra showed similar variations of ±7 nm (±0.02 eV) at 800 W and ±6 nm (±0.02 eV) and 150 W.

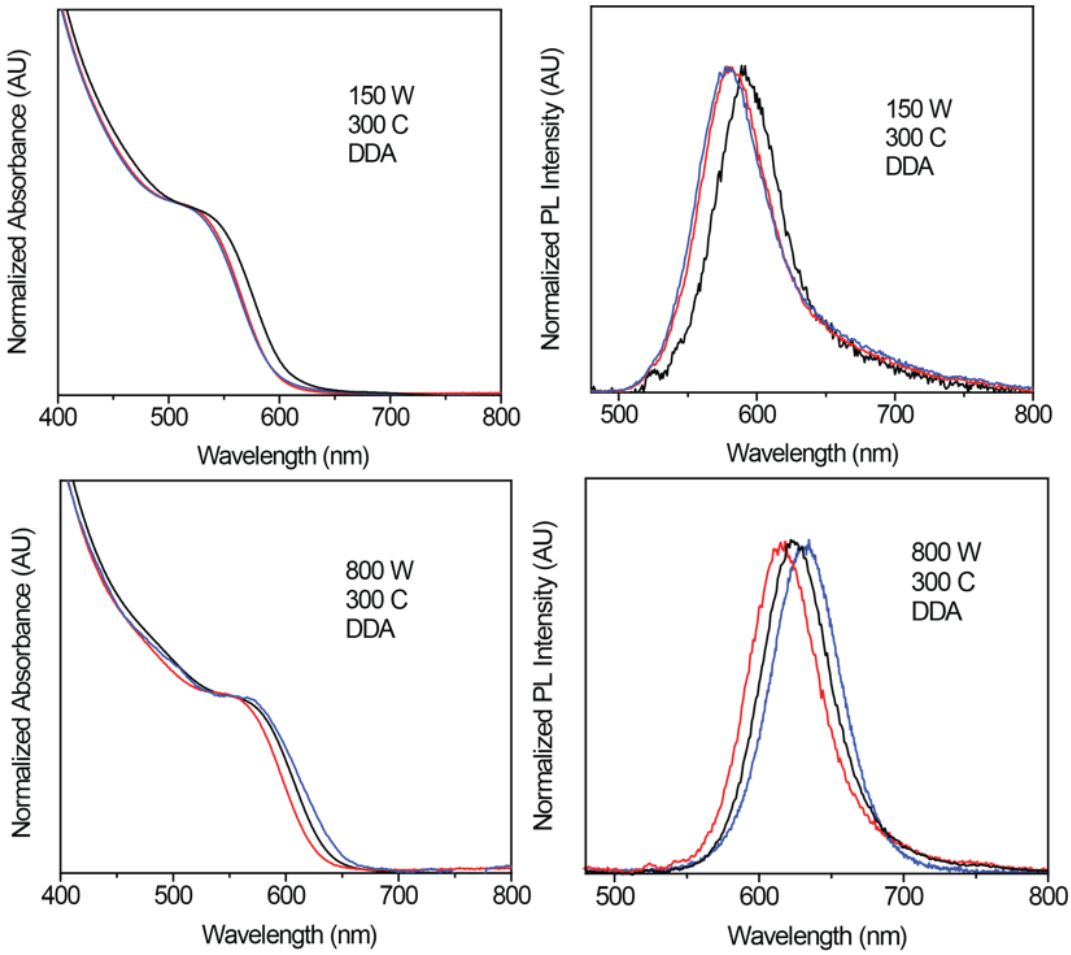

Figure 3.11 Spectra detailing the reproducibility of the syntheses of InP NCs prepared at 300 °C with dodecylamine. These conditions were chosen as they produced the largest diameter NCs (calculated by first abs feature) and deviations in spectral position. (A) UV-Vis absorption spectra of NCs prepared at 800 W show deviations of ±5 nm (±0.02 eV) in the first absorption feature. (B) Photoluminescence spectra (405 nm excitation) of NCs prepared at 800 W show deviations of ±7 nm (±0.02 eV) in the peak position. (C) UV-Vis absorption spectra of NCs prepared at 150 W show deviations of ±7 nm (±0.03 eV) in the first absorption feature. (D) Photoluminescence spectra (405 nm excitation) of NCs prepared at 150 W show deviations of ±6 nm (±0.02 eV) in the peak position.

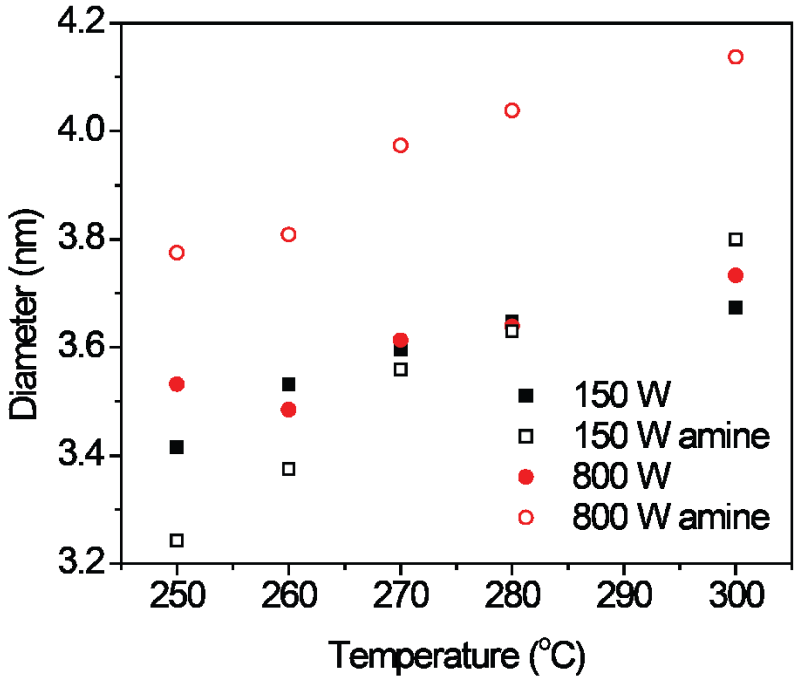

Figure 3.12 InP NC diameter (calculated based on ref 2) vs. reaction temperature for 150 W SP (black filled squares), 150 W SP with amine (black unfilled squares), 800 W SP (red filled circles), and 800 W SP with amine (red unfilled circles). Smaller NCs form at lower temperatures. A larger change in diameter is observed for reactions with amine.

Overall, amine facilitates formation of larger, more red NCs stable for weeks because of precursor activation. Using the first absorption feature, the diameters of the InP NCs were calculated, as described previously.[31,42] Calculated diameters ranging from 3.2 to 4.2 nm were obtained, and a plot of these values for samples prepared at different temperatures and powers is given in the Figure 3.12. TEM images at 800 and 150 W and XRD patterns for samples can also be found in the Figure 3.13, 3.14, and 3.15, respectively. All samples exhibited spherical shape, and, in general, NC diameters increased with increasing temperature. TEM images confirm larger NCs form when amine is used in the reaction and a larger size range is obtained. Size-distributions were similar for samples prepared at 150 and 800 W SP, with larger NCs exhibiting broader

distributions, as observed with samples prepared with no amine. Although luminescence decreases over time, the NCs are stable in solution under ambient conditions for months. Figure 3.16 shows NCs prepared with amine and BMPy BF_4 IL exhibited luminescence after complete drying and exposure to air for 8 months, although the intensity decreased by ~50%.

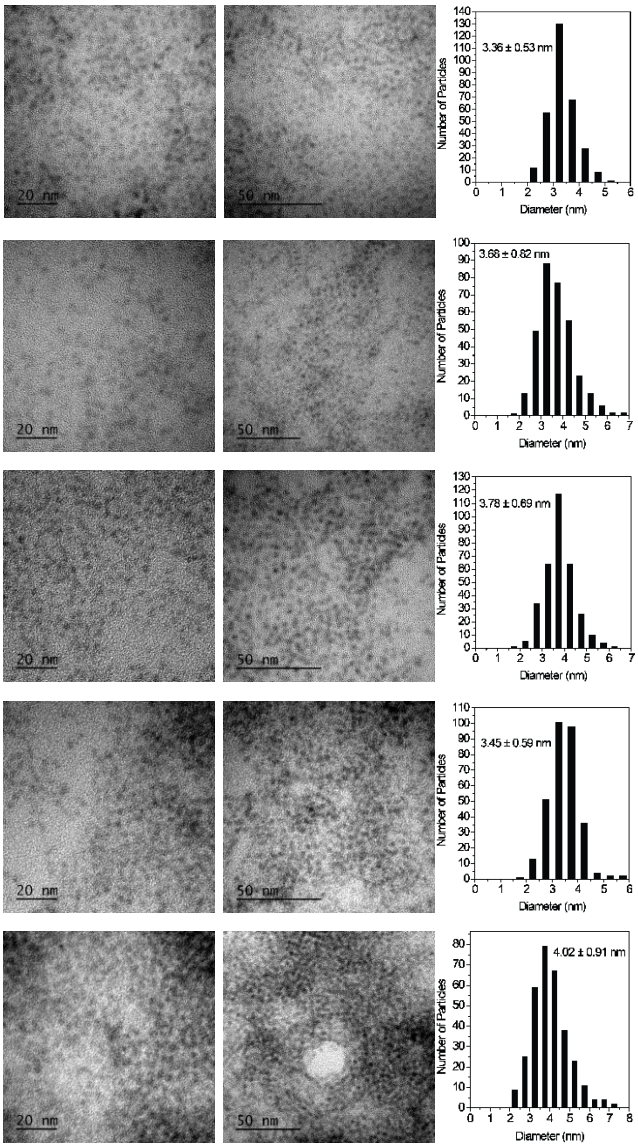

Figure 3.13 TEM images of InP NCs prepared with dodecylamine (DDA) at a SP of 800 W at different set-temperatures. The NCs are spherical in shape and increase in size with increasing temperature.

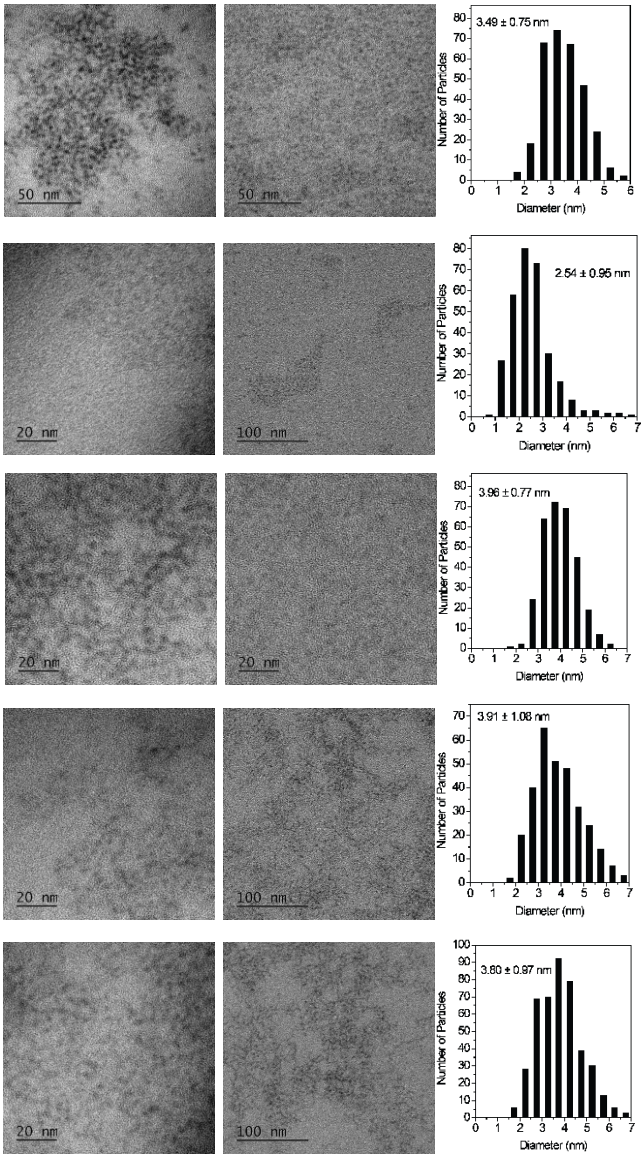

Figure 3.14 TEM images of InP NCs prepared with dodecylamine (DDA) at a SP of 150 W at different set-temperatures. The NCs are spherical in shape, although difficult to image at smaller diameters. Estimated average diameters for the 260 °C reaction were significantly lower than the calculated value possibly due to sample destruction or poor image quality.

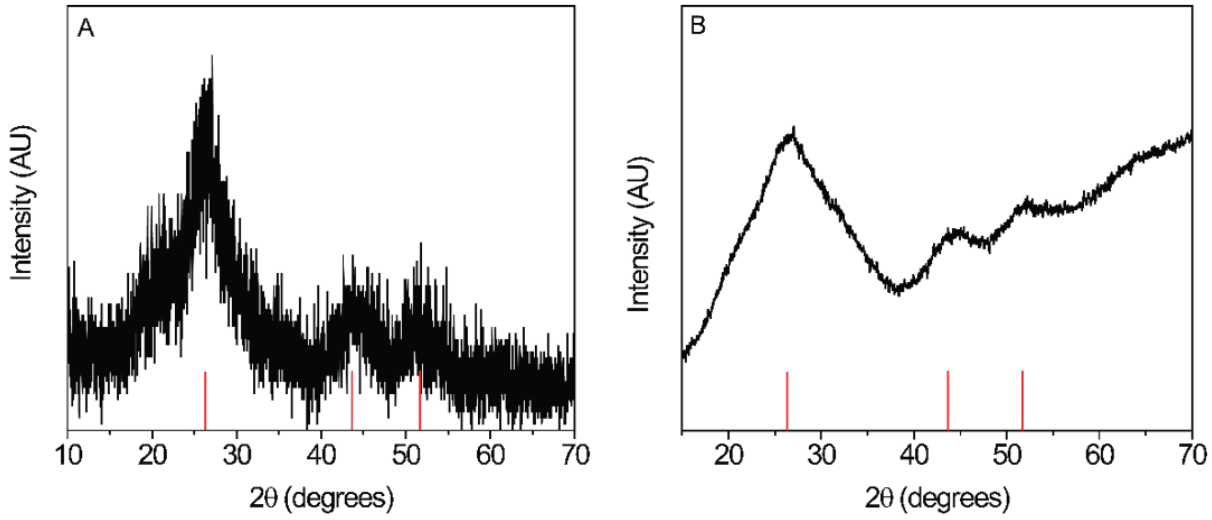

Figure 3.15 Representative powder X-ray diffraction patterns of InP NCs prepared at (A) 300 °C and 800 W and (B) 260 °C and 800 W with amine.

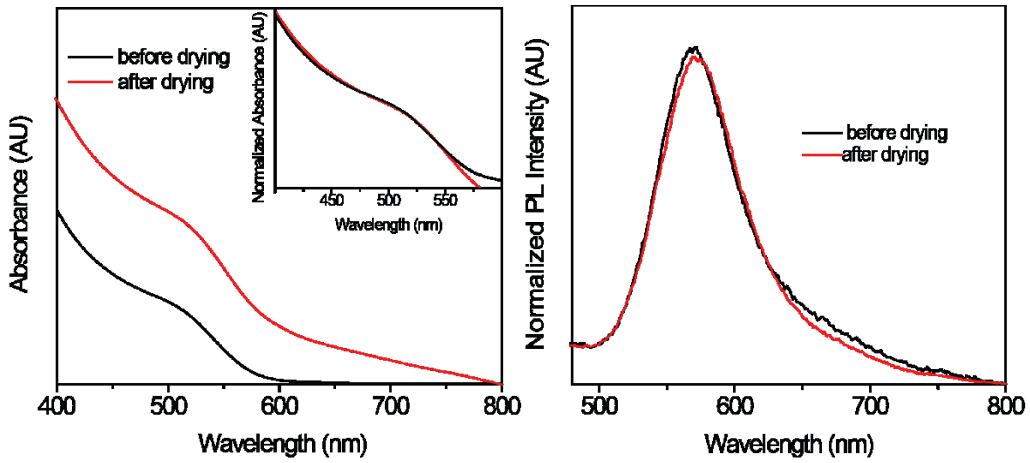

Figure 3.16 Spectra detailing stability of InP NCs prepared at 260 °C and 800 W with dodecylamine. The "after drying" sample was resuspended in toluene after remaining in solid form for 8 months in air. (A) UV-Vis absorption spectra show similar positions of the first absorption feature before and after drying, although the resuspended sample exhibits a great deal of scattering. (B) Photoluminescence spectra (405 nm excitation) show similar peak positions after normalization before and after drying. An overall reduction of PL relative peak intensity of ~50% is observed. The spectra are normalized to their maximum (approximately).

Microwave-Assisted Heating Without IL

To further examine the effects of amine on the synthesis, microwave-assisted syntheses were done without IL. However, the absence of IL is problematic due to slow heating rates. When no IL was used in the Pyrex vessel, the solution failed to reach the desired temperature (300 °C) despite heating as fast as possible at 800 W SP. This is likely due to poor coupling of the precursors to the microwave field, which is expected for these precursors. The dielectric constants of the precursors are 2.3 (palmitic acid), ~3 (phosphine), 2 (decane), and 3.13 (DDA).[79,80]

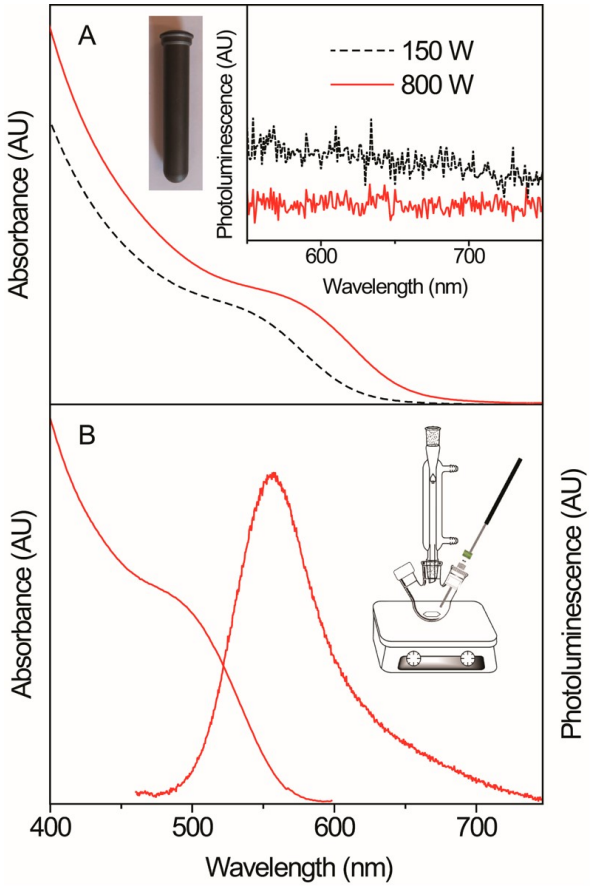

Figure 3.17 (A) UV−vis absorption spectra of InP NCs synthesized in a SiC vessel at 280 °C at set-powers (SPs) of 800 W (red, solid) and 150 W (black, dashed) in the absence of IL. The first absorption peak redshifts from ~530 nm to ~570 nm as the SP changes from 150 to 800 W. In the SiC vessel, heating is predominantly due to convective heating, because there is no IL. The lack

of IL also results in negligible NC luminescence (inset). (B) UV−vis absorption and photoluminescence spectra of InP NCs synthesized in a flask, which was heated to a reaction temperature of 280 °C with a holding time of 15 min. It took around 9 min to reach 280 °C. The PL shoulder indicates poor surface passivation, indicating that it is difficult to synthesize high-quality InP NCs, even at high temperatures (280 °C) in this conventional method.

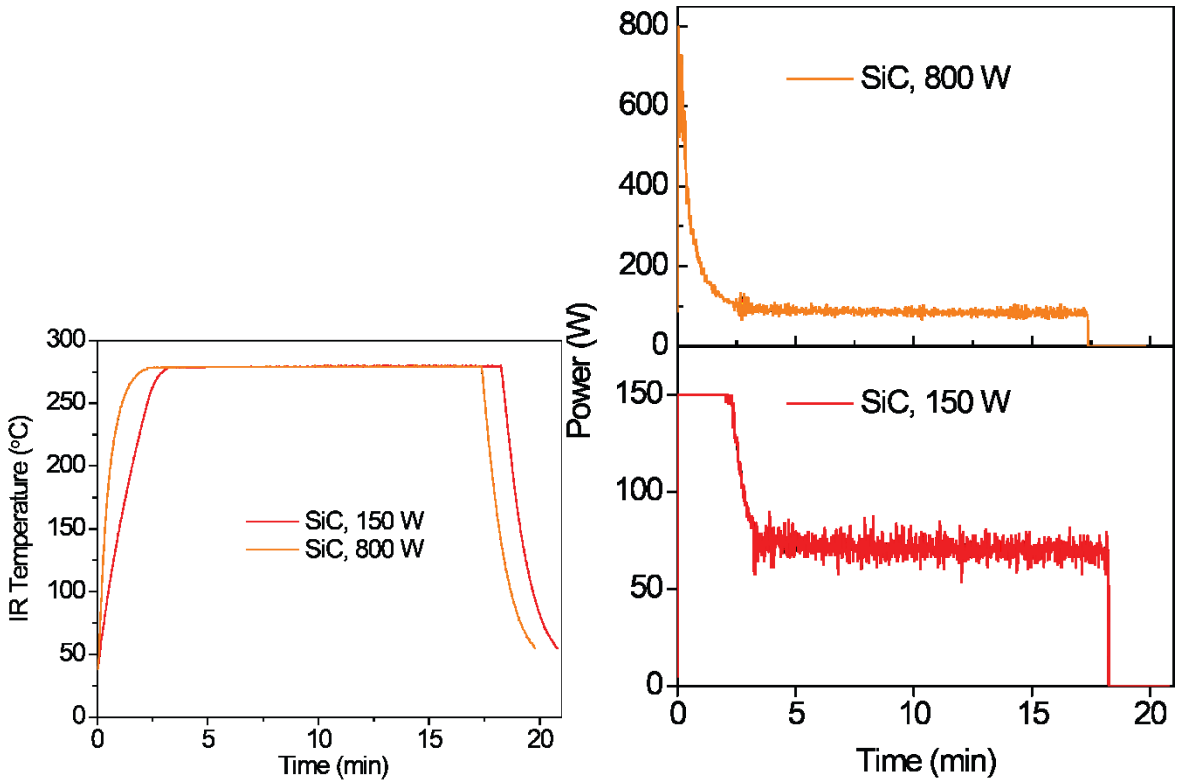

Figure 3.18 Left: Temperature vs time plot for InP NC syntheses in a SiC vessel at 150 W (red) and 800 W (orange) SPs. The reaction done at lower power takes about a minute longer to reach the reaction temperature of 280 °C. The corresponding power vs time plots are shown to the right. As expected, the reaction done at 800 W SP only remains at 800 W for a matter of seconds before decreasing to ~100 W. When 150 W SP is used, the reaction remains at 150 W for a full two minutes before decreasing to ~75 W.

To heat the solution rapidly in the absence of IL, a SiC vessel (Figure 3.17A inset) was used. The SiC vessel efficiently heats the reaction solution through convection, allowing rapid heating in the absence of IL and therefore separation of the effects of amine from the effects of IL on the synthesis.[60,81] The mixture reached reaction temperature (280 °C) in ~3 min at 150 W and ~2 min at 800 W (Figure 3.18). The resulting NCs exhibited no PL (Figure 3.17A inset), and the 150 W SP sample was noticeably smaller than the 800 W SP sample, as indicated by the first absorption features in Figure 3.17A. This is likely because of a discrepancy between internal and external temperature that is well-established in these microwave-assisted syntheses, including in SiC vessels.[60,80,81] Thus, at the higher SP, a higher internal temperature is reached for a longer time than at the lower 150 W SP. Here, the DDA causes a large size difference in the absence of the IL, indicating the size is predominantly a product of DDA and temperature, as previously observed for similar systems.[16,27,28]

Finally, the effect of microwave heating on the reaction was examined by carrying out the synthesis using conventional methods. For this sample, an analogous procedure was followed. As opposed to combining the InP precursor and IL in a microwave vessel, they were combined in a flask fitted with a condenser, thermocouple, and septa, as shown in the Figure 3.17B, inset. The solution was heated to 280 °C using a heating mantle and temperature controller while stirring. Any effects related to microwave heating should be evident from differences between this and the standard MAIL synthesis. Specifically, possible etching related to IL decomposition should occur in the absence of microwaves because fluoride release is a thermal process.[61] The resulting NCs should exhibit luminescence straight out of the synthesis. Absorption and photoluminescence spectra of the resulting NCs are shown in Figure 3.17B. The NCs exhibit PL but not as much as the NCs prepared at 800 W. The PL exhibits a shoulder to the red of the PL peak center, indicating the

surface of the NCs may have more defects than other, more-etched NCs prepared in the microwave. For example, the InP NCs prepared at 280 °C and 800 W SP (Figure 3.2B) exhibit a PL peak centered at 578 nm with a FWHM of 67 nm (0.25 eV), and these NCs have a PL peak centered at 564 nm with a FWHM of 84 nm (0.34 eV). The first absorption feature is also quite broad, resembling that of other samples prepared in the absence of DDA. Although not an exact comparison to the microwave-assisted method, largely because of the 9 min ramp time, the synthesis works in the absence of microwaves. Luminescence ascribed to IL fluoride release and related etching can still occur but does not seem as prominent as in the microwave-assisted syntheses, likely due to the higher T_{start} observed for slower heating rates.[74] Nevertheless, using this IL, it is possible to obtain luminescent InP NCs in the absence of microwaves, highlighting the thermal nature of the overall reaction. Finally, we note that naked NCs form by stripping of oleate ligands from PbSe using BF_3:Et_2O.[44] Here, we generate BF_3 upon IL fluoride loss, and with native palmitate ligands, in situ ligand stripping can occur. However, the products obtained from these syntheses remain suspended in hydrophobic solvent, whereas cationic naked NCs can suspend in polar solvent, and peaks associated with bound palmitate were observed in ^{1}H NMR. Nevertheless, adjusting these initial reaction conditions could provide a pathway to yield an efficient in situ ligand stripping agent and a new method for obtaining naked NCs.

3.4 Summary

In summary, we have investigated the effects of microwave power, reaction temperature, and amine on the microwave-assisted synthesis of InP NCs. Substantial differences in the heating profiles at different SPs and temperatures have been utilized to get InP NCs of different sizes. Although the magnitude of change in NC diameter is small at different SPs, addition of DDA facilitates a high degree of change in size at constant SP. This could be due to a combination of

MAIL heating and precursor activation by amine, since brighter NCs form with DDA. Samples exhibited color-tunable luminescence spanning the visible region, with quantum yields of 20−30%. The IL role was assessed using ILs with different cations and anions, a SiC vessel, and a conventional flask synthesis, confirming ILs with fluoride-containing anions are largely responsible for 1) heating and 2) NC luminescence. However, the presence of fluoride on the NC surface was not observed. The effect of amine on size was confirmed using a SiC vessel in the absence of IL. The advantages of this microwave-assisted synthesis over conventional InP NC syntheses are its simplicity and that a single precursor solution yields luminescent InP NCs of different sizes.

3.5 References

(1) Carey, G. H.; Abdelhady, A. L.; Ning, Z.; Thon, S. M.; Bakr, O. M.; Sargent, E. H. Colloidal Quantum Dot Solar Cells. *Chem. Rev.* **2015**, *115* (23), 12732–12763.

(2) Wood, V.; Bulović, V. Colloidal Quantum Dot Light-Emitting Devices. *Nano Rev.* **2010**, *1*.

(3) Yang, Y.; Zheng, Y.; Cao, W.; Titov, A.; Hyvonen, J.; Manders, J. R.; Xue, J.; Holloway, P. H.; Qian, L. High-Efficiency Light-Emitting Devices Based on Quantum Dots with Tailored Nanostructures. *Nat. Photonics* **2015**, *9* (4), 259–266.

(4) Frecker, T.; Bailey, D.; Arzeta-Ferrer, X.; McBride, J.; Rosenthal, S. J. Review—Quantum Dots and Their Application in Lighting, Displays, and Biology. *ECS J. Solid State Sci. Technol.* **2016**, *5* (1), R3019–R3031.

(5) Bruchez, M.; Moronne, M.; Gin, P.; Weiss, S.; Alivisatos, A. P. Semiconductor Nanocrystals as Fluorescent Biological Labels. *Science* **1998**, *281* (5385), 2013–2016.

(6) Medintz, I. L.; Uyeda, H. T.; Goldman, E. R.; Mattoussi, H. Quantum Dot Bioconjugates for Imaging, Labelling and Sensing. *Nat. Mater.* **2005**, *4* (6), 435–446.

(7) Lifshitz, E.; Siebbeles, L. D. A. Fundamental Processes in Semiconductor Nanocrystals. *Phys. Chem. Chem. Phys.* **2014**, *16* (47), 25677–25678.

(8) Kovalenko, M. V.; Manna, L.; Cabot, A.; Hens, Z.; Talapin, D. V.; Kagan, C. R.; Klimov, V. I.; Rogach, A. L.; Reiss, P.; Milliron, D. J.; et al. Prospects of Nanoscience with Nanocrystals. *ACS Nano* **2015**, *9* (2), 1012–1057.

(9) Boles, M. A.; Ling, D.; Hyeon, T.; Talapin, D. V. The Surface Science of Nanocrystals. *Nat. Mater.* **2016**, *15* (2), 141–153.

(10) Rzigalinski, B. A.; Strobl, J. S. Cadmium-Containing Nanoparticles: Perspectives on Pharmacology and Toxicology of Quantum Dots. *Toxicol. Appl. Pharmacol.* **2009**, *238* (3), 280–288.

(11) Soenen, S. J.; Parak, W. J.; Rejman, J.; Manshian, B. (Intra)Cellular Stability of Inorganic Nanoparticles: Effects on Cytotoxicity, Particle Functionality, and Biomedical Applications. *Chem. Rev.* **2015**, *115* (5), 2109–2135.

(12) Grim, J. Q.; Manna, L.; Moreels, I. A Sustainable Future for Photonic Colloidal Nanocrystals. *Chem. Soc. Rev.* **2015**, *44* (16), 5897–5914.

(13) Cotal, H.; Fetzer, C.; Boisvert, J.; Kinsey, G.; King, R.; Hebert, P.; Yoon, H.; Karam, N. III–V Multijunction Solar Cells for Concentrating Photovoltaics. *Energy Environ. Sci.* **2009**, *2* (2), 174–192.

(14) Friedman, D. J. Progress and Challenges for next-Generation High-Efficiency Multijunction Solar Cells. *Curr. Opin. Solid State Mater. Sci.* **2010**, *14* (6), 131–138.

(15) van Veggel, F. C. J. M. Near-Infrared Quantum Dots and Their Delicate Synthesis, Challenging Characterization, and Exciting Potential Applications. *Chem. Mater.* **2014**, *26* (1), 111–122.

(16) Tamang, S.; Lincheneau, C.; Hermans, Y.; Jeong, S.; Reiss, P. Chemistry of InP Nanocrystal Syntheses. *Chem. Mater.* **2016**, *28* (8), 2491–2506.

(17) Xie, R.; Battaglia, D.; Peng, X. Colloidal InP Nanocrystals as Efficient Emitters Covering Blue to Near-Infrared. *J. Am. Chem. Soc.* **2007**, *129* (50), 15432–15433.

(18) Rowland, C. E.; Liu, W.; Hannah, D. C.; Chan, M. K. Y.; Talapin, D. V.; Schaller, R. D. Thermal Stability of Colloidal InP Nanocrystals: Small Inorganic Ligands Boost High-Temperature Photoluminescence. *ACS Nano* **2014**, *8* (1), 977–985.

(19) Xu, S.; Ziegler, J.; Nann, T. Rapid Synthesis of Highly Luminescent InP and InP/ZnS Nanocrystals. *J. Mater. Chem.* **2008**, *18* (23), 2653–2656.

(20) Baek, J.; Allen, P. M.; Bawendi, M. G.; Jensen, K. F. Investigation of Indium Phosphide Nanocrystal Synthesis Using a High-Temperature and High-Pressure Continuous Flow Microreactor. *Angew. Chem. Int. Ed.* **2011**, *50* (3), 627–630.

(21) Kim, K.; Yoo, D.; Choi, H.; Tamang, S.; Ko, J.-H.; Kim, S.; Kim, Y.-H.; Jeong, S. Halide-Amine Co-Passivated Indium Phosphide Colloidal Quantum Dots in Tetrahedral Shape. *Angew. Chem. Int. Ed Engl.* **2016**, *55* (11), 3714–3718.

(22) Franke, D.; Harris, D. K.; Xie, L.; Jensen, K. F.; Bawendi, M. G. The Unexpected Influence of Precursor Conversion Rate in the Synthesis of III-V Quantum Dots. *Angew. Chem. Int. Ed Engl.* **2015**, *54* (48), 14299–14303.

(23) Mnoyan, A. N.; Kirakosyan, A. G.; Kim, H.; Jang, H. S.; Jeon, D. Y. Electrostatic Stabilized InP Colloidal Quantum Dots with High Photoluminescence Efficiency. *Langmuir* **2015**, *31* (25), 7117–7121.

(24) Tessier, M. D.; Dupont, D.; De Nolf, K.; De Roo, J.; Hens, Z. Economic and Size-Tunable Synthesis of InP/ZnE (E = S, Se) Colloidal Quantum Dots. *Chem. Mater.* **2015**, *27* (13), 4893–4898.

(25) Xie, L.; Harris, D. K.; Bawendi, M. G.; Jensen, K. F. Effect of Trace Water on the Growth of Indium Phosphide Quantum Dots. *Chem. Mater.* **2015**, *27* (14), 5058–5063.

(26) Abolhasani, M.; Coley, C. W.; Xie, L.; Chen, O.; Bawendi, M. G.; Jensen, K. F. Oscillatory Microprocessor for Growth and in Situ Characterization of Semiconductor Nanocrystals. *Chem. Mater.* **2015**, *27* (17), 6131–6138.

(27) Gary, D. C.; Terban, M. W.; Billinge, S. J. L.; Cossairt, B. M. Two-Step Nucleation and Growth of InP Quantum Dots via Magic-Sized Cluster Intermediates. *Chem. Mater.* **2015**, *27* (4), 1432–1441.

(28) Tessier, M. D.; De Nolf, K.; Dupont, D.; Sinnaeve, D.; De Roo, J.; Hens, Z. Aminophosphines: A Double Role in the Synthesis of Colloidal Indium Phosphide Quantum Dots. *J. Am. Chem. Soc.* **2016**, *138* (18), 5923–5929.

(29) Stein, J. L.; Mader, E. A.; Cossairt, B. M. Luminescent InP Quantum Dots with Tunable Emission by Post-Synthetic Modification with Lewis Acids. *J. Phys. Chem. Lett.* **2016**, *7* (7), 1315–1320.

(30) Mićić, O. I.; Smith, B. B.; Nozik, A. J. Core−Shell Quantum Dots of Lattice-Matched $ZnCdSe_2$ Shells on InP Cores: Experiment and Theory. *J. Phys. Chem. B* **2000**, *104* (51), 12149–12156.

(31) Adam, S.; Talapin, D. V.; Borchert, H.; Lobo, A.; McGinley, C.; de Castro, A. R. B.; Haase, M.; Weller, H.; Möller, T. The Effect of Nanocrystal Surface Structure on the Luminescence Properties: Photoemission Study of HF-Etched InP Nanocrystals. *J. Chem. Phys.* **2005**, *123* (8), 084706.

(32) Mićić, O. I.; Cheong, H. M.; Fu, H.; Zunger, A.; Sprague, J. R.; Mascarenhas, A.; Nozik, A. J. Size-Dependent Spectroscopy of InP Quantum Dots. *J. Phys. Chem. B* **1997**, *101* (25), 4904–4912.

(33) Talapin, D. V.; Gaponik, N.; Borchert, H.; Rogach, A. L.; Haase, M.; Weller, H. Etching of Colloidal InP Nanocrystals with Fluorides: Photochemical Nature of the Process Resulting in High Photoluminescence Efficiency. *J. Phys. Chem. B* **2002**, *106* (49), 12659–12663.

(34) Li, L.; Reiss, P. One-Pot Synthesis of Highly Luminescent InP/ZnS Nanocrystals without Precursor Injection. *J. Am. Chem. Soc.* **2008**, *130* (35), 11588–11589.

(35) Lim, J.; Bae, W. K.; Lee, D.; Nam, M. K.; Jung, J.; Lee, C.; Char, K.; Lee, S. InP@ZnSeS, Core@Composition Gradient Shell Quantum Dots with Enhanced Stability. *Chem. Mater.* **2011**, *23* (20), 4459–4463.

(36) Kim, S.; Kim, T.; Kang, M.; Kwak, S. K.; Yoo, T. W.; Park, L. S.; Yang, I.; Hwang, S.; Lee, J. E.; Kim, S. K.; et al. Highly Luminescent InP/GaP/ZnS Nanocrystals and Their Application to White Light-Emitting Diodes. *J. Am. Chem. Soc.* **2012**, *134* (8), 3804–3809.

(37) Yang, X.; Zhao, D.; Leck, K. S.; Tan, S. T.; Tang, Y. X.; Zhao, J.; Demir, H. V.; Sun, X. W. Full Visible Range Covering InP/ZnS Nanocrystals with High Photometric Performance and Their Application to White Quantum Dot Light-Emitting Diodes. *Adv. Mater.* **2012**, *24* (30), 4180–4185.

(38) Wu, K.; Song, N.; Liu, Z.; Zhu, H.; Rodríguez-Córdoba, W.; Lian, T. Interfacial Charge Separation and Recombination in InP and Quasi-Type II InP/CdS Core/Shell Quantum Dot-Molecular Acceptor Complexes. *J. Phys. Chem. A* **2013**, *117* (32), 7561–7570.

(39) Altıntas, Y.; Talpur, M. Y.; Ünlü, M.; Mutlugün, E. Highly Efficient Cd-Free Alloyed Core/Shell Quantum Dots with Optimized Precursor Concentrations. *J. Phys. Chem. C* **2016**, *120* (14), 7885–7892.

(40) Li, C.; Ando, M.; Murase, N. Facile Preparation of Highly Luminescent InP Nanocrystals by a Solvothermal Route. *Chem. Lett.* **2008**, *37* (8), 856–857.

(41) Mićić, O. I.; Sprague, J.; Lu, Z.; Nozik, A. J. Highly Efficient Band-edge Emission from InP Quantum Dots. *Appl. Phys. Lett.* **1996**, *68* (22), 3150–3152.

(42) Reiss, P.; Protière, M.; Li, L. Core/Shell Semiconductor Nanocrystals. *Small Weinh. Bergstr. Ger.* **2009**, *5* (2), 154–168.

(43) Smith, A. M.; Nie, S. Semiconductor Nanocrystals: Structure, Properties, and Band Gap Engineering. *Acc. Chem. Res.* **2010**, *43* (2), 190–200.

(44) Doris, S. E.; Lynch, J. J.; Li, C.; Wills, A. W.; Urban, J. J.; Helms, B. A. Mechanistic Insight into the Formation of Cationic Naked Nanocrystals Generated under Equilibrium Control. *J. Am. Chem. Soc.* **2014**, *136* (44), 15702–15710.

(45) Kagan, C. R.; Murray, C. B. Charge Transport in Strongly Coupled Quantum Dot Solids. *Nat. Nanotechnol.* **2015**, *10* (12), 1013–1026.

(46) MacKinnon, M. A. Hydrofluoric Acid Burns. *Dermatol. Clin.* **1988**, *6* (1), 67–74.

(47) Burgher, F.; Mathieu, L.; Lati, E.; Gasser, P.; Peno-Mazzarino, L.; Blomet, J.; Hall, A. H.; Maibach, H. I. Experimental 70% Hydrofluoric Acid Burns: Histological Observations in an Established Human Skin Explants Ex Vivo Model. *Cutan. Ocul. Toxicol.* **2011**, *30* (2), 100–107.

(48) Baghbanzadeh, M.; Carbone, L.; Cozzoli, P. D.; Kappe, C. O. Microwave-Assisted Synthesis of Colloidal Inorganic Nanocrystals. *Angew. Chem. Int. Ed.* **2011**, *50* (48), 11312–11359.

(49) Horikoshi, S.; Serpone, N. Nanoparticle Synthesis through Microwave Heating. In *Microwaves in Nanoparticle Synthesis*; Horikoshi, S., Serpone, N., Eds.; Wiley-VCH Verlag GmbH & Co. KGaA, 2013; pp 75–105.

(50) Zhu, Y.-J.; Chen, F. Microwave-Assisted Preparation of Inorganic Nanostructures in Liquid Phase. *Chem. Rev.* **2014**, *114* (12), 6462–6555.

(51) Murray, C. B.; Norris, D. J.; Bawendi, M. G. Synthesis and Characterization of Nearly Monodisperse CdE (E = Sulfur, Selenium, Tellurium) Semiconductor Nanocrystallites. *J. Am. Chem. Soc.* **1993**, *115* (19), 8706–8715.

(52) Micic, O. I.; Curtis, C. J.; Jones, K. M.; Sprague, J. R.; Nozik, A. J. Synthesis and Characterization of InP Quantum Dots. *J. Phys. Chem.* **1994**, *98* (19), 4966–4969.

(53) van Embden, J.; Chesman, A. S. R.; Jasieniak, J. J. The Heat-Up Synthesis of Colloidal Nanocrystals. *Chem. Mater.* **2015**, *27* (7), 2246–2285.

(54) Gabriel, C.; Gabriel, S.; Grant, E. H.; Grant, E. H.; Halstead, B. S. J.; Mingos, D. M. P. Dielectric Parameters Relevant to Microwave Dielectric Heating. *Chem. Soc. Rev.* **1998**, *27* (3), 213–224.

(55) Chikan, V.; McLaurin, E. J. Rapid Nanoparticle Synthesis by Magnetic and Microwave Heating. *Nanomaterials* **2016**, *6* (5).

(56) Deetlefs, M.; Seddon, K. Ionic Liquids: Fact and Fiction. *Chim. OGGI-Chem. TODAY* **2006**, *24* (2).

(57) Liu, J.; Yang, X.; Wang, K.; Wang, D.; Zhang, P. Chemical Etching with Tetrafluoroborate: A Facile Method for Resizing of CdTe Nanocrystals under Mild Conditions. *Chem. Commun.* **2009**, *0* (40), 6080–6082.

(58) Hayakawa, Y.; Nonoguchi, Y.; Wu, H.-P.; Diau, E. W.-G.; Nakashima, T.; Kawai, T. Rapid Preparation of Highly Luminescent CdTe Nanocrystals in an Ionic Liquid via a Microwave-Assisted Process. *J. Mater. Chem.* **2011**, *21* (24), 8849–8853.

(59) Ma, M.-G.; Zhu, J.-F.; Zhu, Y.-J.; Sun, R.-C. The Microwave-Assisted Ionic-Liquid Method: A Promising Methodology in Nanomaterials. *Chem. – Asian J.* **2014**, *9* (9), 2378–2391.

(60) Kappe, C. O. Unraveling the Mysteries of Microwave Chemistry Using Silicon Carbide Reactor Technology. *Acc. Chem. Res.* **2013**, *46* (7), 1579–1587.

(61) Leadbeater, N. E.; Torenius, H. M. A Study of the Ionic Liquid Mediated Microwave Heating of Organic Solvents. *J. Org. Chem.* **2002**, *67* (9), 3145–3148.

(62) Hallett, J. P.; Welton, T. Room-Temperature Ionic Liquids: Solvents for Synthesis and Catalysis. 2. *Chem. Rev.* **2011**, *111* (5), 3508–3576.

(63) Lorbeer, C.; Cybinska, J.; Mudring, A.-V. Facile Preparation of Quantum Cutting GdF_3 : Eu^{3+} Nanoparticles from Ionic Liquids. *Chem. Commun.* **2010**, *46* (4), 571–573.

(64) Lovingood, D. D.; Strouse, G. F. Microwave Induced In-Situ Active Ion Etching of Growing InP Nanocrystals. *Nano Lett.* **2008**, *8* (10), 3394–3397.

(65) Gerbec, J. A. Methods of Synthesis of Colloidal Nanoparticles. Ph.D. Thesis, University of California, Santa Barbara: California, United States, 2006.

(66) Gerbec, J. A.; Magana, D.; Washington, A.; Strouse, G. F. Microwave-Enhanced Reaction Rates for Nanoparticle Synthesis. *J. Am. Chem. Soc.* **2005**, *127* (45), 15791–15800.

(67) Magde, D.; Rojas, G. E.; Seybold, P. G. Solvent Dependence of the Fluorescence Lifetimes of Xanthene Dyes. *Photochem. Photobiol.* **1999**, *70* (5), 737–744.

(68) Magde, D.; Wong, R.; Seybold, P. G. Fluorescence Quantum Yields and Their Relation to Lifetimes of Rhodamine 6G and Fluorescein in Nine Solvents: Improved Absolute Standards for Quantum Yields. *Photochem. Photobiol.* **2002**, *75* (4), 327–334.

(69) Jhung, S. H.; Jin, T.; Hwang, Y. K.; Chang, J.-S. Microwave Effect in the Fast Synthesis of Microporous Materials: Which Stage Between Nucleation and Crystal Growth Is Accelerated by Microwave Irradiation? *Chem. – Eur. J.* **2007**, *13* (16), 4410–4417.

(70) Washington II, A. L.; Strouse, G. F. Microwave Synthesis of CdSe and CdTe Nanocrystals in Nonabsorbing Alkanes. *J. Am. Chem. Soc.* **2008**, *130* (28), 8916–8922.

(71) Bose, D. N.; Ramprakash, Y.; Basu, S. Characterization of N-InP Surfaces before and after Surface Modification. *Mater. Lett.* **1989**, *8* (9), 364–368.

(72) Sun, Y.; Liu, Z.; Machuca, F.; Pianetta, P.; Spicer, W. E. Optimized Cleaning Method for Producing Device Quality InP(100) Surfaces. *J. Appl. Phys.* **2005**, *97* (12), 124902.

(73) Fu, H.; Zunger, A. InP Quantum Dots: Electronic Structure, Surface Effects, and the Redshifted Emission. *Phys. Rev. B* **1997**, *56* (3), 1496–1508.

(74) Cao, Y.; Mu, T. Comprehensive Investigation on the Thermal Stability of 66 Ionic Liquids by Thermogravimetric Analysis. *Ind. Eng. Chem. Res.* **2014**, *53* (20), 8651–8664.

(75) Morris-Cohen, A. J.; Malicki, M.; Peterson, M. D.; Slavin, J. W. J.; Weiss, E. A. Chemical, Structural, and Quantitative Analysis of the Ligand Shells of Colloidal Quantum Dots. *Chem. Mater.* **2013**, *25* (8), 1155–1165.

(76) Protière, M.; Reiss, P. Amine-Induced Growth of an In_2O_3 Shell on Colloidal InP Nanocrystals. *Chem. Commun.* **2007**, (23), 2417–2419.

(77) Allen, P. M.; Walker, B. J.; Bawendi, M. G. Mechanistic Insights into the Formation of InP Quantum Dots. *Angew. Chem. Int. Ed.* **2010**, *49* (4), 760–762.

(78) Buffard, A.; Dreyfuss, S.; Nadal, B.; Heuclin, H.; Xu, X.; Patriarche, G.; Mézailles, N.; Dubertret, B. Mechanistic Insight and Optimization of InP Nanocrystals Synthesized with Aminophosphines. *Chem. Mater.* **2016**, *28* (16), 5925–5934.

(79) Dielectric Constant (DC Value) Compendium; Endress+Hauser: Weil am Rhein, Germany, 2000.

(80) Kappe, C. O. How to Measure Reaction Temperature in Microwave-Heated Transformations. *Chem. Soc. Rev.* **2013**, *42* (12), 4977–4990.

(81) Ashley, B.; Lovingood, D. D.; Chiu, Y.-C.; Gao, H.; Owens, J.; Strouse, G. F. Specific Effects in Microwave Chemistry Explored through Reactor Vessel Design, Theory, and Spectroscopy. *Phys. Chem. Chem. Phys.* **2015**, *17* (41), 27317–27327.

Chapter 4 - Synthesis of Polar InP Nanocrystals via In Situ Ligand Stripping

4.1 Introduction

Though semiconductor NCs are associated with low-cost solution processability and tunable optical and electrical properties, for integrating into devices such as field effect transistors and photovoltaics, NCs surface structure and environment play a key role since the interface between individual NCs and charge transport layers is important in determining efficiency of the devices. Charge transfer from the NCs is strongly affected by ligands since smaller ligands facilitate electronic communication between NCs.[1] One of the problems associated with the surface chemistry of colloidal InP NCs from a synthetic perspective is to synthesize them with short inorganic ligands. The synthesized InP NCs can have potential applications in optoelectronic and bio-imaging.

For modifying surface of the semiconductor NCs, standard methods of ligand exchange, namely solution phase ligand exchange or solid-state ligand exchange is often used since NCs isolation and stabilization is achieved by long-chain organic ligands.[1] With this method NCs surfaces are modified to have short inorganic ligands like metal-chalcogenides,[2] halides, pseudohalides, halometallates,[3] metal-free inorganic ligands,[4] metal halides, and lead halide perovskites,[5] or stabilizing them in inorganic matrices[6] over the years. Because of ionic shells on the NCs surface, their solubility changes from non-polar solvent (toluene or hexane) to polar solvents like hydrazine, DMSO, N-methylformamide (NMF), or Formamide (FA). Reported inorganic ligands that stabilize InP NCs surfaces are sulfide (S^{-2}), azide (N^{3-}), molecular metal chalcogenide complex ($Sn_2S_6^{4-}$), and $InCl_3$. Hexylphosphonic acid exchanges initial oleate ligands on InP NCs surface by gel permeation chromatography (GPC) but solubility of the NCs retains in non-polar

solvent only.[7] Post-etching method is reported for electrostatically stabilizing InP NC surface by sulfate (SO_4^{2-}) ions along with carbonyl coordination of polar solvent by using fluoric and sulfuric acids.[8] Our experiments on InP NCs synthesis by a microwave-assisted method produced InP NCs that have solubility in DMSO and DMF solvents. So, these NCs are called polar InP NCs in this work.

HF etching is used for obtaining luminescent InP NCs but they are still soluble in non-polar solvent (toluene) because of long alkyl chain ligands.[9] *In situ* etching is reported for InP NCs synthesis by a microwave-assisted method to get luminescent InP NCs with solubility in toluene.[10] Helms group reported that colloidal stabilization of PbSe NCs during ligand stripping process can be obtained by BF_4^- and their solubility in a polar solvent (DMF) is achieved.[11] In our synthesis, *in situ* ligand stripping is occurring in a reaction of microwave-assisted method resulting in InP NCs that have luminescence and solubility in DMSO solvent. This *in situ* ligand stripping is afforded by decomposition of hexafluorophosphate (PF_6^-) ion containing ionic liquids (ILs) used for the microwave synthesis. The luminescence and solubility obtained for the InP NCs is the first synthesis from a synthetic perspective for any colloidal NCs from III-V semiconductors. The presented synthesis and characterization paves for similar synthesis of other III-V semiconductor NCs.

4.2 Experimental Section

Chemicals

Indium acetate ($In(OAc)_3$, 99.99%), tris(trimethylsilyl)phosphine (TMSP), min. 98%) (10% in hexane) from Strem; palmitic acid (PA, ≥99%), 1-butyl-3-methylimidazolium hexafluorophosphate(BMIm PF_6, ≥97%), 1-butyl-4-methylpyridinium hexafluorophosphate, (BMPy PF_6, ≥97%), 1-butyl-2,3-dimethylimidazolium hexafluorophosphate (BDMIm PF_6, ≥97%), 1-butyl-3-methyl-imidazolium tetrafluoroborate (BMIm BF_4, BASF quality, ≥98%),

decane (anhydrous, ≥99%), indium acetate ($In(OAc)_3$, 99.99% trace metals basis), dimethylsulfoxide, ≥99.5% (GC), and methanol, ACS reagent, ≥99.8% from Sigma Aldrich; toluene, certified ACS, chloroform, certified ACS, ethanol certified ACS from fisher scientific; dimethylsulfoxide-d_6, 99.9% and chloroform-d, 99.8% from Cambridge isotope laboratories; 1-octadecene (1-ODE), 90%, tech from Acros Organics; Rhodamine B from Fisher Scientific.

Indium Palmitate (InPA)

InPA is synthesized using a method adopted from Strouse and co-workers.[12] A 100 mL two-neck round-bottom (RB) flask is attached to a Schlenk line using a condenser; a rubber septum is attached, and the flask was put under vacuum. After filling the flask with N_2, 0.605 g (2.36 mmol) of PA is added. The solid is heated under vacuum while stirring in an oil bath at 105 °C for 5−10 min. After cooling the PA to room temperature under vacuum, the flask is put under N_2, and 0.207 g (0.710 mmol) of $In(OAc)_3$ is added. After putting the flask under vacuum, the solids are heated to 150 °C. Any solid that formed on the walls of the flask is melted using a heat gun. This process is repeated until the pressure reached baseline, about an hour. The flask is cooled to room temperature under vacuum, yielding a white solid.

InP Precursor

In an inert atmosphere glovebox, decane (47 mL) is added to the flask containing the InPA and left stirring until the solid is well-suspended (12 h). In the glovebox, $P(TMS)_3$ (1.15 mL, 0.393 mmol) is diluted in decane (3 mL) and slowly added to the InPA suspension. After obtaining an orange solution (1−2 h), the InP precursor solution is transferred to a Schlenk line and heated in an oil bath set to 65 °C under N_2. After the solution turned optically clear (∼10 min), the flask is returned to the glovebox. The orange solution is immediately used as the precursor for the InP NC syntheses. This is essential for formation of high quality NCs reproducibly.

Microwave-Assisted Synthesis of InP NCs

The following methods are used for the synthesis of NCs. All samples are prepared in a glovebox under inert atmosphere in tightly capped 10 mL microwave vessels with a stir bar. The microwave method used the "heat as fast as possible" mode and a reaction time (holding time) of 15 min, unless otherwise indicated, followed by cooling to 55 °C using compressed air.

If red solution of decane layer is formed after the microwave synthesis, it is separated from the dark-brown IL side product, which settled at the bottom, by a pipet. The sample is precipitated using acetone. The solid is isolated after centrifugation at 5100 rpm for 5 min and suspended in toluene. The precipitation and suspension procedures are repeated two more times, and the NCs are suspended in toluene for characterization. If red/red-brown precipitate is formed after the microwave synthesis, decane layer is separated from the precipitate by a pipet. The precipitate sample is washed with toluene by centrifugation at 5100 rpm for 5 min and suspended in DMSO. Precipitation and the suspension procedures are repeated two more times, and the NCs are suspended in DMSO for characterization.

InP precursor (3 mL) is combined with IL in a Pyrex microwave vessel. The vessel is capped, brought out of the glovebox, and put in the microwave reactor immediately. The mixture is heated to 280 °C at 800 W set-power (SP), unless otherwise mentioned, for a holding time of 15 minutes.

Method I Amounts of BMIm PF_6 IL used are 26 (0.128 mmol), 86 (0.426 mmol), and 172 (0.852 mmol) μL for 1:3, 1:10, and 1:20 ratio reactions of In:IL.

Method II Microwave powers applied to 1:10 reactions using BMIm PF_6 IL are 100, 500, and 800 W.

Method III 0.12 g (0.426 mmol) of BMIm PF_6 IL is used for 1:10 reaction of BMIm PF_6 IL.

Method IV 0.12 g (0.426 mmol) and 0.36 g (1.278 mmol) of BDMIm PF_6 IL is used for 1:10 and 1:30 reactions, respectively for microwave reactions of BDMIm PF_6 IL.

For washing the NCs from the 1:30 reaction, 2 mL MeOH is used for centrifugation at 5100 rpm for 5 min. Brown-red color NCs are stuck to the wall so supernatant is separated for centrifugation in toluene at 5100 rpm for 5 minutes to get a precipitate of red color NCs.

Method V Amounts of BMIm BF_4 IL used were 78 (0.426 mmol), 468 (2.556 mmol), and 780 (4.260 mmol) μL for 1:10, 1:60, and 1:100 ratio reactions of In:IL at 290 °C and 300 W SP.

For washing NCs from these three reactions, EtOH is used instead of acetone.

Conventional synthesis of InP NCs by hot-injection method

Synthesis of InP precursor is same as described above for microwave-assisted synthesis with the only exception is 17 mL freshly degassed 1-ODE is used instead of 50 mL of decane. A 3-necked 20 mL RB flask is attached to Schlenk line and 2 mL of 1-ODE is added to it to degas at 110 °C for 30 minutes. Then under N_2 gas supply, temperature is raised to 300 °C. In a 3 mL syringe, 1 mL of InP precursor and 86 μL of BMIm PF_6 IL are taken together and brought out of glove box and immediately injected rapidly into 1-ODE solvent at 300 °C. During 20-minute reaction, aliquots are collected at different time intervals of 2.5, 5, 10, and 20 minutes into chloroform solvent for absorption and photoluminescence measurements. Obtained solid after the reaction in the flask is collected with a few drops of DMSO after separating supernatant from it. For washing the final NCs, 1 mL of toluene is added to NCs and washed three times at 13.3 krpm for 5 minutes.

Characterization methods

UV-Visible absorption spectroscopy

UV-vis absorption spectroscopy measurements are recorded in either toluene, chloroform, or DMSO in Cary 5000 UV-vis-NIR spectrophotometer. InP NCs from the 1:3 reaction are washed with acetone 2 times by centrifuging for 5 min. at 5k rpm. These NCs are recorded in toluene. NCs

from the 1:10 and 1:20 reaction prior to measurements in DMSO are washed with toluene 2 times by centrifuging for 5 min. at 5k rpm. In some instances of stability studies of NCs from the 1:10 and 1:20 reactions, NCs are washed with a mixture of EtOH (1 mL) and MeOH (0.5 mL) by centrifuging three times for 5 min. at 13.3 krpm at 15 °C.

Photoluminescence spectroscopy

Photoluminescence measurements are recorded in either toluene, chloroform, or DMSO using PTI Quanta Master 400 fluorometer with 405 nm excitation wavelength. InP NCs from the 1:3 reaction are washed with acetone twice by centrifuging for 5 min. at 5k rpm. These NCs are recorded in toluene. NCs from the 1:10 and 1:20 reaction prior to measurements in DMSO are washed with toluene 2 times by centrifuging for 5 min. at 5k rpm. In some instances of stability studies of NCs from the 1:10 and 1:20 reactions, NCs are washed with a mixture of EtOH and MeOH (3:1, volume ratio) by centrifuging three times for 7 min. at 13.3 krpm at 15 °C. Quantum yields are measured with Rhodamine B dye in water as reference by using the following equation.

$$\Phi_{sam} = (\Phi_{ref})\left(\frac{A_{ref}}{A_{sam}}\right)\left(\frac{I_{sam}}{I_{ref}}\right)\left(\frac{\eta_{sam}}{\eta_{ref}}\right)^2$$

where Φ, η, A, and I are quantum yield, refractive index, absorbance, and integrated area of the emission, respectively

Time-corelated single photon counting (TCSPC) measurements

TCSPC measurements are carried out in LifeSpec II, Edinburgh Instruments. TCSPC measurements are recorded with emission detected at 575, 615, and 598 nm for the NCs from 1:3, 1:10, and 1:20 microwave reactions, respectively with 377 nm excitation wavelength. Curve fitting is done by tri-exponential decay in the instrument using F980 spectrometer software. Chi-Square (χ^2) is used to judge goodness of the fit by 1 ± 0.1. The following equation is used to calculate average lifetime (τ_{avg}) of the InP NCs.[13]

$$\tau_{avg} = \frac{\alpha_1\tau_1^2 + \alpha_2\tau_2^2 + \alpha_3\tau_3^2}{\alpha_1\tau_1 + \alpha_2\tau_2 + \alpha_3\tau_3} = f_1\tau_1 + f_2\tau_2 + f_3\tau_3$$

Where τ, α, and f are the lifetime, pre-exponential factor, and fractional contribution of each decay component.

Transmission electron microscopy

TEM images are recorded using an FEI Tecnai G2 Spirit copper BioTWIN microscope. A drop of colloidal NCs solution in either toluene or DMSO solvent is dried on a grid. NCs are washed with a mixture of EtOH and MeOH (2:1, volume ratio) in 2.5 mL micro centrifuge tubes three times at 7 min at 13.3k rpm prior to taking NCs into DMSO solvent. Then, Cu grid of NCs is vacuum dried to evaporate DMSO.

X-ray photoelectron spectroscopy

NCs from 1:10 reaction are washed with a mixture of EtOH and MeOH (2:1, volume ratio) in a 2.5 mL micro centrifuge tube 3 times for 7 min. at 13.3k rpm. After drying the solid for 1 day, NCs are placed on a carbon film to record XPS measurements on PerkinElmer PHI 5400 using achromatic Al Ka radiation (1486.60 eV). 285.0 eV for Carbon (C) element is used as binding energy (BE) standard for charge correction of the substrate and XPS spectra are subjected to Shirley background subtraction.

FT- IR spectroscopy

NCs from the 1:10 and 1:20 reaction are washed with a mixture of EtOH and MeOH (2:1, volume ratio) in 2.5 mL micro centrifuge tubes 3 times for 7 min. at 13.3k rpm. FT-IR measurements of BMIm PF_6 IL, crude InP NCs, and InP NCs after washing from 1:10 and 1:20 reactions are carried out on a Nicolet Nexus 670 FT-IR spectrometer with KBr plates and a Nicolet 380 FT-IR spectrometer using ATR (attenuated total reflection) technique and ZnSe as the crystal.

Zeta potential measurements

NCs are washed with a mixture of EtOH and MeOH (2:1, volume ratio) and filtered through 0.2 μm nylon filter. Zeta potentials are measured in DMSO solvent on a ZetaPALS zeta potential analyzer, Brookhaven Instruments Corporation. Though the solvent DMSO option is not available in the instrument, experiments are still carried out in DMSO since solvent dielectric constant cannot change sign of the zeta potential.

^{1}H, ^{19}F, and ^{31}P NMR measurements

Crude InP NCs from the 1:10 reaction are taken into DMSO-d_6 solvent whereas crude InP NCs of decane layer from 1:100 reaction using BMIm BF_4 are taken into $CDCl_3$ solvent to record ^{1}H, ^{19}F, and ^{31}P NMR spectra on Varian 400 MHz NMR spectrometer.

4.3 Results & Discussion

Microwave reactions with BMIm PF_6 IL are carried out with three different ratios of 1:3, 1:10, and 1:20 (In:IL). Figure 4.1 shows a plot of temperature and power against time for 1:3, 1:10, and 1:20 ratios (Indium to IL). At smaller amounts of IL, the temperature curve is smooth and power curve has smaller magnitude of oscillations. However, as the IL amount increases magnitude of oscillations of temperature and power increases. Figure 4.2 shows absorption and photoluminescence spectra of InP NCs obtained at 1:3, 1:10, and 1:20 ratios. After microwave reaction of 1:10, a red-brown precipitate is formed at the bottom of the vessel separating from decane layer shown in the middle vessel of the photograph in Figure 4.2A. The precipitate is not soluble in toluene but has emission. A red precipitate is observed at higher amount of IL (1:20) as shown in the inset photograph of Figure 4.2A on the right. Precipitates from the 1:10 and 1:20 reactions are dispersible in DMSO (dielectric constant, ε = 46.7) and N,N-DMF (ε = 36.7)

indicating probable coordination of the solvent to NC surface since in other polar solvents like acetonitrile and water the precipitates are dispersible but not optically clear.

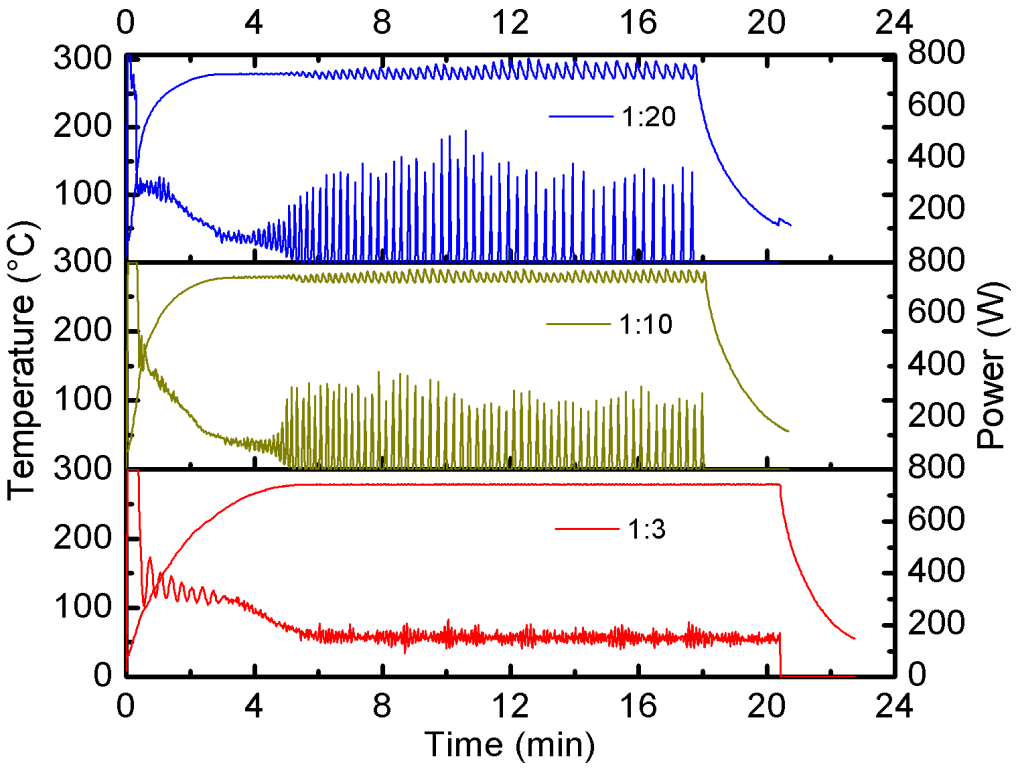

Figure 4.1 Plots of temperature and power vs. time during microwave reactions. Because of the small amount of IL in the reaction mixture for the 1:3 (In:IL) reaction, ramp time to reach 280 °C is around 318 seconds and to complete the reaction is around 1362 seconds. In the beginning of the reaction, applied power is constant at applied 800 W for around 24 seconds and in the later stage smaller power oscillations in between 114 to 224 W from 330 to 1230 seconds are observed. Because the power of the microwave varies to stabilize temperature at reaction temperature. For the 1:10 reaction, ramp time and time to complete the reactions are around 162 and 1248 seconds, respectively. For the 1:20 reaction, ramp time and time to complete the reactions are around 180 and 1248 seconds, respectively. Power is constant at 800 W for 24 seconds and 6 seconds for the 1:10 and 1:20 reactions, respectively. Power oscillates in between 0 to 500 W from 270 seconds

to 1062 seconds for the 1:20 reaction whereas it oscillates from 0 to 370 W for the 1:10 reaction from 270 to 1080 seconds.

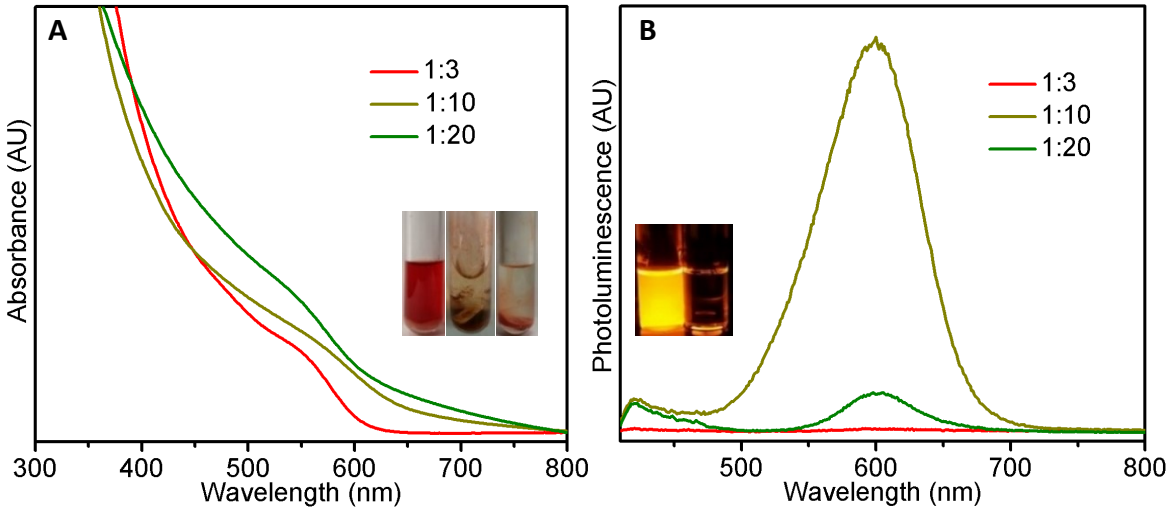

Figure 4.2 UV-Visible absorption (A) and photoluminescence spectra (B) of InP nanocrystals prepared with different amounts of IL, BMIm PF_6. The inset picture in (A) shows NCs dispersed in the decane phase for a 1:3 (In:IL) reaction whereas NCs congregated at the bottom of the reaction vessels for the 1:10 and 1:20 ratios. The inset picture in (B) depicts the dispersibility of InP NCs from a 1:10 ratio reaction in polar solvent (dimethylsulfoxide, DMSO) on the left and congregation in non-polar solvent (toluene) at the bottom of the vessel on the right. Both solutions are under UV light. NCs from the 1:3 reaction have a relatively narrow first absorption feature when compared with spectra of the 1:10 and 1:20 reactions. The PL FWHMs of NCs from the 1:10 and 1:20 reactions are 0.31 and 0.23 eV, respectively. Here, the NCs from 1:10 and 1:20 are washed with toluene only.

The first absorption feature of these NCs in DMSO confirm NC formation and their broad absorption features around 575 and 565 nm from the 1:10 and 1:20 reactions could be due to sample polydispersity of the NCs, which might be due to etching as reported for InP NCs in a post-synthetic HF etching.[15] Since NCs stabilization also takes place by steric effect, IL amount is

reduced to 1:3 (indium to IL) and then a red colored solution of NCs is formed after the reaction as shown in the photograph of Figure 4.2A on the left. The first excitonic peak is centered around 550 nm and the NCs are dispersible in non-polar solvents (toluene and chloroform) only. Lifetimes of individual components and Chi-Square (χ^2) are shown in Appendix B.

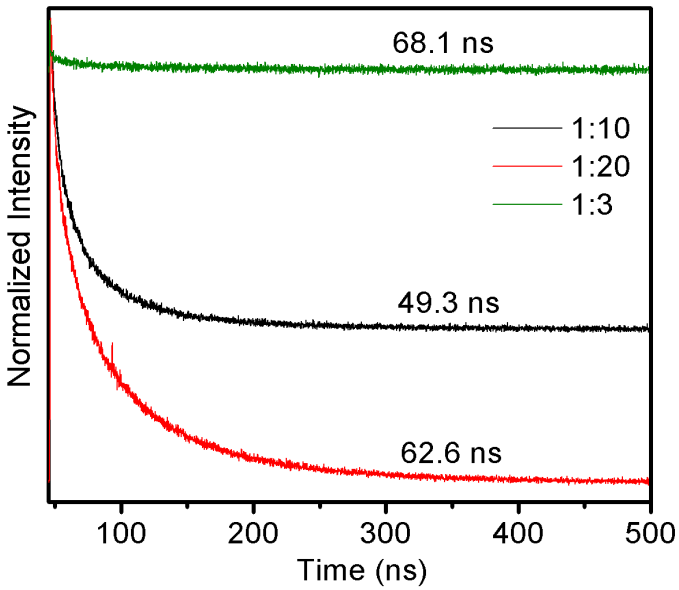

Figure 4.3 Time-corelated single photon counting (TCSPC) measurements of InP NCs synthesized from the 1:3, 1:10, and 1:20 ratio microwave reactions. The average lifetimes for the NCs from the 1:10 and 1:20 reactions are found to be 41.2 ± 8 and 47.3 ± 15 ns, respectively for two batches of samples.

In the photoluminescence spectra of Figure 4.2B, the NCs obtained from the 1:3 reaction have very weak emission with no distinct emission peak. As the amount of IL increases to 1:10 a peak appears around 599 nm. The dispersibility of the NCs changes from non-polar (toluene) to polar (DMSO) solvent suggesting surface modification at higher amounts of IL in the reaction mixture. The inset picture in Figure 4.2B shows the NCs dispersed in DMSO with yellow-orange emission but are not dispersible in toluene. These NCs have a quantum yield of 30% in DMSO with toluene

washing. Upon washing with ethanol and methanol, QY fall below 5%. NCs from the 1:20 reaction have an emission peak around 602 nm and are dispersible in DMSO but not in non-polar solvent (toluene). The emission peak in between 410-450 nm might be due to solvent (DMSO) emission. Time corelated single photon counting (TCSPC) measurements are shown in Figure 4.3.

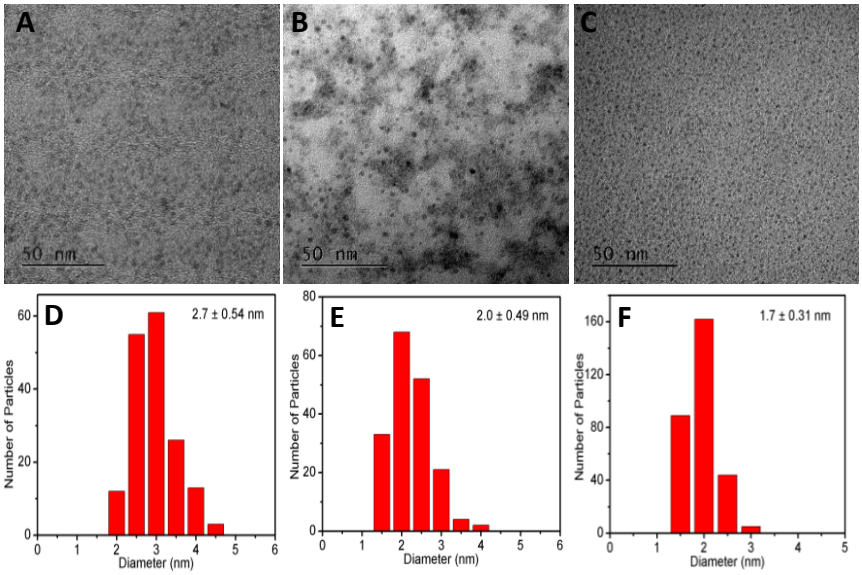

Figure 4.4 TEM images and histograms of InP NCs. NCs are spherical in shape and their diameters are 2.7 ± 0.54 nm (# NPs 170), 2.0 ± 0.49 nm (# NPs 180), and 1.7 ± 0.31 nm (# NPs 300) for 1:3 (A), 1:10 (B), and 1:20 (C) reactions, respectively, indicating decrease of diameter of the NCs as IL amount increases in the reaction mixture. For each microwave reaction under each TEM image respective histogram is shown.

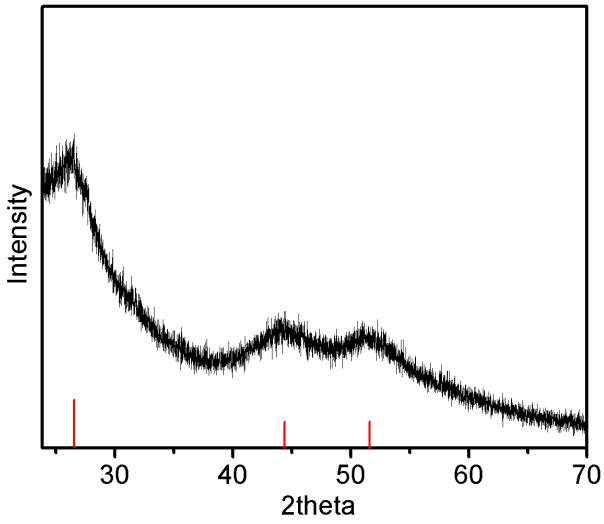

Figure 4.5 X-ray diffraction spectrum of InP NCs obtained from the 1:10 microwave reaction have zinc blende structure. Red lines correspond to bulk InP reflections.

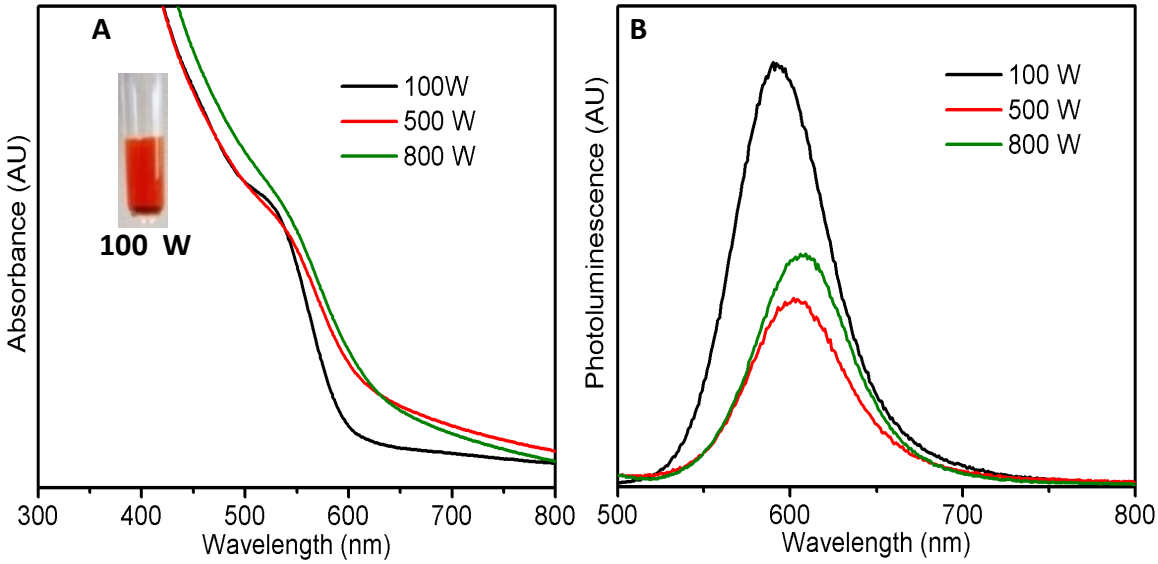

Figure 4.6 UV-Visible absorption (A) and photoluminescence (B) spectra of InP NCs obtained at 100, 500, and 800 W set-powers and 1:10 ratios. NCs are suspended in the decane phase after the MW reaction at 100 W, as shown in the inset of (A). These NCs are dispersible in non-polar solvent like toluene. NCs obtained at higher powers (500 W and 800 W) are suspended in the IL layer and are dispersible in polar solvent (DMSO). NCs are photoluminescent (B).

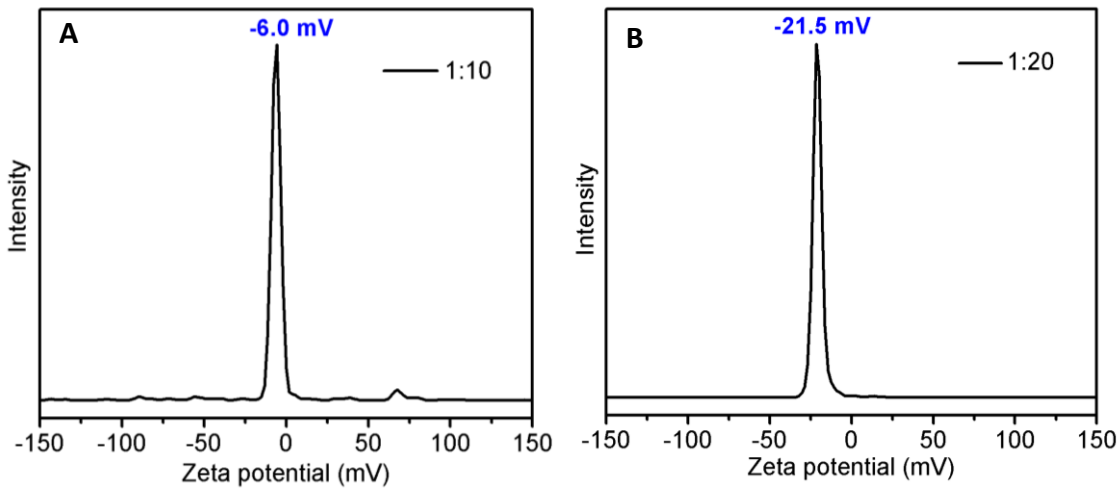

Figure 4.7 Zeta potential measurements of the NCs from the 1:10 (A) and 1:20 (B) reactions, respectively. Negative charges indicate the presence of anions on the NC surface. The average negative charges for the NCs from the 1:10 and 1:20 reactions are found to be -5.0 ± 1 and -17.2 ± 4 mV, respectively for two batches of samples.

TEM images in Figure 4.4A-C show the NCs have spherical shape and as the amount of BMIM PF_6 IL increases, the average size of the NCs is 2.7 ± 0.5, 2.0 ± 0.5, and 1.7 ± 0.3 nm for 1:3 (A), 1:10 (B), and 1:20 (C) reactions. Their histograms are as shown in Figure 4.4. The percent size deviations (% SD) are 40, 49, and 36 for InP NCs from 1:3, 1:10, and 1:20 microwave reactions, respectively. The Crystallinity and zinc blende structure is confirmed by X-ray diffraction as shown in Figure 4.5 for the NCs from the 1:10 reaction. NCs dispersibility can not only be changed by varying IL amount but also does by changing set-power of microwave without altering reaction temperature and IL amount. Figure 4.6 shows absorption and photoluminescence spectra of the NCs synthesized at different SPs 100, 500, and 800 W. NCs prepared after the 100 W microwave reaction are dispersed in decane layer as shown in the picture of absorption spectra. However, NCs are precipitated from the decane layer for 500 and 800 W microwave reactions. Different heating rates of MW reactions might be causing to alter amount of IL decomposing, which in turn led to different degrees of ligand stripping on the NCs surface.

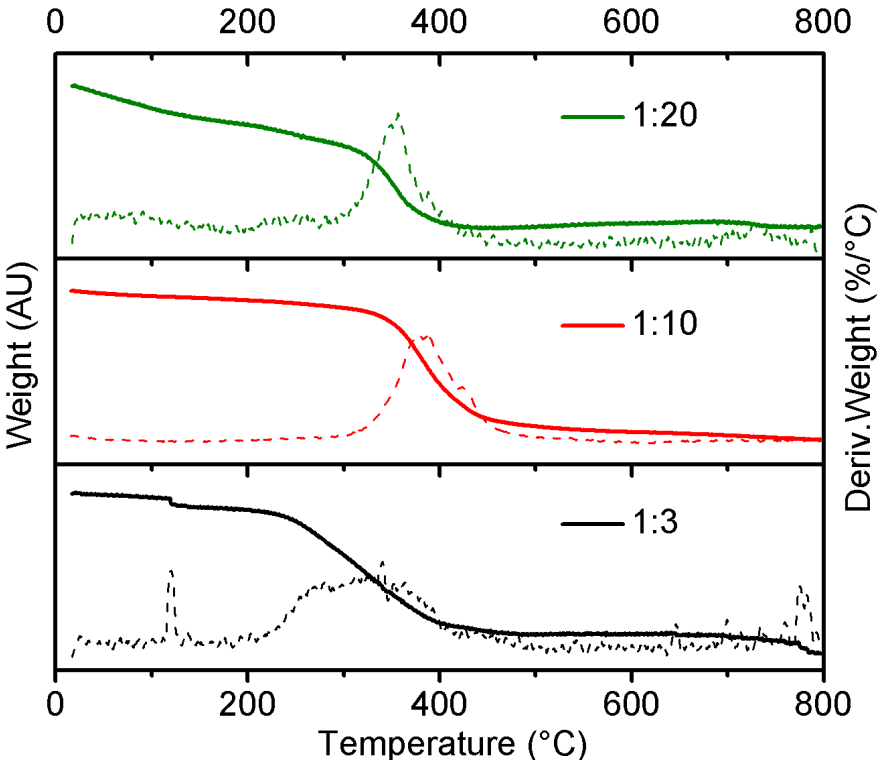

Figure 4.8 Thermogravimetric analysis (TGA) curves of the InP NCs from the 1:3, 1:10, and 1:20 reactions. Derivative curves (of weight percent) are dashed. Predominant mass loss starts above 300 °C for NCs from the 1:10 and 1:20 reactions supporting ionic nature of the ligands on NCs surface. For 1:3 reaction, the mass loss starts above 220 °C as can be seen from the derivative curve. The mass loss above 300 °C might be due to palmitate ligands on NCs surface. Weight loss at 120 °C for the NCs from 1:3 reaction is due to evaporation of toluene adsorbed on the NCs.

Zeta potential measurements are shown in Figure 4.7 for surface characterization. Zeta potentials of the NCs from the 1:10 (A) and 1:20 (B) reactions are -6.0 and -21.5 mV, respectively. The negative values indicate anionic surface due to presence of anions.[2,5,16] Thermogravimetric analysis is also done as shown in Figure 4.8. Weight loss above 300 °C for the NCs supports ionic ligands presence on NC surface.[17] Predominant weight loss of ligands for the NCs from the 1:10 and 1:20 reactions start from around 300 °C, whereas it starts from around 220 °C for the NCs

from the 1:3 reaction. Weight loss above 300 °C for NCs from the 1:3 reaction might be due to ionic ligation of palmitic ligand. Surface of the NCs from the 1:10 and 1:20 reactions have ionic ligands on the surface.

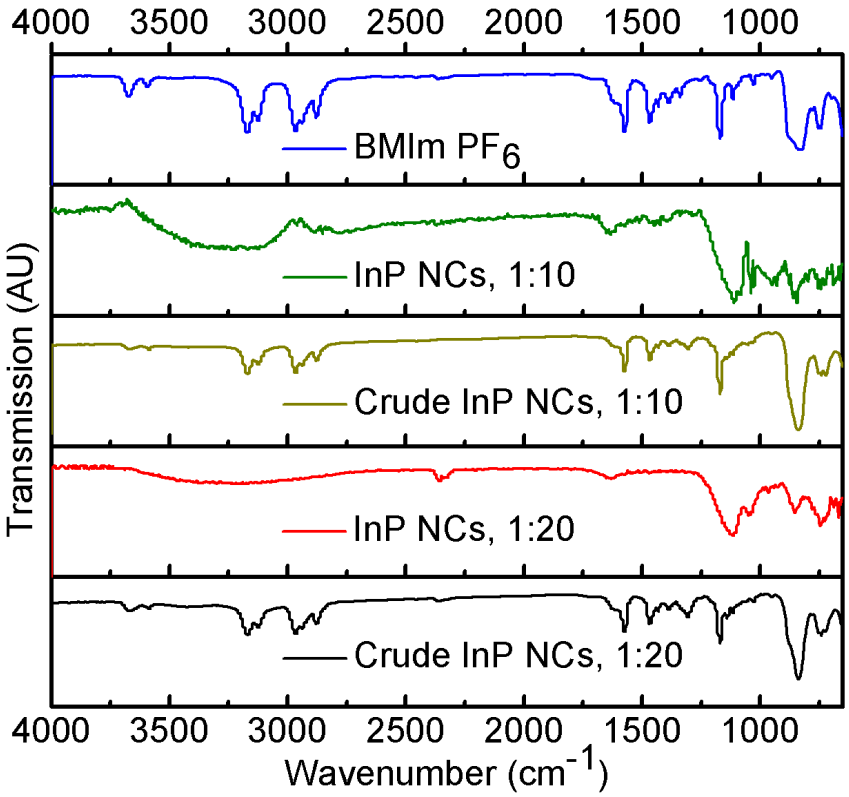

Figure 4.9 Fourier Transform Infrared (FT-IR) spectra of (A) BMIm PF_6, (C & E) crude InP NCs, and (B & D) InP NCs washed with a mixture of ethanol and methanol. C-H stretching in the range 3200-2800 cm^{-1} seen for the crude NCs is absent for the washed InP NCs indicating the absence of PA and BMIm of IL. The intense peak at 838 cm^{-1} corresponds to F-P-F asymmetric stretching of PF_6^- in the crude InP NCs of 1:10 and 1:20 reactions and BMIm PF_6 IL. However, after washing NCs from both the 1:10 and 1:20 reactions with a mixture of methanol and ethanol, the intense peak of F-P-F asymmetric stretching of PF_6^- is absent indicating the absence of the PF_6^- ion. For the washed NCs, broad signals around 3600-2800 cm^{-1} might be due to EtOH and MeOH washing.

FT-IR spectra of the NCs from the 1:10 and 1:20 reactions are shown in Figure 4.9. FT-IR spectra of precipitate (crude NCs) after separating it from the decane phase of the MW reactions exhibit aliphatic and aromatic C-H stretches in the regions 2800-3000 cm^{-1} and 3000-3200 cm^{-1}, respectively, suggesting possibility of BMIm of IL in the crude mixture. To verify if the BMIm of IL is really present, NCs are washed with a mixture of ethanol and methanol. These NCs after washing do not have any peaks corresponding to aliphatic and aromatic C-H stretches showing absence of the BMIm of the IL. As C-H stretches are absent for the washed NCs it can be implied that palmitic ligand is also not present on the surface of the NCs. The intense peak at 838 cm^{-1} correspond to F-P-F asymmetric stretching of PF_6^- in the crude InP NCs of 1:10 and 1:20 reactions and BMIm PF_6 IL.[18] However, after washing NCs from both the 1:10 and 1:20 reactions with mixture of methanol and ethanol, intense peak of F-P-F asymmetric stretching of PF_6^- is absent indicating absence of PF_6^- ion. So, the NCs are getting trapped in the unreacted IL because of ionic surface and settle as precipitate at the bottom of the vessel in the unreacted IL layer after microwave reaction.

NMR spectroscopy is used to characterize the surface of polar NCs in DMSO-d_6. ^1H NMR spectrum in Figure 4.10 shows presence of BMIm of IL for the crude NCs from the 1:10 reaction. Figure 4.11 and Figure 4.12 show ^{19}F and ^{31}P NMR spectra of the crude mixture of NCs from the 1:10 reaction. The resonances at -69.7 and -71.6 ppm in ^{19}F NMR spectrum and at -143.1 ppm as a septet in ^{31}P NMR show presence of PF_6^- ions. The resonances at -77.9 and -80.4 ppm in ^{19}F NMR spectrum and at -14.1 ppm as a triplet in ^{31}P NMR confirm presence of $PO_2F_2^-$ ions,[19] formed from the IL decomposition in the crude NCs mixture. The Peaks at -148.72 and -148.77 ppm in ^{19}F NMR spectrum correspond to BF_4^- formation because of microwave vessel (Pyrex) etching.[20]

These results confirm presence of unreacted BMIM PF_6 IL along with formation of $PO_2F_2^-$ in the crude NCs mixture.

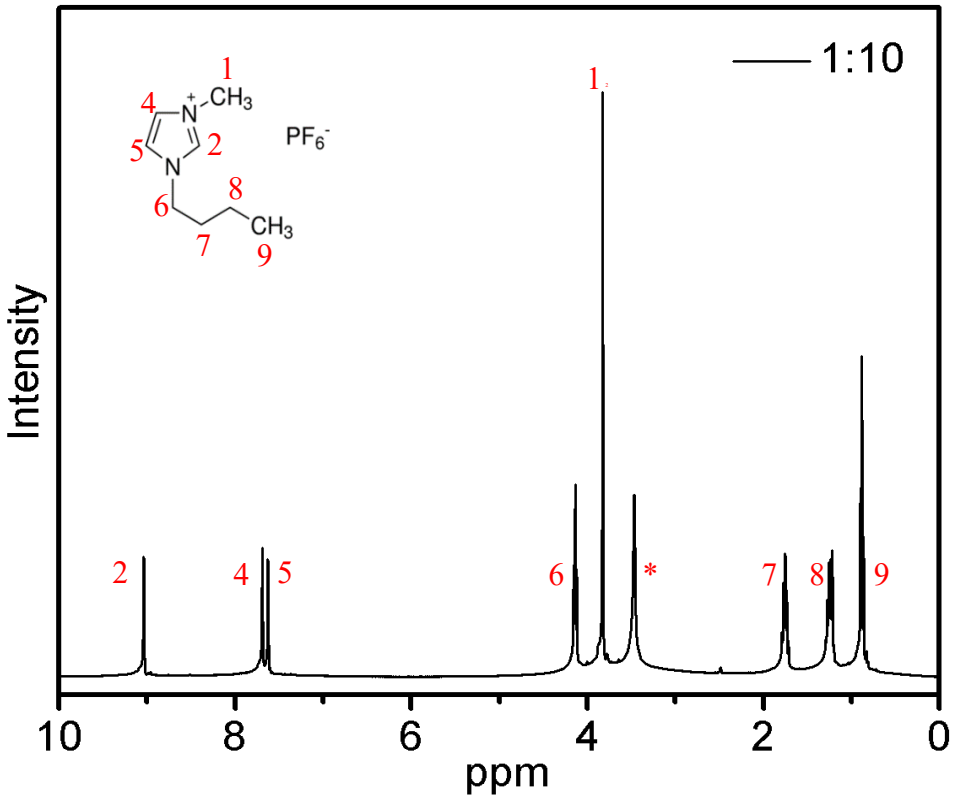

Figure 4.10 ^{1}H NMR spectrum of the crude InP NCs mixture for the 1:10 microwave reaction in DMSO-d6. The presence of peaks at 0.8, 1.2, 1.8, 3.8, 4.1, 7.7, 7.6, and 9.1 ppm indicates unreacted BMIm PF_6 IL is in the crude mixture. A new peak at 3.46 ppm corresponds to a by-product formed after the microwave reaction.

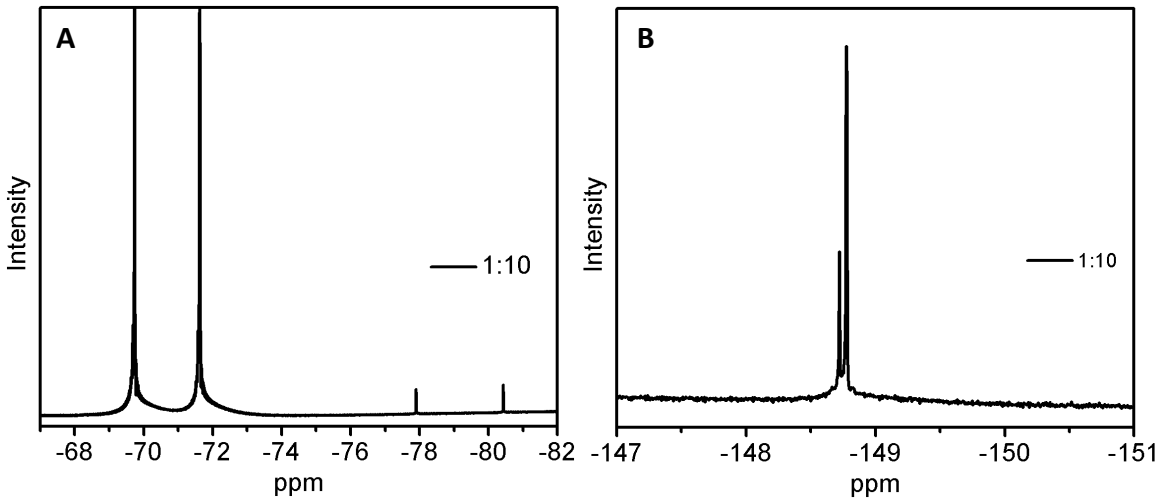

Figure 4.11 ^{19}F NMR spectra of the crude InP NC mixture for the 1:10 microwave reaction in DMSO-d6. The intense peaks at -69.7 and -71.6 ppm correspond to PF_6^- and peaks at -77.9 and -80.4 ppm correspond to $PO_2F_2^-$ in (A). The peaks around -148.8 ppm in (B) correspond to BF_4^-, likely formed from etching of the microwave vessel (Pyrex).

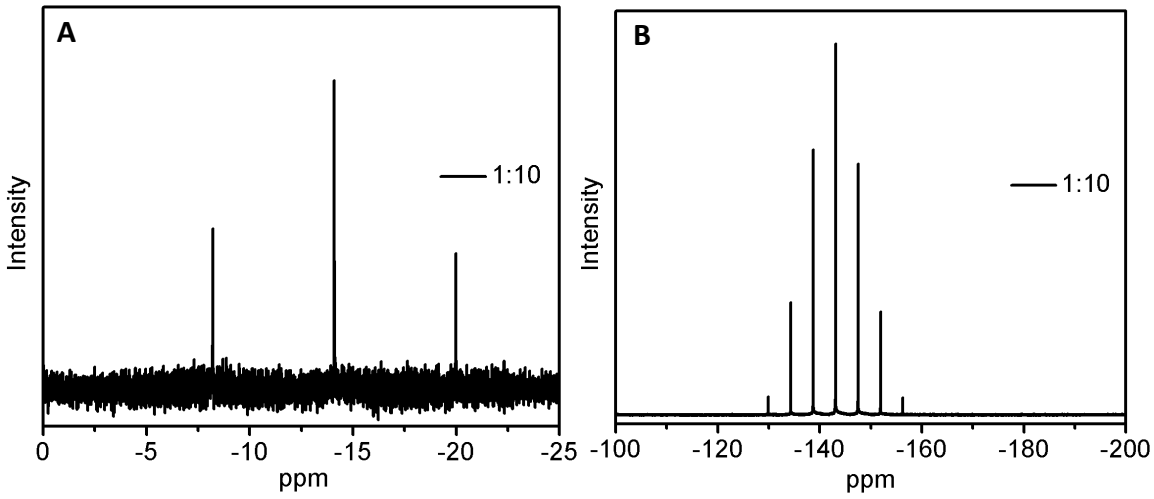

Figure 4.12 ^{31}P NMR spectra of the crude InP NCs mixture for the 1:10 microwave reaction in DMSO-d_6. The intense septet peak at -143.1 ppm in (B) confirms PF_6^- ions and the triplet peak at -14.1 ppm in (A) confirm presence of $PO_2F_2^-$, formed from IL decomposition.

Since the sample used for NMR measurements is the crude NCs and no broadening of any of the NMR signals is observed, the ions identified PF_6^-, BF_4^-, and $PO_2F_2^-$ might be either in the crude InP NCs mixture or in equilibrium with itself present on the NC surface. For NMR measurements with higher concentrations of the crude NCs mixture resulted in NCs getting stuck to wall of the NMR test tube so we had to rely on X-ray photoelectron spectroscopy technique for further surface characterization.

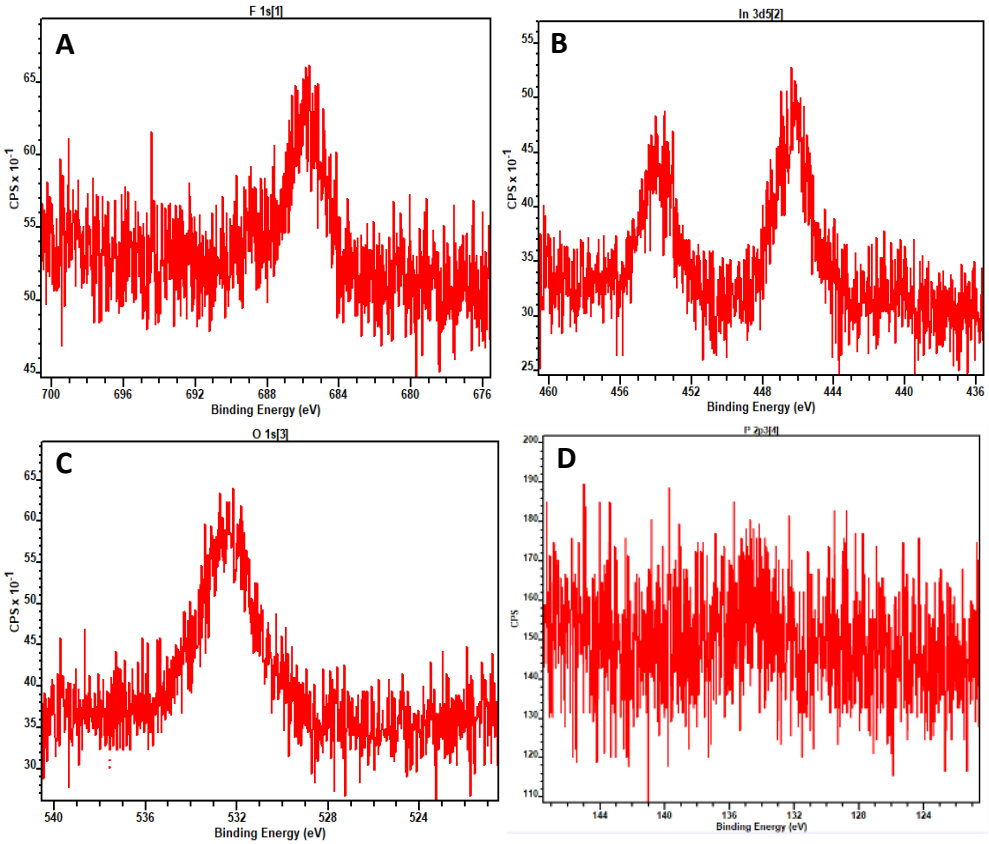

Figure 4.13 X-ray photoelectron spectroscopy (XPS) spectra of F 1s (A), In 3d (B), O 1s (C), and P 2p (D) of washed InP NCs from the 1:10 reaction with a mixture of methanol and ethanol. The main peak at 685.7 eV in the F 1s spectrum corresponds to the $PO_2F_2^-$ ion whereas peaks at 446.2 eV and 532.38 eV correspond to phosphates $(PO_y)_x$ in the In 3d and O 1s spectra, respectively. No significant peak features are observed besides large noise in the P 2p spectrum.

X-ray photoelectron spectroscopy (XPS) is done on the washed InP NCs from the 1:10 reaction by a mixture of ethanol and methanol to remove unreacted IL in the crude mixture and the resulting spectra are shown in Figure 4.13. We could not get any distinguishable peak for the P 2p XPS spectrum. Figure 4.14D shows P 2p XPS spectrum. The main peak in F 1s spectrum (A) at 685.7 eV corresponds to the $PO_2F_2^-$ ion.[21] The two peaks in In 3d (B) at 446.2 eV and 454.1 eV correspond to $3d_{5/2}$ and $3d_{3/2}$ splittings, which might belong to indium binding to phosphate groups, $(PO_y)_x$.[22] In accordance, in O 1s spectrum (C) the peak at 532.4 eV might correspond to phosphates, $(PO_y)_x$.[22] Deconvolutions of all these spectra are not presented because of noise in the observed spectra and hence only main peaks are assigned. Since BE value (687.9 eV) of F in PF_6^- is off from the F1s peak, presence of PF_6^- on NC surface can be eliminated.[23] Owing to the fact that PF_6^- and BF_4^- are soft bases their presence on NC surface can be less likely because In^{3+} is a hard acid. Synthesis of BMIm PO_2F_2 is reported[24] but it's formation can also be ruled out because after washing NCs with alcohols, absence of cationic moiety (BMIm) is observed in FT-IR spectra. So, presence of $PO_2F_2^-$ can be confirmed on the InP NC surface by XPS and ^{19}F and ^{31}P NMR spectroscopy. Hence, PF_6^- peak in ^{19}F NMR spectrum in Figure 4.14 can be attributed to unreacted IL after the MW reaction

Conventional flask synthesis is widely used for synthesis of colloidal semiconductor NCs so it is tested to check feasibility of polar InP NCs synthesis. So, hot-injection method is used as it can yield monodisperse NCs.[25] To synthesize the polar InP NCs, InP precursor and BMIm PF_6 IL are injected together into 1-ODE solvent at 300 °C. A direct evidence of *in situ* ligand stripping for polar InP NCs synthesis is demonstrated. Absorption and photoluminescence spectra of the NCs are shown in Figure 4.14. During the initial stages of the reaction, NCs are dispersible in chloroform. As time goes by, the NCs separate from the chloroform and settle at the bottom of the

vials. They exhibit yellow luminescence under UV light shown inset (A). NCs formed after the reaction are dispersible in DMSO (polar solvent). Their excitonic and emission peaks are shown inside spectra of the absorption and PL spectra, respectively.

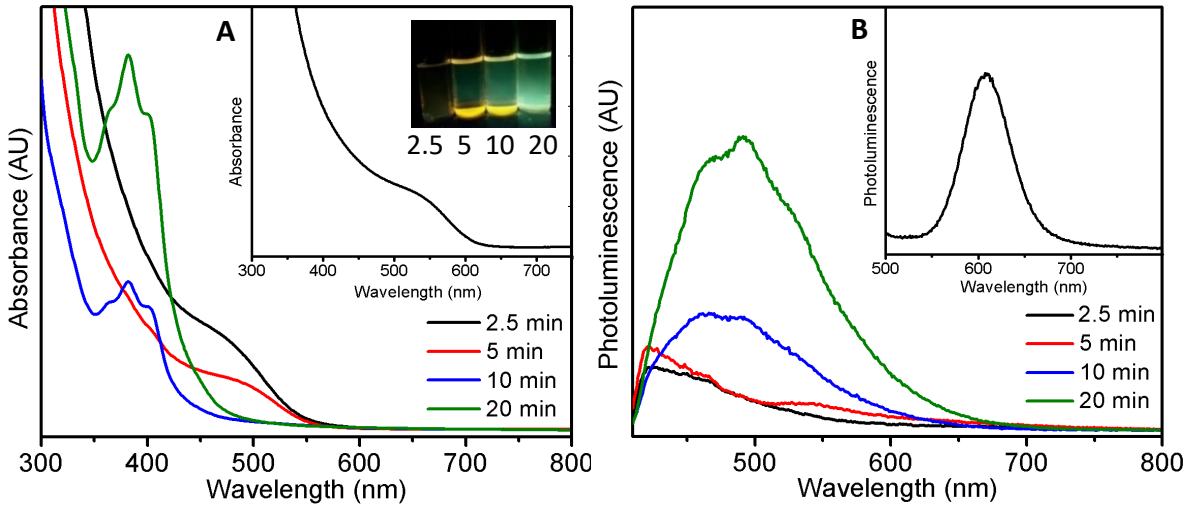

Figure 4.14 UV-Visible absorption (A) and photoluminescence (B) spectra of InP NCs synthesized by hot-injection method. Aliquots collected with the same volume at different time intervals (minutes) in chloroform are shown inset (A). NCs are precipitated for aliquots of 5 and 10 min. By 20 minutes of the reaction, NCs are stuck to wall of the glass flask so they are not collected into 20 min. aliquot. Hence, 20 min. aliquot does not show excitonic and emission feature of InP NCs. Excitonic peak can be observed for 2.5 and 5 min. However, as NCs are settling fast at the bottom of the vial for aliquot of 10 min, excitonic peak is not observed in $CHCl_3$. In the PL spectra, small emission peak corresponding to 5 min. only can be seen around 550 nm. For 10 and 20 min. aliquots, the emission around 500 nm and absorption around 380 nm might be due to by-product(s) of the reaction. Absorption and PL spectrum of InP NCs in DMSO after the reaction are shown inside the absorption and PL spectra, respectively.

Effect of Anion of the IL

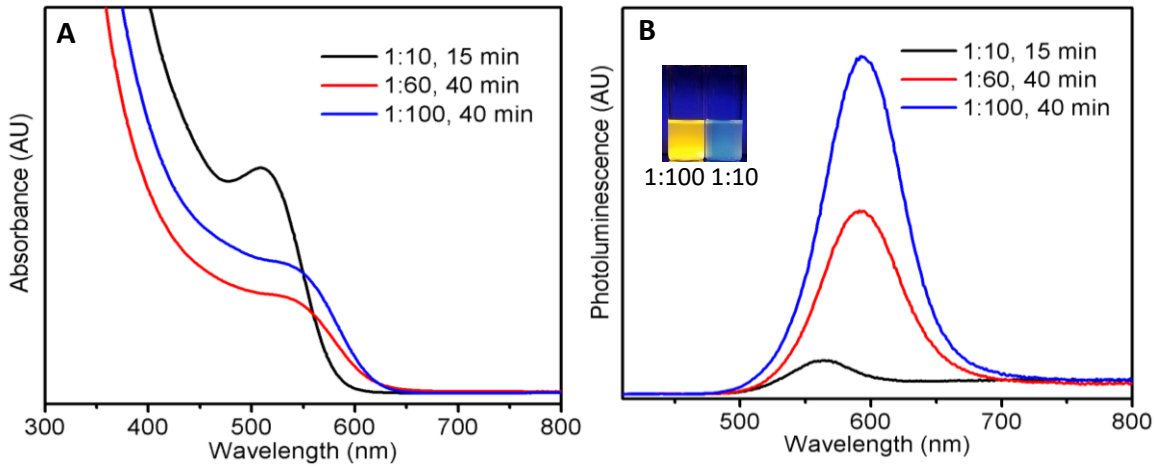

Figure 4.15 UV-Visible absorption (A) and photoluminescence (B) spectra of InP NCs synthesized using BMIm BF_4 IL. Smaller amounts of IL produce a narrow absorption peak, whereas increasing the IL amount leads to a broader absorption as seen by red-shift of the excitonic peak. In the photoluminescence spectra as the IL amount increases, the emission peak red-shifts with FWHM values of 0.26, 0.25, and 0.25 eV for 1:10, 1:60, and 1:100 ratio reactions. Upon washing with ethanol some of the NCs remain in ethanol layer for 1:100 reaction but not for the 1:10 reaction as shown in the inset picture of photoluminescence spectra.

Similar to PF_6^- containing ILs, upon decomposition at high temperatures BF_4^- containing ILs also produce a Lewis acid (BF_3), which could also be responsible for ligand stripping on InP NC surface. So, BMIm BF_4 IL is tested for polar NCs synthesis. Figure 4.15 shows the UV-Vis absorption (A) and photoluminescence (B) spectra of InP NCs synthesized with BMIm BF_4 IL at 290 °C and 300 W with different reaction holding times (HTs) and indium to IL ratios. These conditions are chosen to increase decomposition of the IL and to avoid sparks in reaction mixture so that auto-stopping of the microwave reaction be prevented. As the amount of IL and HT increases, the absorption and emission peaks red shift and excitonic peak broadens whereas increase in IL amount from 1:60 to 1:100 ratio causes very little change in excitonic and emission

peak wavelengths. Though IL amount increased to 1:100 microwave reaction, a red color solution of decane layer is formed after the microwave reaction indicating presence of NCs in decane layer.

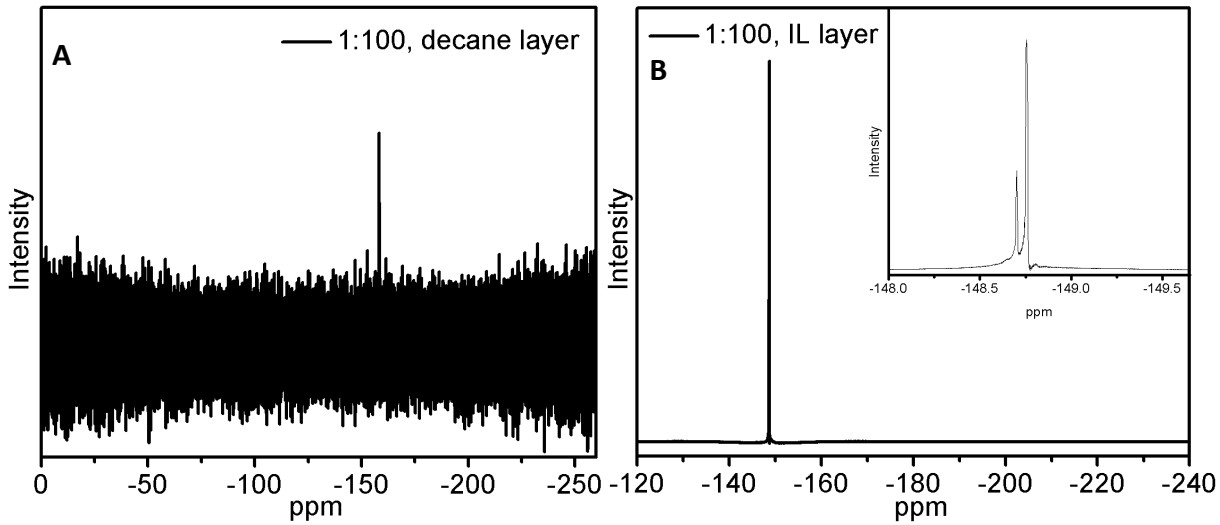

Figure 4.16 ^{19}F NMR spectra of decane layer (A) and IL layer (B) separated from each other after 1:100 microwave reaction of using BMIm BF_4 IL. The peak at -158.4 ppm might be due to $FSiMe_3$ formed during the microwave reaction. The peaks at -148.70 and -148.75 ppm are due to undecomposed BMIm BF_4 IL in the IL layer. In ^{31}P NMR spectra for both decane and IL layers, no peaks are observed.

After precipitating the NCs with EtOH for the 1:100 reaction some of the NCs remain in the EtOH, whereas for the 1:10 reaction none of the NCs go into EtOH as shown in the inset picture of the emission of the EtOH layer under UV radiation showing yellow emission from the 1:100 reaction. This might be due to partial modification of surface of the InP NCs by BMIm BF_4 IL at higher amounts and longer holding times. Probably because of high dissociation energy of B-F bond (613 $KJ.mol^{-1}$) than that of P-F bond (490 $KJ.mol^{-1}$), decompositon of BMIm BF_4 IL may not be high enough to produce polar NCs.

^{19}F NMR spectra for both decane layer and IL layer after the 1:100 microwave reaction are shown in Figure 4.16. In decane layer a fluorinated species, $FSiMe_3$ is observed at -158.4 ppm. In IL layer

no fluorinated species other than BF_4^- at -148.70 and -148.75 ppm is observed. It is reported that surface etching of InP NCs might generate PF_3 species so we recorded ^{31}P NMR spectra for both decane and IL layer and no corresponding peak is observed in any of the two layers. It can be inferred that ligand stripping in microwave reactions using BMIm PF_6 IL is because of PF_3 or PF_5 generated by decomposition of the BMIm PF_6 IL but not from the PF_3 generated after surface etching of the InP NCs. However, we could not identify any species of PF_3 or PF_5 in the crude mixture nor decane layer of InP NCs after the 1:10 microwave reaction using BMIm PF_6 IL.

Scheme 4.2 Probable Mechanism of Ligand Stripping

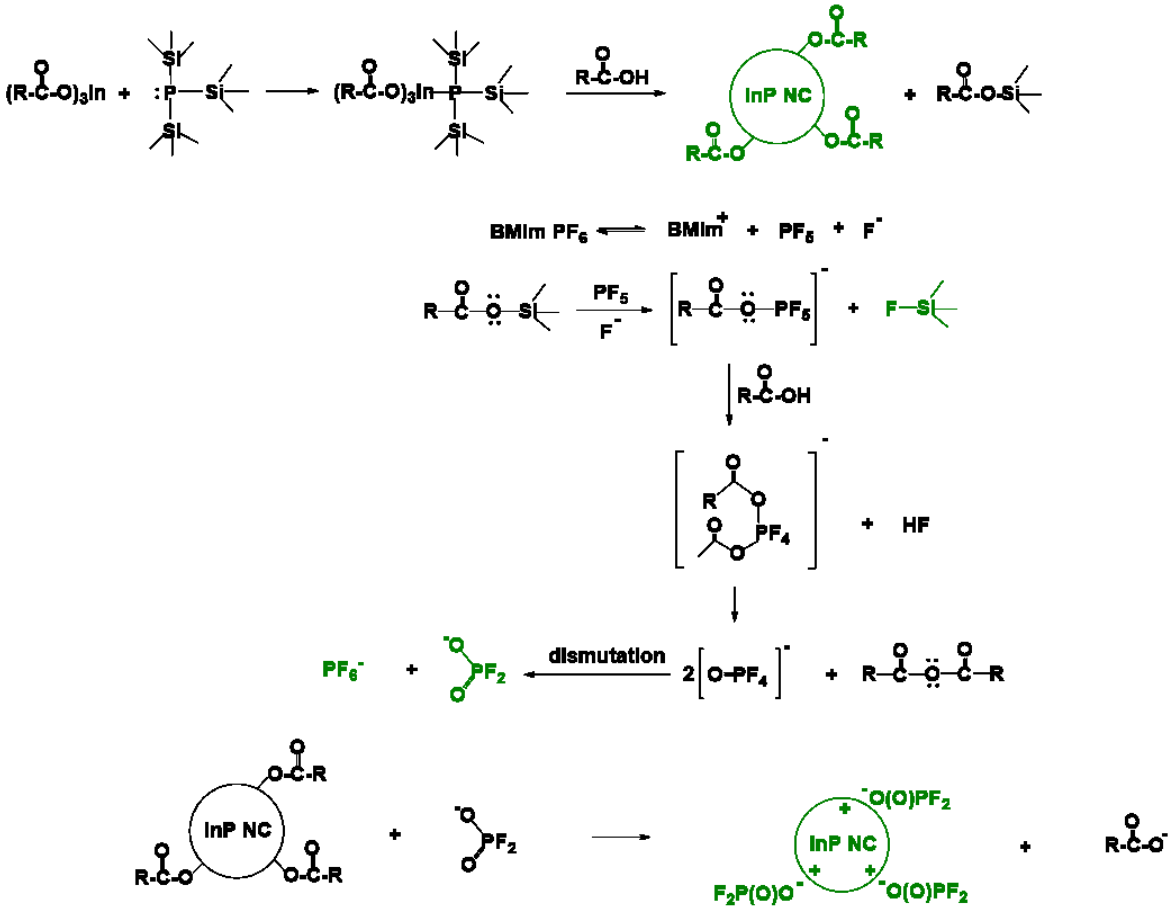

Scheme 4.2 Probable mechanism of ligand stripping depicting $PO_2F_2^-$ ion formation via IL decomposition. Initial palmitic ligands on the surface of the NCs are stripped by $PO_2F_2^-$ ion. Chemical structures shown in green color are identified in the characterization of the InP NCs.

Following this characterization, a mechanism for the polar InP NCs formation via *in situ* ligand stripping is proposed as shown in Scheme 4.2. In this mechanism, an acid-base reaction between indium palmitate (InPA) and tris(trimethylsilyl)phosphine (TMSP) occurs to give a complex.[26] Carboxylic acids are known to break the P-Si bonds so PA forms silylcarboxylates in addition to coordinating with InP NCs.[26] At high temperatures BMIm PF_6 IL will be in equilibrium with Lewis acid, PF_5, and fluoride ion. Because of oxophilic nature of phosphorous, a reaction of silylcarboxylate with PF_5 (Lewis acid) can be predicted to yield trimethylsilylfluoride and an intermediate. As there is excess PA in the reaction mixture, it can extract fluoride from the intermediate, which undergoes intra-molecular bond rearrangement to generate POF_4^- intermediate and HF. The released HF is likely to etch borosilicate glass to produce BF_4^-. POF_4^- is thermally highly unstable and dismutates even at -140 to -130 °C to stable difluorophosphate ($PO_2F_2^-$) and PF_6^-.[19] Had $PO_2F_2^-$ ion formed by hydrolysis of PF_6^-, there would have been further hydrolysis of difluorophosphate to give monofluorophosphate. So, $PO_2F_2^-$ generation takes place via decomposition of the IL. In the final step, the $PO_2F_2^-$ strips carboxylate ligand on the NC surface to end up on the NC surface.

Reproducibility & Stability

Reproducibility data of InP NCs synthesized at two different ratios 1:10 and 1:20 are shown in Figure 4.17. Since absorptions and photoluminescence spectra of the NCs is broad, scattered plot of the reproducibility data is not shown but instead absorption and photoluminescence curves are compared. Absorption curves are located around 570 nm for both NCs from the 1:10 and 1:20 reactions and their broad absorption nature makes it difficult to compare from one batch to another batch synthesis. From photoluminescence spectra, a better comparison can be made. Emission peaks are located at 600 (FWHM, 0.31 eV or 88 nm), 608 (FWHM, 0.22 eV or 65 nm), and 591

(FWHM, 0.25 eV or 72 nm) nm for NCs from the 1:10 reaction whereas they are observed at 602 (FWHM, 0.23 eV or 70 nm), 613 (FWHM, 0.21 eV or 67 nm), and 569 (FWHM, 0.34 eV or 85 nm) nm for NCs from the 1:20 reaction. In other words, for two batch sets emission peak wavelengths are little higher for NCs from the 1:20 reaction than that of the 1:10 reaction. In all cases the NCs are associated with higher FWHMs values indicating broad size distribution. To sum up, polar NCs from the 1:10 and 1:20 microwave reactions can be reproduced with some deviations in the absorption and emission.

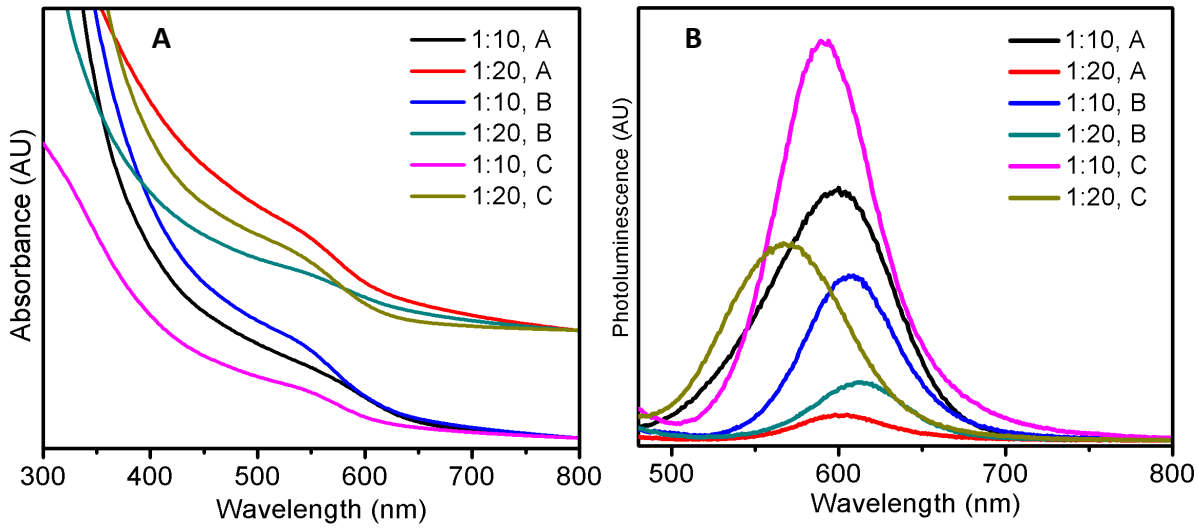

Figure 4.17 Reproducibility data of the polar InP NCs synthesis. UV-Visible absorption (A) and photoluminescence (B) spectra. Absorption peaks are broad for polar NCs and are located at wavelength regions around 570 nm. Emission peaks are located closely for NCs from the 1:10 reaction however, for NCs from the 1:20 reactions, emission peak is deviating by higher wavelength difference (30 nm) for one batch. Labels A, B, and C in the spectra denote different batches of NCs synthesis.

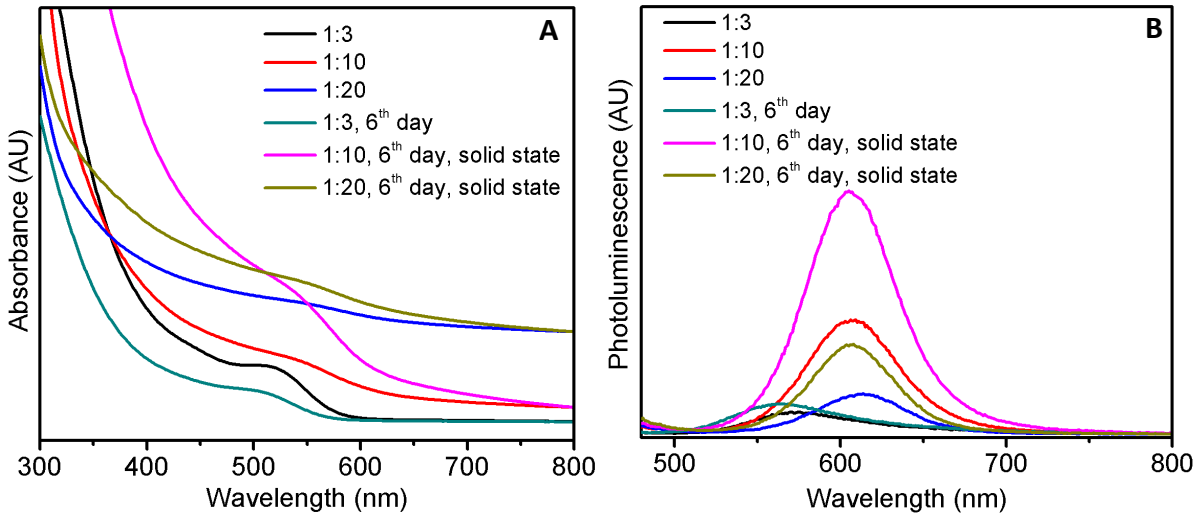

Figure 4.18 Stability of the InP NCs in solid state. UV-Vis absorption (A) and photoluminescence spectra (B) of InP NCs. After washing NCs with a mixture of methanol and ethanol, polar InP NCs stored in solid state have deviations in absorption but emission peaks appear to have similar features after 6 days. NCs from the 1:3 reaction are stored in colloidal form in toluene only and their absorption and emission features are distorted.

Stability of the NCs is compared both in solid state and colloidal form. Figure 4.18 shows absorption (A) and photoluminescence (B) spectra of the NCs stored in solid state after washing with a mixture of methanol and ethanol. For polar NCs, absorption features have deviations on sixth day. In emission spectra the differences can be seen easily. NCs from the 1:10 reaction have similar emission features whereas NCs from the 1:20 reaction have little blue shift in the emission peak on sixth day. Figure 4.19 shows absorption (A) and photoluminescence (B) spectra of the NCs stored in colloidal form in DMSO after washing with a mixture of methanol and ethanol. NCs from both the 1:10 reaction and 1:20 reaction lose absorption and emission features significantly by 6 days indicating instability of the polar NCs in DMSO after washing with methanol and ethanol mixture. It could be probably because of oxidation of the NCs surface by alcohols or replacing the

$PO_2F_2^-$ ion on the NCs surface. It is reported that short chain alcohols strip carboxylate ligands on CdSe and PbSe NCs and quench their luminescence[27] and extensive washing of InP NCs with ethanol can partially remove TOPO-TOP ligands from the surface[28]. The changes in absorption and emission features are not observed to the same extent in solid state because after washing with alcohols, alcohols present on the NCs surface might be evaporated because of low boiling temperatures.

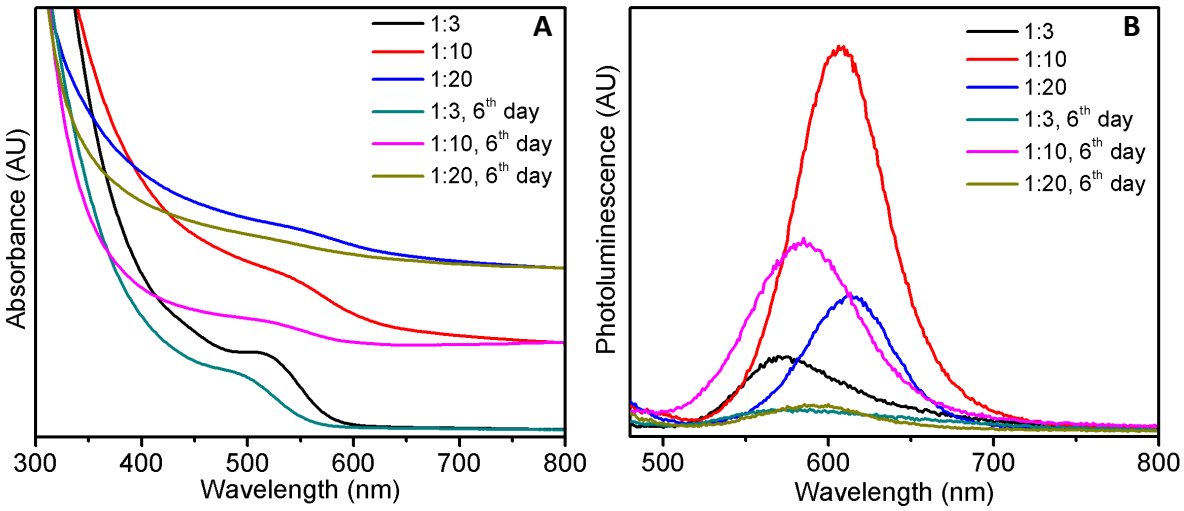

Figure 4.19 Stability of the InP NCs in colloidal form. UV-Visible absorption (A) and photoluminescence spectra (B) of InP NCs. After washing NCs with mixture of methanol and ethanol, NCs are stored in DMSO solvent. NCs lose absorption and emission features significantly after 6 days with loss in intensity indicating instability in colloidal form after washing with mixture of methanol and ethanol.

Figure 4.20 shows absorption and photoluminescence spectra of InP NCs from the 1:10 and 1:20 reactions. Here, NCs are not subjected to any kind of alcohol washing and stored in DMSO as colloidal form for about one year. After 360 days, NCs from the 1:10 reaction lose their absorption and emission features significantly. However, NCs from the 1:20 reaction still retain the absorption and emission features with blue shift and loss in intensity probably because of more

electrostatically stabilized surface. The blue shift is 20 and 15 nm in absorption and emission spectra, respectively. From all the stability studies it can be concluded that polar NCs from the 1:20 reaction retain colloidal stability in DMSO if they are not washed with alcohols. In contrast, if polar NCs are washed with alcohols, they will lose their absorption and emission features within 6 days. However, if NCs are stored in solid state even after washing with alcohols they will retain their absorption and emission features to some extent in the solid state.

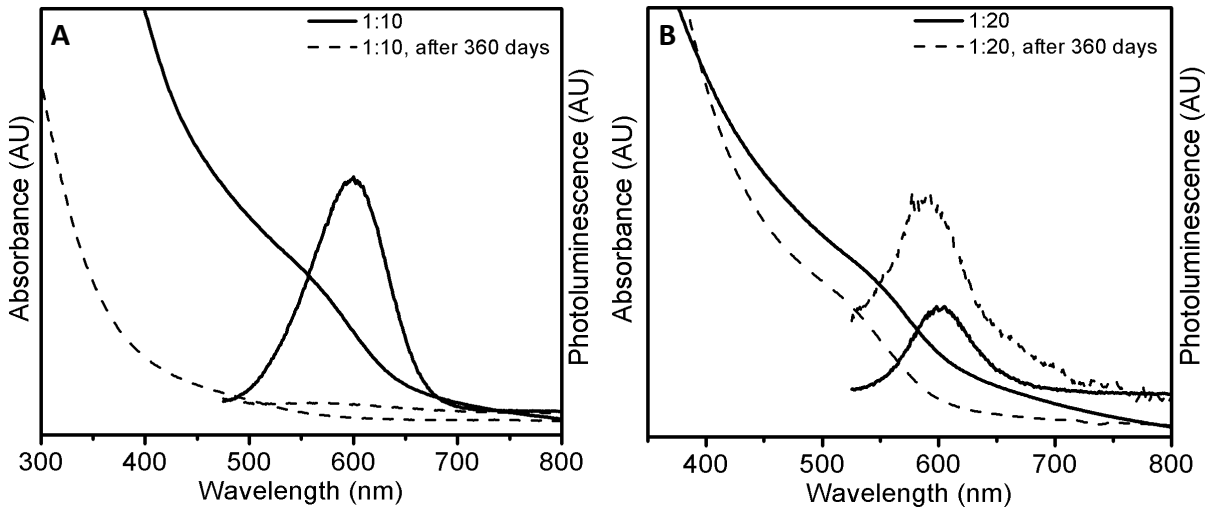

Figure 4.20 Stability studies of InP NCs stored in colloidal form in DMSO without washing with mixture of MeOH and EtOH. UV-Visible absorption and photoluminescence spectra of InP NCs compared after 360 days (dashed curves) from the 1:10 (A) and 1:20 (B) reactions. NCs from the 1:10 reaction lose absorption and emission features almost completely after 360 days whereas NCs from the 1:20 reaction retain absorption and emission features, but with a blue shift of 20 and 15 nm in absorption and emission, respectively with loss of intensity.

Effect of Cations of the IL

Having synthesized polar InP NCs using imidazolium based hexafluorophosphate IL, BMIm PF_6, it prompted us to examine effect of other counter-cations of PF_6 IL on the polar NCs synthesis by microwave-assisted method. Figure 4.21 shows absorption and photoluminescence spectra of InP NCs synthesized with BMPy PF_6, BDMIm PF_6, and BMIm PF_6 ionic liquids with 1:10 ratio of

In:IL. A narrow absorption feature is observed for BDMIm PF_6, which produces InP NCs dispersed in decane solvent after the reaction as shown in the middle vessel of the inset picture in Figure 4.21A. TGA plot is shown in Figure 4.22 for BDMIm PF_6 and BMIm PF_6 to compare their thermal stability. 99% of the BMIm PF_6 IL decomposes by 400 °C, whereas only 81% of the BDMIm PF_6 IL decomposes even at 800 °C denoting its high decomposition temperatures although its decomposition starts lower than that of BMIM PF_6. Although it does not necessarily

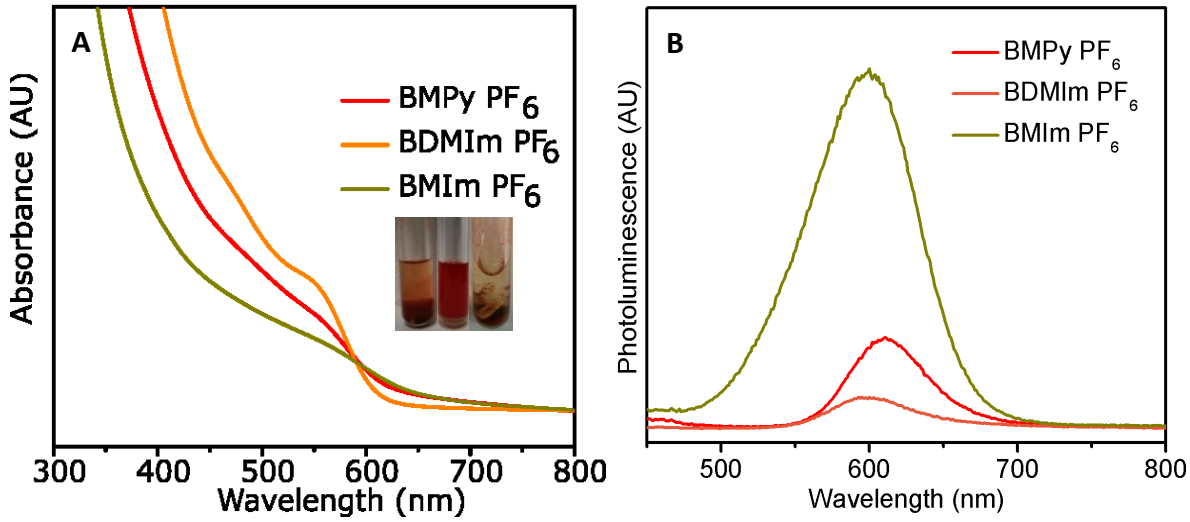

Figure 4.21 UV-Visible absorption (A) and photoluminescence (B) spectra of InP NCs synthesized using different PF_6^- containing ionic liquids. Similar to the BMIm PF_6 IL, BMPy PF_6 yielded a precipitate of NCs (inset, A) at 280 °C dispersible in DMSO. However, BDMIm PF_6 produces NCs dispersed in the decane layer as shown in the inset photo. NCs from the BDMIm PF_6 reaction have relatively narrow absorption peak whereas NCs from the BMPy PF_6 and BMIm PF_6 reactions have broad absorptions peaks. NCs from these three reactions have emission peak around 600 nm with FWHM values of 0.21, 0.22, and 0.31 eV for the BMPy PF_6, BDMIm PF_6 IL, and BMIm PF_6 IL, respectively.

mean same decomposition temperatures in InP NCs synthesis for these two ILs, absence of acidic proton at C2 position might also be a reason for high decomposition temperature of BDMIm PF_6 IL. Probably because of high decomposition temperature of BDMIm PF_6 IL, there might be lower ligand stripping leading the NCs to have dispersibility in toluene only. To test if polar NCs can be

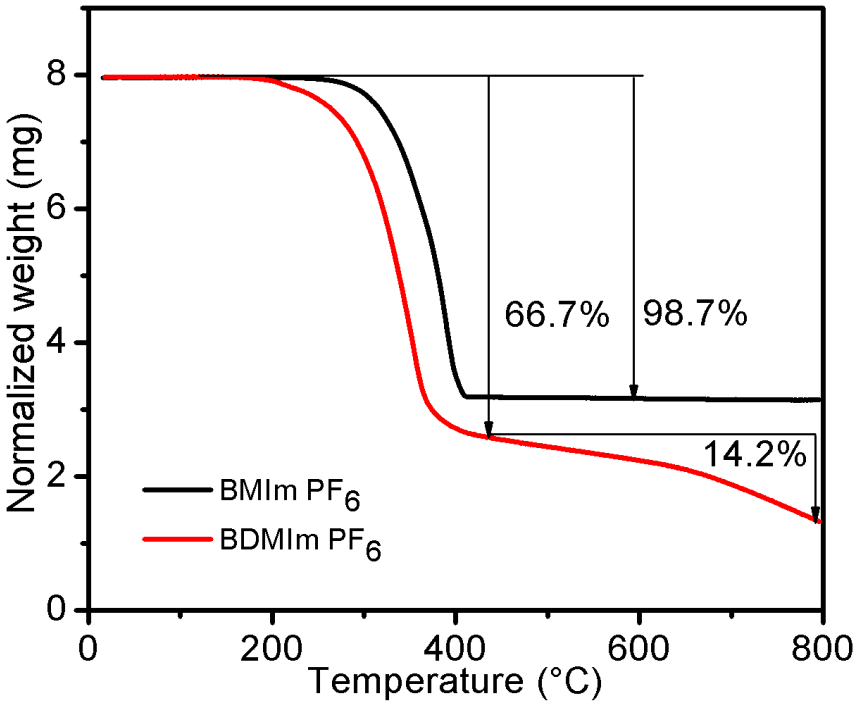

Figure 4.22 Thermogravimetric analysis (A) of BMIm PF_6 and BDMIm PF_6. Most (99%) of the BMIm PF_6 IL decomposes by 400 °C, whereas only 81% of the BDMIm PF_6 IL decomposes, even at 800 °C.

synthesized, amount of BDMIm PF_6 is increased to do a microwave reaction with a ratio of 1:30 of In:IL. Absorption and photoluminescence spectra of the NCs synthesized are shown in Figure 4.23. After washing the NCs, spectra are recorded in DMSO. The NCs obtained are of two different solids of colors brown-red and red, which are dispersible in DMSO. In addition, InP NCs synthesized using BMPy PF_6 IL at 280 °C and 800 W have a majority of the NCs settling at bottom of the vessel with a broad excitonic peak as shown in Figure 4.21A. FWHMs for the NCs from

BMPy PF_6 and BMIm PF_6 reactions are found to be 0.21 and 0.31 eV, respectively in Figure 4.21B. In our previous work it is shown that MW reaction using BMPy PF_6 IL at lower temperature (260 °C and 150 W) yielded InP NCs dispersible in toluene.[14]

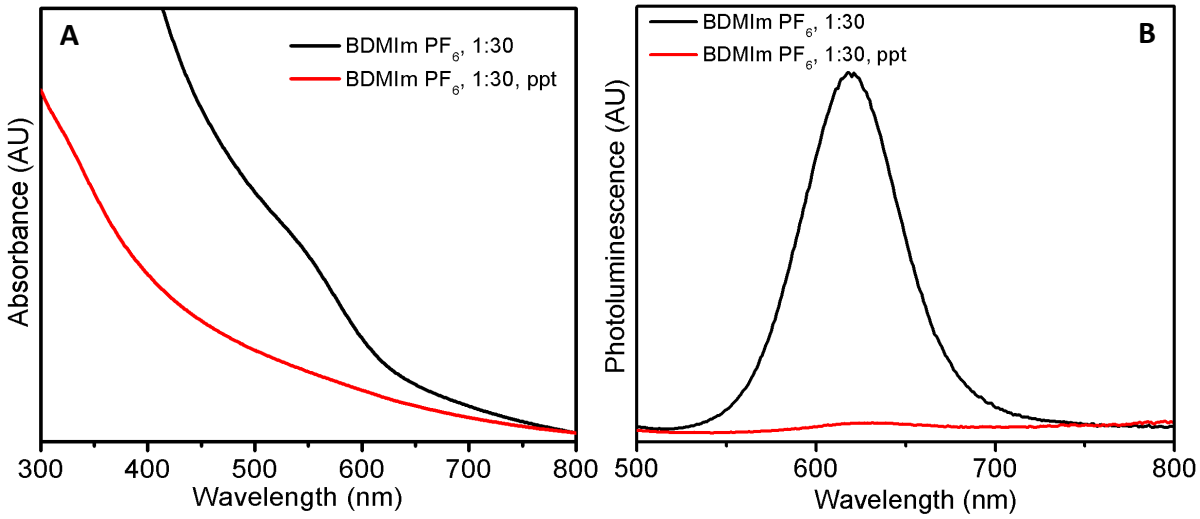

Figure 4.23 Absorption (A) and photoluminescence (B) spectra of red and red-brown precipitate of InP NCs in DMSO synthesized from 1:30 reaction using BDMIm PF_6 IL. Red precipitate of NCs has broad absorption peak (black curve) whereas red-brown precipitate has no absorption peak (red curve). Red precipitate of NCs has distinct emission peak around 625 nm whereas red-brown precipitate of NCs has a very little hump around 630 nm.

4.4 Summary

Polar InP NCs are synthesized via *in situ* ligand stripping by microwave-assisted method. NCs dispersibility changes from toluene to DMSO by varying amount of BMIM PF_6 IL in reaction mixture. Polar NCs have broad absorption features though their size distribution improves as IL amount increases. Negative zeta potentials confirm presence of anions on the NC surface. Presence of $PO_2F_2^-$ is identified by ^{19}F and ^{31}P NMR and XPS spectroscopy and a probable mechanism of *in situ* ligand stripping is proposed. In situ ligand stripping is confirmed by conventional hot-injection method. Polar NCs can also be synthesized by other PF_6^- containing ILs, BMPy PF_6 and

BDMIm PF_6. BMIm BF_4 IL could not produce polar NCs but is partially modifying the surface even at higher amounts of the IL and longer holding times. The synthesized polar NCs can pave a way for other polar semiconductor NCs synthesis of InAs and InSb by *in situ* ligand stripping. Synthesized NC materials can have potential applications in optoelectronics.

4.5 References

(1) Boles, M. A.; Ling, D.; Hyeon, T.; Talapin, D. V. The Surface Science of Nanocrystals. *Nat. Mater.* **2016**, *15* (2), 141–153.

(2) Liu, W.; Lee, J.-S.; Talapin, D. V. III–V Nanocrystals Capped with Molecular Metal Chalcogenide Ligands: High Electron Mobility and Ambipolar Photoresponse. *J. Am. Chem. Soc.* **2013**, *135* (4), 1349–1357.

(3) Zhang, H.; Jang, J.; Liu, W.; Talapin, D. V. Colloidal Nanocrystals with Inorganic Halide, Pseudohalide, and Halometallate Ligands. *ACS Nano* **2014**, *8* (7), 7359–7369.

(4) Nag, A.; Kovalenko, M. V.; Lee, J.-S.; Liu, W.; Spokoyny, B.; Talapin, D. V. Metal-Free Inorganic Ligands for Colloidal Nanocrystals: S^{2-}, HS^{-}, Se^{2-}, HSe^{-}, Te^{2-}, HTe^{-}, TeS_3^{2-}, OH^{-}, and NH^{2-} as Surface Ligands. *J. Am. Chem. Soc.* **2011**, *133* (27), 10612–10620.

(5) Dirin, D. N.; Dreyfuss, S.; Bodnarchuk, M. I.; Nedelcu, G.; Papagiorgis, P.; Itskos, G.; Kovalenko, M. V. Lead Halide Perovskites and Other Metal Halide Complexes As Inorganic Capping Ligands for Colloidal Nanocrystals. *J. Am. Chem. Soc.* **2014**, *136* (18), 6550–6553.

(6) Zhang, H.; Dasbiswas, K.; Ludwig, N. B.; Han, G.; Lee, B.; Vaikuntanathan, S.; Talapin, D. V. Stable Colloids in Molten Inorganic Salts. *Nature* **2017**, *542* (7641), 328–331.

(7) Roberge, A.; Stein, J. L.; Shen, Y.; Cossairt, B. M.; Greytak, A. B. Purification and In Situ Ligand Exchange of Metal-Carboxylate-Treated Fluorescent InP Quantum Dots via Gel Permeation Chromatography. *J. Phys. Chem. Lett.* **2017**, *8* (17), 4055–4060.

(8) Mnoyan, A. N.; Kirakosyan, A. G.; Kim, H.; Jang, H. S.; Jeon, D. Y. Electrostatic Stabilized InP Colloidal Quantum Dots with High Photoluminescence Efficiency. *Langmuir* **2015**, *31* (25), 7117–7121.

(9) Talapin, D. V.; Gaponik, N.; Borchert, H.; Rogach, A. L.; Haase, M.; Weller, H. Etching of Colloidal InP Nanocrystals with Fluorides: Photochemical Nature of the Process Resulting in High Photoluminescence Efficiency. *J. Phys. Chem. B* **2002**, *106* (49), 12659–12663.

(10) Lovingood, D. D.; Strouse, G. F. Microwave Induced In-Situ Active Ion Etching of Growing InP Nanocrystals. *Nano Lett.* **2008**, *8* (10), 3394–3397.

(11) Doris, S. E.; Lynch, J. J.; Li, C.; Wills, A. W.; Urban, J. J.; Helms, B. A. Mechanistic Insight into the Formation of Cationic Naked Nanocrystals Generated under Equilibrium Control. *J. Am. Chem. Soc.* **2014**, *136* (44), 15702–15710.

(12) Gerbec, J. A.; Magana, D.; Washington, A.; Strouse, G. F. Microwave-Enhanced Reaction Rates for Nanoparticle Synthesis. *J. Am. Chem. Soc.* **2005**, *127* (45), 15791–15800.

(13) Lakowicz, J. R. *Principles of Fluorescence Spectroscopy*, 3rd ed.; Springer US, 2006.

(14) Siramdas, R.; McLaurin, E. J. InP Nanocrystals with Color-Tunable Luminescence by Microwave-Assisted Ionic-Liquid Etching. *Chem. Mater.* **2017**, *29* (5), 2101–2109.

(15) Li, C.; Ando, M.; Murase, N. Facile Preparation of Highly Luminescent InP Nanocrystals by a Solvothermal Route. *Chem. Lett.* **2008**, *37* (8), 856–857.

(16) Kovalenko, M. V.; Scheele, M.; Talapin, D. V. Colloidal Nanocrystals with Molecular Metal Chalcogenide Surface Ligands. *Science* **2009**, *324* (5933), 1417–1420.

(17) Shen, Y.; Gee, M. Y.; Tan, R.; Pellechia, P. J.; Greytak, A. B. Purification of Quantum Dots by Gel Permeation Chromatography and the Effect of Excess Ligands on Shell Growth and Ligand Exchange. *Chem. Mater.* **2013**, *25* (14), 2838–2848.

(18) Talaty, E. R.; Raja, S.; Storhaug, V. J.; Dölle, A.; Carper, W. R. Raman and Infrared Spectra and Ab Initio Calculations of C2-4MIM Imidazolium Hexafluorophosphate Ionic Liquids. *J. Phys. Chem. B* **2004**, *108* (35), 13177–13184.

(19) Christe, K. O.; Dixon, D. A.; Schrobilgen, G. J.; Wilson, W. W. Tetrafluorophosphate Anion. *J. Am. Chem. Soc.* **1997**, *119* (17), 3918–3928.

(20) Gelmboldt, V. O.; Ganin, E. V.; Fonari, M. S.; Simonov, Y. A.; Koroeva, L. V.; Ennan, A. A.; Basok, S. S.; Shova, S.; Kählig, H.; Arion, V. B.; et al. Two New “onium” Fluorosilicates, the Products of Interaction of Fluorosilicic Acid with 12-Membered Macrocycles: Structures and Spectroscopic Properties. *Dalton Trans.* **2007**, *0* (27), 2915–2924.

(21) Yang, G.; Shi, J.; Shen, C.; Wang, S.; Xia, L.; Hu, H.; Luo, H.; Xia, Y.; Liu, Z. Improving the Cyclability Performance of Lithium-Ion Batteries by Introducing Lithium Difluorophosphate (LiPO2F2) Additive. *RSC Adv.* **2017**, *7* (42), 26052–26059.

(22) Faur, M.; Faur, M.; Jayne, D. T.; Goradia, M.; Goradia, C. XPS Investigation of Anodic Oxides Grown on P-Type InP. *Surf. Interface Anal.* **1990**, *15* (11), 641–650.

(23) Dedryvère, R.; Leroy, S.; Martinez, H.; Blanchard, F.; Lemordant, D.; Gonbeau, D. XPS Valence Characterization of Lithium Salts as a Tool to Study Electrode/Electrolyte Interfaces of Li-Ion Batteries. *J. Phys. Chem. B* **2006**, *110* (26), 12986–12992.

(24) Matsumoto, K.; Hagiwara, R. A New Series of Ionic Liquids Based on the Difluorophosphate Anion. *Inorg. Chem.* **2009**, *48* (15), 7350–7358.

(25) de Mello Donegá, C.; Liljeroth, P.; Vanmaekelbergh, D. Physicochemical Evaluation of the Hot-Injection Method, a Synthesis Route for Monodisperse Nanocrystals. *Small Weinh. Bergstr. Ger.* **2005**, *1* (12), 1152–1162.

(26) Gary, D. C.; Glassy, B. A.; Cossairt, B. M. Investigation of Indium Phosphide Quantum Dot Nucleation and Growth Utilizing Triarylsilylphosphine Precursors. *Chem. Mater.* **2014**, *26* (4), 1734–1744.

(27) Hassinen, A.; Moreels, I.; De Nolf, K.; Smet, P. F.; Martins, J. C.; Hens, Z. Short-Chain Alcohols Strip X-Type Ligands and Quench the Luminescence of PbSe and CdSe Quantum Dots, Acetonitrile Does Not. *J. Am. Chem. Soc.* **2012**, *134* (51), 20705–20712.

(28) Adam, S.; Talapin, D. V.; Borchert, H.; Lobo, A.; McGinley, C.; de Castro, A. R. B.; Haase, M.; Weller, H.; Möller, T. The Effect of Nanocrystal Surface Structure on the Luminescence Properties: Photoemission Study of HF-Etched InP Nanocrystals. *J. Chem. Phys.* **2005**, *123* (8), 084706.

Chapter 5 - Conclusions

In this dissertation, microwave-assisted ionic liquid (MAIL) etching of InP NCs synthesis is investigated. Luminescent InP NCs are synthesized using ionic liquids (ILs) containing tetrafluoroborate (BF_4^-) and hexafluorophosphate (PF_6^-) ions. In a silicon carbide (SiC) vessel, bigger NCs form than from the Pyrex vessel because of the higher reactions temperatures in the SiC vessel. In addition, they have surface defects but these defects are minimized by increasing holding time of the microwave reaction. Postreaction etching by ILs on InP NCs result in complete digestion of the NCs.

A novel method of *in situ* ligand stripping and etching is reported for synthesis of InP NCs by microwave-assisted ionic liquid (MAIL) etching method using hexafluorophosphate (PF_6^-) salts. InP NCs solubility can be changed from non-polar (toluene) to polar solvent (DMSO) without requiring any second step of ligand exchange method for modifying surface. The unique nature of these NCs is they still have emission without requiring any HF etching step. The presented *in situ* ligand stripping and etching can also be applied in conventional flask synthesis. This novel synthesis paves a way to synthesize other In-V NCs like InSb with inorganic ligands on surface involving aliphatic acids during the synthesis. Some of the problems to address further in this study to reduce broadness of absorption peaks, improve size distribution, and obtaining water solubility. If water solubility is achieved, they can have potential applications in bio-imaging.

For tuning the size of the InP NCs, same MAIL etching is used by leveraging carefully microwave set-powers (SPs), reaction temperature, and amine. The presented method avoids typical methods of sequential addition of InP precursors, multiprecursors of P, or changing ligand concentration.

In all these three methods, InP NCs still lack luminescence so postreaction processing like HF etching or shell growth (ZnS or ZnSe) is required. However, because of *in situ* etching in MAIL etching method, InP NCs emit different colors in our method. So, size and emission of the InP NCs can be tuned simultaneously. Hence, the reported MAIL etching method is advantageous over conventional InP synthesis for luminescent InP NCs formation. This method can be applied to other semiconductor NCs like InGaP for tuning the size and emission simultaneously. Some of the problems to address further in this study to improve quantum yields and size distributions of the InP NCs.

To sum up, MAIL etching can be used to tune size, emission, and solubility of the InP NCs without using conventional methods. Throughout this work for synthesizing InP NCs reproducibly, maintaining air-free and moisture-free conditions during the synthesis holds the key owing to the sensitivity of InP precursor towards air and moisture.

Acknowledgements

I would like to thank Department of Chemistry, Kansas State University and National Science Foundation (NSF) for providing funding for my PhD work.

Appendix A - Synthesis of Indium Sulfide Nanoparticles from Bulk Materials

A.1 Synthesis

In a 3-neck round-bottom flask indium wire (0.03 g) and elemental S (0.0045g) are taken as Indium and sulfur precursor along with 1-dodecanethol (1.87 mL) as ligand. Moles ratio of In:S:DDT is 1:0.5:30. The flask is equipped with a temperature sensor and a condenser opened to atmosphere. First, a precursor is prepared by heating reaction mixture to 160 °C and then it is heated to 180 °C for over an hour. During this stage aliquots are collected from the reaction mixture to record absorption and photoluminescence.

A.2 Results & Discussion

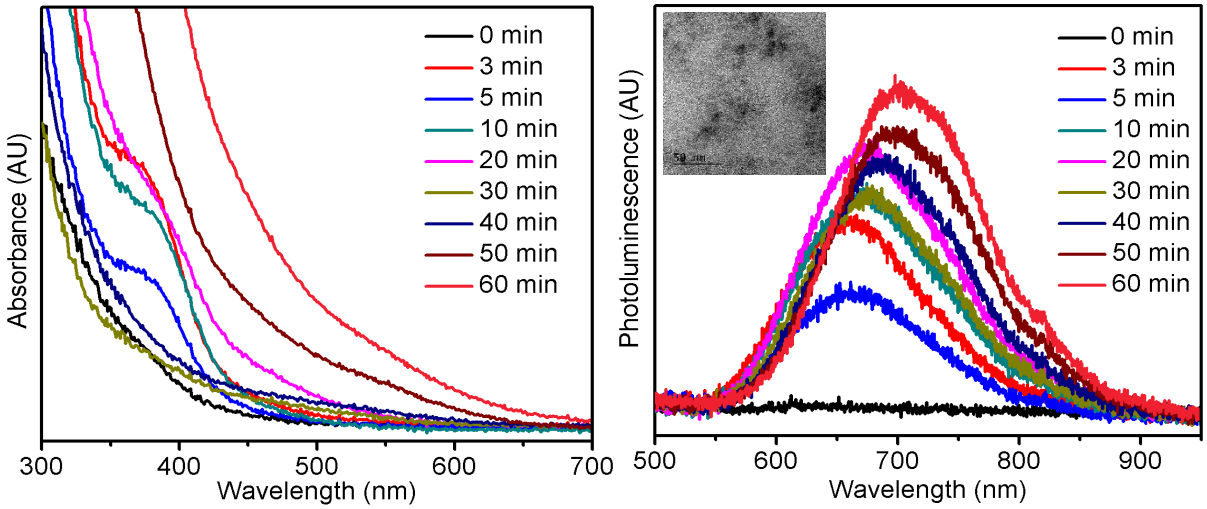

Figure. A. 1 UV-Vis absorption and photoluminescence (PL) spectra of indium sulfide nanoparticles collected at different time intervals at 180 °C. As time increases evolution of absorption peak is observed whereas broad emission is observed probably because of surface traps on the nanoparticles. Inside the photoluminescence spectra TEM image is shown.

Fig. A.1 shows absorption and photoluminescence (PL) spectra of indium sulfide nanoparticles. As time increases to 3 minutes absorption peak is appeared and as the time further increases to 60 minutes absorption peak broadens and will have a red shift probably because of growth and broad size distribution of the nanoparticles. The nanoparticles have emission features as shown in the photoluminescence spectra. As time increases to 60 minutes emission peak has red shift with a range of FWHMs (144-150 nm). TEM image inside photoluminescence spectra indicates formation of the nanoparticles.

Appendix B - Table of lifetime components of InP NCs

Sample	1:3	1:10	1:20
τ_1	**20.0**	**5.8**	**3.0**
α_1	0.015	0.067	0.046
τ_2	**40.0**	**25.8**	**19.0**
α_2	-0.037	0.068	0.081
τ_3	**50.0**	**86.4**	**75.0**
α_3	0.030	0.018	0.081
χ^2	1.051	1.059	1.066
τ_{avg} **(average lifetime, ns)**	**68.1**	**49.3**	**62.6**